DTIC FILE COPY

AD-A202 601

VERIFICATION AND LIMITATIONS OF THE MONOSTATIC-BISTATIC RADAR CROSS SECTION DERIVED BY KELL

THESIS

Jeffrey M. MacLennan
Captain, USAF

AFIT/GE/ENG/88D-24

DTIC
ELECTE
JAN 1 8 1989
S
D

DISTRIBUTION STATEMENT A
Approved for public release;
Distribution Unlimited

DEPARTMENT OF THE AIR FORCE
AIR UNIVERSITY
AIR FORCE INSTITUTE OF TECHNOLOGY

Wright-Patterson Air Force Base, Ohio

89 1 17 110

(1)

AFIT/GE/ENG/88D-24

DTIC
ELECTE
JAN 1 8 1989
S D
Dc

VERIFICATION AND LIMITATIONS OF THE MONOSTATIC-BISTATIC RADAR CROSS SECTION DERIVED BY KELL

THESIS

Jeffrey M. MacLennan
Captain, USAF

AFIT/GE/ENG/88D-24

Approved for public release; distribution unlimited

AFIT/GE/ENG/88D-24

VERIFICATION AND LIMITATIONS OF THE MONOSTATIC-BISTATIC RADAR CROSS SECTION RELATIONSHIP DERIVED BY KELL

THESIS

Presented to the Faculty of the School of Engineering
of the Air Force Institute of Technology
Air University
In Partial Fulfillment of the
Requirements for the Degree of
Master of Science in Electrical Engineering

Jeffrey M. MacLennan, B.S.E.E.
Captain, USAF

December 1988

DTIC
COPY
INSPECTED
6

Accesion For
NTIS CRA&I
DTIC TAB
Unannounced
Justification
By
Distribution /
Availability Codes
Dist | Avail and / or Special
A-1

Approved for public release: distribution unlimited

Preface

The purpose of this study was to verify the mathematical correctness and to determine some of the limitations of the monostatic-bistatic radar cross section (RCS) relationship developed by Robert E. Kell. Potentially, the Radar Target Scattering Facility, Holloman AFB, NM, could apply this relationship to reduce testing time and costs.

A detailed mathematical formulation is provided. It begins with the monostatic-bistatic equivalence theorem (MBET). The MBET is a physical optics approximation relating monostatic and bistatic RCS. The derivation of Kell's relationship is built upon the MBET and is mathematically sound within the prescribed bounds.

Kell's relationship was tested using computer models. The results of the testing show Kell's method of determining bistatic RCS from monostatic RCS measurements has some merit. Measurements are needed to establish the limits to which Kell's method may be applied. Also, the complexity of the targets must be increased in order to gage the accuracy of Kell's method under a variety of conditions.

In performing this study I have received help from others. Of course, I am indebted to my faculty advisor, Major Harry Barksdale, whose insight and guidance kept me moving in the right direction. I would also like to thank

Captain Bill Oetting who never failed to respond positively to my panicked cries for help and Captain Dennis Tackett who devoted a great deal of time and effort in the actual production of this thesis. And, finally, a special thanks to my wife, Debbie, who endured it all with a smile.

Table of Contents

	Page
Preface	ii
List of Figures	vi
Abstract	xi
I. Introduction	1
Overview	1
Background	2
Bistatic RCS measurement	2
Bistatic RCS prediction	3
Statement of Problem	4
Scope	4
Approach	5
Summary of Remaining Chapters	6
II. Theory	7
Background	7
Monostatic-Bistatic Equivalence Theorem	7
Proof	9
Documentation supporting the MBET	13
Kell's Method	14
Mathematical formulation	15
The determination of bistatic RCS	18
Implementing Kell's method	20
Summary	20
III. Results	22
Testing Kell's Hypothesis	22
Sphere	23
Approach	23
Near resonant size sphere results	26
Large sphere results	35
Flat Plate	42
Approach	42
Flat plate results	44
Cylinder	51
Approach	51
Cylinder results	53

Page

IV. Conclusion 71

Conclusions 72
Bistatic angle 72
Electrical size 72
Angle of incidence 73
Surface continuity 73
Recommendations for Further Study . . . 74

Appendix A: Derivation of Kell's Method 76

Appendix B: Sphere RCS Computer Programs 84

Appendix C: Square Flat Plate RCS Models and Computer Programs 92

Appendix D: Cylinder RCS Models and Computer Programs 96

Bibliography 110

VITA 112

List of Figures

Figure		Page
1.	Bistatic Scattering Geometry Depicting the Bistatic-Monostatic Relationship	8
2.	Bistatic Coordinate System with Antennas in the x-z Plane	15
3.	Scattering Geometry for a Sphere	25
4.	Creeping Wave Scattering in the x-y Plane . .	26
5.	Sphere (ka = 1; Vertical Polarization): Bistatic RCS and Equivalent Monostatic RCS . .	29
6.	Sphere (ka = 1; Vertical Polarization): Difference in RCS (Bistatic - Monostatic) . .	29
7.	Sphere (ka = 1; Horizontal Polarization): Bistatic RCS and Equivalent Monostatic RCS . .	30
8.	Sphere (ka = 1; Horizontal Polarization): Difference in RCS (Bistatic - Monostatic) . .	30
9.	Sphere (ka = 3; Vertical Polarization): Bistatic RCS and Equivalent Monostatic RCS . .	31
10.	Sphere (ka = 3; Vertical Polarization): Difference in RCS (Bistatic - Monostatic) . .	31
11.	Sphere (ka = 3; Horizontal Polarization): Bistatic RCS and Equivalent Monostatic RCS . .	32
12.	Sphere (ka = 3; Horizontal Polarization): Difference in RCS (Bistatic - Monostatic) . .	32
13.	Sphere (ka = 5; Vertical Polarization): Bistatic RCS and Equivalent Monostatic RCS . .	33
14.	Sphere (ka = 5; Vertical Polarization): Difference in RCS (Bistatic - Monostatic) . .	33
15.	Sphere (ka = 5; Horizontal Polarization): Bistatic RCS and Equivalent Monostatic RCS . .	34
16.	Sphere (ka = 5; Horizontal Polarization): Difference in RCS (Bistatic - Monostatic) . .	34

Figure Page

17. Sphere (ka = 10; Vertical Polarization): Bistatic RCS and Equivalent Monostatic RCS . . 36

18. Sphere (ka = 10; Vertical Polarization): Difference in RCS (Bistatic - Monostatic) . . 36

19. Sphere (ka = 10; Horizontal Polarization): Bistatic RCS and Equivalent Monostatic RCS . . 37

20. Sphere (ka = 10; Horizontal Polarization): Difference in RCS (Bistatic - Monostatic) . . 37

21. Sphere (ka = 30; Vertical Polarization): Bistatic RCS and Equivalent Monostatic RCS . . 38

22. Sphere (ka = 30; Vertical Polarization): Difference in RCS (Bistatic - Monostatic) . . 38

23. Sphere (ka = 30; Horizontal Polarization): Bistatic RCS and Equivalent Monostatic RCS . . 39

24. Sphere (ka = 30; Horizontal Polarization): Difference in RCS (Bistatic - Monostatic) . . 39

25. Sphere (ka = 50; Vertical Polarization): Bistatic RCS and Equivalent Monostatic RCS . . 40

26. Sphere (ka = 50; Vertical Polarization): Difference in RCS (Bistatic - Monostatic) . . 40

27. Sphere (ka = 50; Horizontal Polarization): Bistatic RCS and Equivalent Monostatic RCS . . 41

28. Sphere (ka = 50; Horizontal Polarization): Difference in RCS (Bistatic - Monostatic) . . 41

29. Bistatic Scattering Geometry for a Square Flat Plate 42

30. Equivalent Monostatic Scattering Geometry for a Square Flat Plate 43

31. Square Flat Plate (ϕ = 0°): Bistatic RCS and Equivalent Monostatic RCS 45

32. Square Flat Plate (ϕ = 0°): Difference in RCS (Bistatic - Monostatic) . . 45

Figure Page

33. Square Flat Plate (θ = 8°): Bistatic RCS and Equivalent Monostatic RCS 46

34. Square Flat Plate (θ = 8°): Difference in RCS (Bistatic - Monostatic) . . 46

35. Square Flat Plate (θ = 16°): Bistatic RCS and Equivalent Monostatic RCS 47

36. Square Flat Plate (θ = 16°): Difference in RCS (Bistatic - Monostatic) . . 47

37. Square Flat Plate (θ = 24°): Bistatic RCS and Equivalent Monostatic RCS 48

38. Square Flat Plate (θ = 24°): Difference in RCS (Bistatic - Monostatic) . . 48

39. Square Flat Plate (θ = 32°): Bistatic RCS and Equivalent Monostatic RCS 49

40. Square Flat Plate (θ = 32°): Difference in RCS (Bistatic - Monostatic) . . 49

41. Square Flat Plate (θ = 40°): Bistatic RCS and Equivalent Monostatic RCS 50

42. Square Flat Plate (θ = 40°): Difference in RCS (Bistatic - Monostatic) . . 50

43. Cylinder Geometry 51

44. Cylinder (θ = 0°; Vertical Polarization): Bistatic RCS and Equivalent Monostatic RCS . . 55

45. Cylinder (θ = 0°; Horizontal Polarization): Bistatic RCS and Equivalent Monostatic RCS . . 55

46. GTD Applied to Right-Circular Cylinder to Show Contributions from Illuminated Edges . . 56

47. Cylinder (θ = 15°; Vertical Polarization): Bistatic RCS and Equivalent Monostatic RCS . . 59

48. Cylinder (θ = 15°; Vertical Polarization): Difference in RCS (Bistatic - Monostatic) . . 59

49. Cylinder (θ = 15°; Horizontal Polarization): Bistatic RCS and Equivalent Monostatic RCS . . 60

Figure Page

50. Cylinder (ϕ = 15°; Horizontal Polarization): Difference in RCS (Bistatic - Monostatic) . . 60

51. Cylinder (ϕ = 30°; Vertical Polarization): Bistatic RCS and Equivalent Monostatic RCS . . 61

52. Cylinder (ϕ = 30°; Vertical Polarization): Difference in RCS (Bistatic - Monostatic) . . 61

53. Cylinder (ϕ = 30°; Horizontal Polarization): Bistatic RCS and Equivalent Monostatic RCS . . 62

54. Cylinder (ϕ = 30°; Horizontal Polarization): Difference in RCS (Bistatic - Monostatic) . . 62

55. Cylinder (ϕ = 45°; Vertical Polarization): Bistatic RCS and Equivalent Monostatic RCS . . 63

56. Cylinder (ϕ = 45°; Vertical Polarization): Difference in RCS (Bistatic - Monostatic) . . 63

57. Cylinder (ϕ = 45°; Horizontal Polarization): Bistatic RCS and Equivalent Monostatic RCS . . 64

58. Cylinder (ϕ = 45°; Horizontal Polarization): Difference in RCS (Bistatic - Monostatic) . . 64

59. Cylinder (ϕ = 60°; Vertical Polarization): Bistatic RCS and Equivalent Monostatic RCS . . 65

60. Cylinder (ϕ = 60°; Vertical Polarization): Difference in RCS (Bistatic - Monostatic) . . 65

61. Cylinder (ϕ = 60°; Horizontal Polarization): Bistatic RCS and Equivalent Monostatic RCS . . 66

62. Cylinder (ϕ = 60°; Horizontal Polarization): Difference in RCS (Bistatic - Monostatic) . . 66

63. Cylinder (ϕ = 75°; Vertical Polarization): Bistatic RCS and Equivalent Monostatic RCS . . 67

64. Cylinder (ϕ = 75°; Vertical Polarization): Difference in RCS (Bistatic - Monostatic) . . 67

65. Cylinder (ϕ = 75°; Horizontal Polarization): Bistatic RCS and Equivalent Monostatic RCS . . 68

66. Cylinder (ϕ = 75°; Horizontal Polarization): Difference in RCS (Bistatic - Monostatic) . . 68

Figure		Page
67.	Cylinder (Φ = 90°; Vertical Polarization): Bistatic RCS and Equivalent Monostatic RCS . .	70
68.	Cylinder (Φ = 90°; Horizontal Polarization): Difference in RCS (Bistatic - Monostatic) . .	70
69.	Bistatic Coordinate System with Antennas in the x-z Plane	78
70.	Scattering Geometry for a Square Flat Plate .	92
71.	Diffraction at Edge of Conducting Wedge . . .	97
72.	Diffraction by a Right Circular Cylinder . . .	98
73.	Angular Relationships for Geometric Factors .	100
74.	Phase of a Diffracted Ray	101

Abstract

Robert Kell developed a relationship between monostatic radar cross section (RCS) and bistatic RCS whereby bistatic RCS can be predicted from monostatic RCS measurements under certain conditions. This study found Kell's relationship to be mathematically sound given certain assumptions. Kell's relationship was then tested by comparing computer generated bistatic and monostatic cross sections for simple shapes. Four parameters were varied during testing in order to discern possible limitations of Kell's method: bistatic angle, angle of incidence, electrical size of the target, and continuity. Results of the testing show Kell's method has some merit. The difference between the bistatic RCS and its related monostatic RCS for electrically large spheres is less than 1-dB up to bistatic angles of 80°. For electrically large flat and singly curved surfaces the monostatic and bistatic cross sections were within 3-dB for angles of incidence up to 30° from broadside and bistatic angles up to 15°. Finally, the accuracy of Kell's relationship proved to be polarization dependent when surface discontinuities in the form of 90° wedges were present.

VERIFICATION AND LIMITATIONS OF THE MONOSTATIC-BISTATIC RADAR CROSS SECTION RELATIONSHIP DERIVED BY KELL

I. Introduction

Overview

One method used to reduce the detectability of an aircraft by radar is to shape it so the energy from the radar is reflected away from the radar's receiver. By reflecting the incident energy away from the receiver the aircraft presents a smaller radar cross section (RCS) and, therefore, is more difficult to detect. Monostatic radar, a radar in which the radar's transmitter and receiver antennas are collocated, is more common than bistatic radar, a radar with separated transmitter and receiver antennas. For this reason, most aircraft designed to present a low RCS reflect energy away from the direction of the transmitting source. However, reducing the RCS in one direction using shaping techniques results in an increased RCS in another direction (Knott, 1985:10). Thus, even today's most stealthy aircraft, those designed to hinder detection by radar at common flight aspects, may still be detectable by bistatic radar receivers (Adams, 1988:27).

For military planners to project a weapon system's ability to penetrate enemy air defenses, it is necessary to perform both monostatic and bistatic RCS analyses.

Unfortunately, however, the evolution of bistatic RCS prediction and measurement techniques has not kept pace with that of monostatic techniques (Hunka, 1978:243). Because of the threat bistatic radars pose for even stealth aircraft and the need to plan for and reduce that threat, methods need to be developed that accurately predict bistatic RCS.

Background

The earliest radars were bistatic, but with the appearance of monostatic radar in the 1930's bistatic radar faded from prominence. Bistatic radar interest surfaced again in the mid 1950's leading to bistatic radar applications in satellite tracking systems and guidance control in low altitude cruise missiles (Skolnik, 1961:20; Biggs and McMillen, 1979:1). However, the development of bistatic RCS prediction and measurement techniques did not receive the attention monostatic RCS techniques enjoyed until later.

Bistatic RCS measurements. Bistatic RCS measurements are inherently more difficult and complex than monostatic measurements simply because the receiving antenna must be moved for each measurement (Hunka,1977:243). The Air Force Radar Target Scatter Facility (RATSCAT), an outdoor radar range at Holloman AFB, New Mexico, uses a bistatic mobile receiver van to enhance the mobility of their receiving antenna (Dynalectron Corp., 1985:43). However, they must still deal with the complexities involved in bistatic RCS

measurements not suffered by monostatic measurements. Each repositioning of the receiver calls for recalibration. This means the target of interest must be replaced with a calibration target so that background returns can be identified. Multipath scattering must also be accounted for with each position change. And, when all is ready, the target, sometimes as large as a full scale model of a B1-B, must be remounted. All of this takes a great deal more time and costs considerably more than monostatic measurements (Tomko, 1988).

Bistatic RCS prediction. Before the 1950's, the scientific community in general felt the theoretical calculation of a complex target's RCS was beyond the capabilities of the known technology. By the early 1950's, approximation techniques began evolving that allowed the estimation of the RCS for such complex shapes as airplanes, missiles, and satellites. Through experience and the appearance of high speed computers the theoretical estimation of an average monostatic cross section circa 1958 was within 4 dB of measured values (Crispin and others, 1968:v). Bistatic prediction methods were also developed during this period, but there was no experimental data with which to compare their accuracy (Siegel and others, 1955:305).

One could easily speculate that the previously

mentioned problems regarding bistatic RCS measurements were the reason why bistatic RCS experimental data was in short supply. Because monostatic RCS measurements are much easier to perform than bistatic measurements, if a means of predicting bistatic RCS from monostatic measurements were possible, it would be less costly and faster than performing bistatic RCS measurements. This approach to bistatic RCS prediction would be beneficial to operations such as the RATSCAT.

Statement of the Problem

In 1965, Robert Kell presented a relationship between monostatic and bistatic radar cross section which appears to offer a means of predicting bistatic RCS using monostatic measurements under certain conditions. The purpose of this thesis is to verify the theoretical accuracy of Kell's relationship and to determine the physical limitations with which Kell's method has practical application.

Scope

The basis for Kell's method is developed first. This development begins with a description of the monostatic-bistatic equivalence theorem (MBET), the foundation of Kell's method. Following this is the mathematical formulation of Kell's hypothesis.

The results from an investigation in which Kell's method is theoretically applied to specific shapes whose

bistatic cross section can be accurately modeled are presented. The accuracy of Kell's method when subjected to changes in either bistatic angle, electrical size, or surface discontinuity will then be discussed.

Approach

The limitations of Kell's method can be found theoretically by comparing computer generated bistatic radar cross sections to the equivalent monostatic cross sections produced using Kell's hypothesis. Computer programs either in use by Air Force agencies or developed from proven monostatic and bistatic RCS models will be used.

Kell suggests his method is most accurate in the high frequency regime to about 10° of bistatic angle using targets dominated by specular returns (Kell, 1965:987). This investigation will apply Kell's method to targets meeting these conditions in order to verify the accuracy of this method. The parameters of bistatic angle, electrical size, angle of incidence, and surface continuity will then be varied so some of the limitations of Kell's method might be brought out. In the case of surface continuity, a target with 90° wedges will be used to determine the limitations of Kell's relationship when surface discontinuities are present.

Summary of Remaining Chapters

Chapter II is a development of Kell's method. It begins with a description of the monostatic-bistatic equivalence theorem (MBET). A review of the literature regarding the MBET is then provided. This is followed by the mathematical formulation of Kell's method.

Chapter III describes RCS models for the sphere, flat plate, and cylinder for both the bistatic case and Kell's equivalent monostatic case. Chapter III then presents the results from the comparison of the two cases.

Chapter IV contains the conclusions reached from this study and recommendations for further research in this area.

II. Theory

Background

Robert Kell implies his method extends the monostatic bistatic equivalence theorem (MBET) to include more general cases (Kell, 1965:983). In an effort to offer a more complete development of Kell's method, this chapter first presents the MBET and documentation supporting the concept of predicting bistatic RCS from monostatic RCS. Unfortunately, there has been little research performed in this area. It will be seen that the MBET relies upon physical optics approximations, and therefore, it is applicable to only those targets fitting into the limitations set by physical optics techniques. The development of Kell's method shows his approach relies upon the interaction between individual scattering centers. Kell uses the concept of reradiation lobe patterns of the individual scattering centers to define the bistatic scattering pattern in terms of the monostatic pattern and bistatic angle (Kell, 1965:983).

Monostatic-Bistatic Equivalence Theorem

In general, discussions of bistatic RCS are divided into two areas. The first is concerned with bistatic angles less than 180°. The second case takes into account bistatic angles approximately equal to 180°. This is known as

forward scattering. It has significantly different behavior than bistatic scattering and is not addressed in this study.

In considering the case where the bistatic angle is less than 180°, Crispin and others developed what has come to be known as the monostatic-bistatic equivalence theorem (MBET). Referring to Figure 1, this theorem claims as the wavelength becomes small compared to target size the bistatic cross section obtained with a transmitter direction $\hat{R}$ and a receiver direction $\hat{n}_o$ approaches the RCS obtained when the transmitter and receiver are collocated at $\hat{R} + \hat{n}_o$ assuming the target is sufficiently smooth (Crispin and others, 1968:158). More succinctly, the MBET is saying the bistatic RCS is equal to the monostatic RCS in the direction of the bisector of the bistatic angle as the wavelength becomes very small.

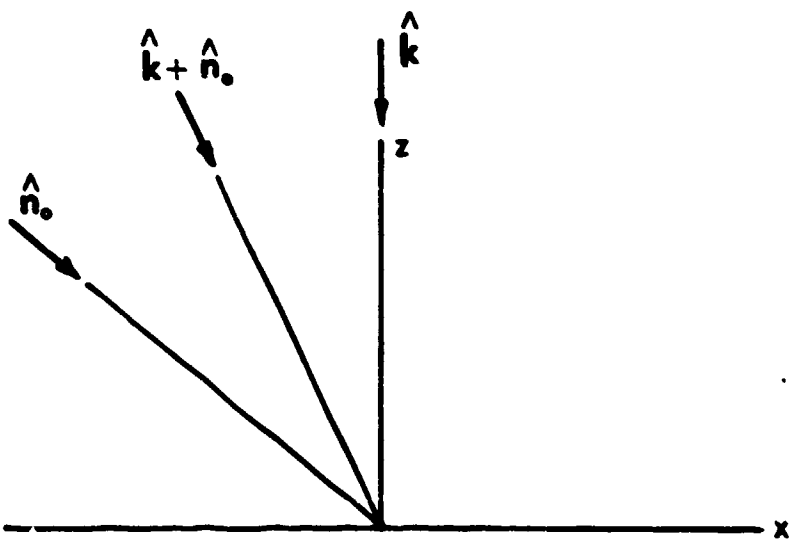

Figure 1. Bistatic Scattering Geometry Depicting the Bistatic-Monostatic Relationship

Proof. Crispin offers the following proof for the MBET (Crispin and others, 1968:158). Radar Cross Section as a function of transmitter and receiver position is derived as follows (Siegel and others, 1955:10). Assuming the surface of the scattering body is perfectly conducting the equation for the scattered magnetic field is given by

$$\bar{H}_{sc} = \frac{1}{4\pi} \int_S (\hat{n} \times \bar{H}_t) \times \nabla \left(\frac{e^{-ikR}}{R}\right) ds \qquad (1)$$

where $\bar{H}_{sc}$ = scattered magnetic field

$\hat{n}$ = the unit vector normal to the surface

$\bar{H}_t$ = tangential component of the magnetic field on the target's surface

R = distance between the receiver and the integrat on point

$k = 2\pi/\lambda$ (wave number)

S = region of integration (target's surface)

By assuming the incident field is an infinite plane wave, $\bar{H}_t$ can be approximated as twice the tangential component of the incident magnetic field on the illuminated side. Letting the incident magnetic field have a magnitude $\bar{H}_o$ and direction $\hat{a}$ allows $\bar{H}_t$ to be written as

$$\bar{H}_t = 2\bar{i}_t H_o e^{-ik(\hat{r} \cdot \bar{r}')} \quad \text{on the target's illuminated side} \qquad (2)$$

$$= 0 \quad \text{on the target's shadow side}$$

where $\hat{R}$ = a unit vector directed from the transmitter, assumed to be in the far field, to the origin of the coordinate system

$\bar{r}'$ = radius vector from origin to any point on the target's surface

$\bar{f}_t = \hat{a} - (\hat{a} \cdot \hat{n})\hat{n}$

Using far field approximations

$$\frac{\nabla(e^{-ikR})}{R} = \frac{-ik\hat{n}_o e^{-ikR}}{R'} \qquad (3a)$$

and

$$R = R' - \cos\alpha_o \qquad (3b)$$

where R' = distance from the origin to the receiver.

$\hat{n}_o$ = a unit vector directed from the receiver to the origin

$$\cos\alpha_o = -\frac{\hat{n}_o \cdot \bar{r}'}{|\bar{r}'|}$$

Letting $H_o = 1$, substituting eqs.(2) and (3) into (1) gives

$$\bar{H}_{sc} = \frac{e^{-ikR'}}{R'} \bar{F} \qquad (4)$$

where $$\bar{F} = \frac{ik}{2\pi}[(\hat{n}_o \cdot \hat{a})\bar{f} - (\hat{n}_o \cdot \bar{f})\hat{a}] \qquad (5a)$$

and $$\bar{f} = \int_{s'} \hat{n} e^{ik\bar{r} \cdot (\hat{n}_o + \hat{R})} ds \qquad (5b)$$

s' = illuminated region of the target

The RCS can now be expressed as (Crispin and others, 1968:158)

$$\sigma = 4\pi[\,|F_x|^2 + |F_y|^2 + |F_z|^2\,] \tag{6}$$

In Figure 1, the transmitter is placed on the x axis and the receiver is constrained to lie in the y-z plane. With this configuration the monostatic case is defined by

$$\hat{n}_o = \hat{y}\mathrm{Sin}\theta - \hat{z}\mathrm{Cos}\theta \tag{7a}$$

$$\hat{R} = \hat{y}\mathrm{Sin}\theta - \hat{z}\mathrm{Cos}\theta \tag{7b}$$

$$\hat{a} = \hat{x}\mathrm{Cos}\phi + \hat{y}\mathrm{Sin}\phi\mathrm{Cos}\theta + \hat{z}\mathrm{Sin}\phi\mathrm{Sin}\theta \tag{7c}$$

while in the bistatic case

$$\hat{n}_o = \hat{y}\mathrm{Sin}2\theta - \hat{z}\mathrm{Cos}2\theta \tag{8a}$$

$$\hat{R} = -\hat{z} \tag{8b}$$

$$\hat{a} = \hat{x}\mathrm{Cos}\phi + \hat{y}\mathrm{Sin}\phi \tag{8c}$$

Considering the vector $\bar{f}$ as the wavelength becomes small compared to the target

$$\bar{f} = -\frac{(\hat{n}_o+\hat{R})}{|\hat{n}_o+\hat{R}|}\int_s [e^{ik\bar{r}'}\cdot(\hat{n}_o+\hat{R})]ds \tag{9}$$

For the monostatic case, eq. (9) becomes

$$\bar{f} = \bar{p}\int_s [e^{ik\bar{r}'}\cdot(\hat{n}_o+\hat{R})]ds \tag{10}$$

And in the bistatic case, eq. (9) becomes

$$\bar{f} = \bar{p} \int_{s'} [e^{ik\bar{r}'} \cdot (2\hat{\beta}\cos\theta)]_{ds} \qquad (11)$$

where $\hat{\beta} = \hat{y}\sin\theta - \hat{z}\cos\theta$

Evaluating eqs.(10) and (11) by stationary phase yields

$$\bar{f} = [\hat{y}A\sin\theta - \hat{z}A\cos\theta] \exp(ikC) \quad \text{(monostatic case)} \qquad (12)$$

$$f = [\hat{y}A\tan\theta - \hat{x}A] \exp(ikC\cos\theta) \quad \text{(bistatic case)} \qquad (13)$$

Substituting eqs. (7) and (10) for the monostatic case into eq. (5)

$$\bar{F} = \frac{ik}{2\pi} [Ae^{ikC}(\hat{x}\cos\phi + \hat{y}\sin\phi\cos\theta + \hat{z}\sin\phi\sin\theta] \qquad (14)$$

Applying eq. (14) to eq. (6) gives the monostatic RCS

$$\sigma_m = (kA)^2/\pi \qquad (15)$$

Now, substituting eqs.(8) and (11) for the bistatic case into eq. (5)

$$\bar{F} = \frac{ik}{2\pi} [A \exp(ikC\cos\theta)][(\sin\theta\sin2\theta)(\hat{y}\tan\theta - \hat{z}) - (\tan\theta\sin2\theta + \cos2\theta)(\hat{x}\cos\phi + \hat{y}\sin\phi)] \qquad (16)$$

Again, applying eq. (16) to (6) gives the bistatic RCS

$$\sigma_b = (kA)^2/\pi \qquad (17)$$

Comparing eqs. (15) and (17), it can be seen that as wavelength becomes small compared to target size the monostatic RCS taken on the bisector of the bistatic angle is equivalent to the bistatic RCS.

The equations the MBET is developed from, eqs. (1) and (2), are derived using physical optics techniques (Siegel and others, 1953:10). Therefore, the MBET is valid only if the restrictions required by physical optics are satisfied. Those restrictions are given below (Skinner and Jost, 1988:2):

1. The target must have a large enough RCS that higher order effects do not make a significant difference.

2. The target must be significantly larger than a wavelength.

3. A significant amount of the target's surface should be within approximately 45° of the normal of the bisector of the transmitter and receiver.

4. The target must be perfectly conducting.

These restriction limit the applicability of the MBET. Two studies were found, however, in which the MBET was used to determine bistatic RCS.

Documentation supporting the MBET. Biggs and McMillen, in their efforts to formulate the bistatic RCS of a prolate spheroid, found the MBET returned accurate results. The two discrepancies these researchers noted when comparing measured data with data obtained using the MBET were within

one percent and were attributed to the fact the MBET requires the target be infinitely removed from the transmitter and the receiver. When it is not, the bistatic receiver is not looking at the exact same spot as the monostatic receiver (Biggs and McMillen, 1979:13).

Coleman, while testing an aircraft RCS computer prediction method, MISCAT III, against measured data of the F-5 aircraft, found bistatic angles up to 16° had little effect on the RCS. This made the MBET attractive. By taking advantage of this approximation he was able to reduce program running time for the bistatic case for small bistatic angle to that of the monostatic case. At the same time, he was able to resolve some inaccuracies by avoiding certain elements within the bistatic RCS derivation (Coleman, 1977:34).

In the process of applying the MBET, Coleman developed error estimates for parallel, perpendicular, and cross polarizations. His interpretation of the error estimates reach the same conclusions that Kell does in the development of his approach. First, the RCS is determined by the relationships between scattering center. The second, that the equivalent monostatic RCS includes the factor $\cos(\beta/2)$ where β is the bistatic angle (Coleman, 1977:43).

Kell's Method

Kell developed a method to obtain bistatic RCS using monostatic RCS measurements. His method uses the concept of

reradiation lobe patterns from individual scattering centers to define the bistatic RCS in terms of monostatic patterns and the bistatic angle. Kell's approach uses the MBET by relating the bistatic RCS to the monostatic RCS viewed on the bisector of the bistatic angle by a factor of $\cos(\beta/2)$ (Kell, 1965:983).

Mathematical formulation. The geometry Kell used is given in Figure 2.

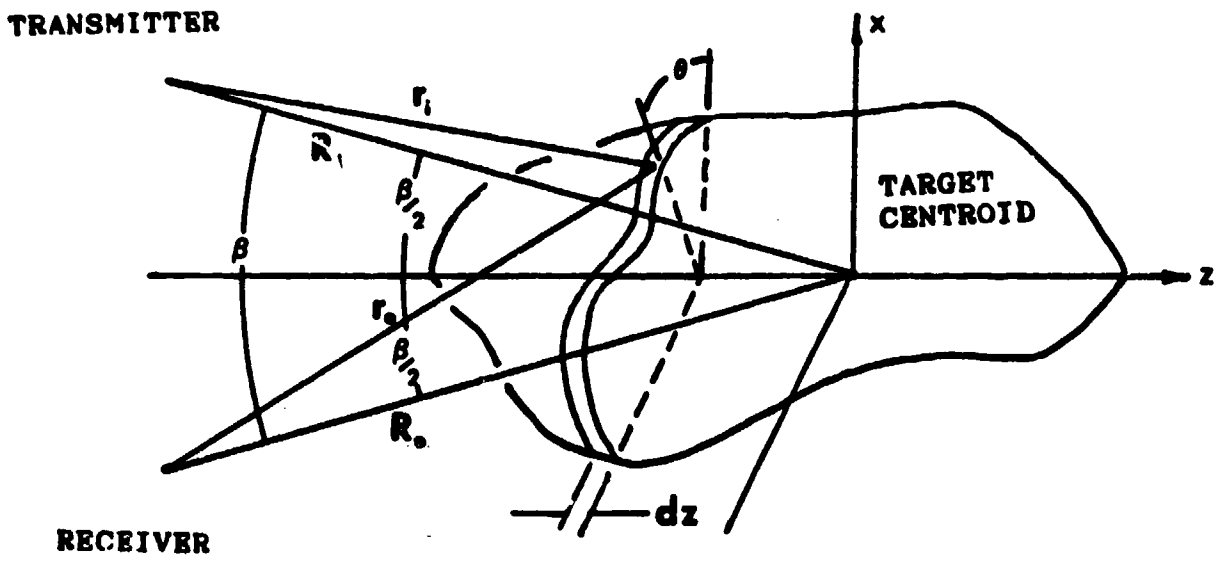

Figure 2. Bistatic Coordinate System with Antennas in the x-z Plane

It can be seen in Figure 2 that Kell aligns the bisector of the the bistatic angle, β, and the centroid of the target along the z axis. Applying the Stratton-Chu equation for

the scattered magnetic field to this geometry, Kell arrives at the following expression for the bistatic RCS (Kell, 1965:985)

$$\sigma = \frac{\pi}{\lambda^2} \left| \int I(z) \exp[ik2z\cos(\beta/2)]\, dz \right|^2 \qquad (18a)$$

where

$$I(z) = \int [(\hat{n} \times \bar{h}_s) \times \hat{f}_o(e^{i\phi}) + (\hat{n}\cdot\bar{h}_s)(e^{i\phi})\hat{f}_o - (\hat{n} \times \bar{e}_s)e^{i\phi}] \times p(\theta,z)\, d\theta \qquad (18b)$$

The derivation of eq. (18) can be found in appendix A.

Kell made the following observations regarding eq. (18) (Kell, 1965:985):

a) I(z) is an exact description of the surface geometry, illuminating and observing ray geometry, and surface wave propagation effects

b) While eq. (18) has the form of a physical optics expression it is not a physical optics expression because I(z), in this case, is exact as opposed to a physical optics approximation

c) Eq. (18) can be divided into a sum of subintegrals whose end points correspond to scattering centers. The end points of each subintegral are determined by the range in z over which the respective integrands are continuous.

According to Kell, the phase of a given scattering center plays a large role in the contribution that scattering center makes to the total RCS. The magnitude of the contributrion of an individual scattering center to the overall return is directly related to the area covered by the scattering center. The size of the area of the scattering center is directly related, in turn, to the phase of the scattering center. All points with phases within $\pi/2$ of the scattering center's phase contribute positively with the scattering center's return. The greater the area within $\pi/2$ of the scattering center's phase the greater the contribution from that scattering center. This concept applies equally to both monostatic and bistatic RCS (Kell, 1965:985).

Differences will often arise between bistatic RCS and monostatic RCS viewed on the bisector of the bistatic angle as the bistatic angle changes. Kell relates these differences to the following changes in the scattering centers (Kell, 1965:985):

a) Changes in the phase of scattering centers relative to other centers

b) Changes in strength of the radiation from a given scattering center

c) Change in the number of scattering centers.

Looking at eq. (18), phase is clearly dependent on the bistatic angle by a factor of $\cos(\beta/2)$. Kell couples this

factor with the wave number k and then views a change in bistatic angle as a change in wavelength. As the relative wavelength changes with bistatic angle the area within $\pi/2$ wavelengths of the scattering centers also changes (Kell, 1965:985).

The radiation strength of a scattering center is dependent on the strength of the surface current, among other things, at that location. With changes in the bistatic angle there can be changes in the tangential components of the incident field resulting in a change in the surface currents.

Kell describes the appearance and disappearance of scattering centers as aspect angle and target geometry dependent and declines further explanation (Kell, 1965:985).

The determination of bistatic RCS. Kell approximates the target by breaking it into a collection of discrete scattering centers. Those centers directly illuminated by the incident wave are termed simple centers while those illuminated by reflections from other parts of the target are termed reflex centers. Kell's addresses only the simple scattering centers. Using the concept of discrete scattering centers, Kell then derives the total RCS by summing the product of the individual center's RCS and a relative phase term (Kell, 1965:986):

$$\sigma = \left| \sum_{m=1}^{M} [(\sigma_m)^{1/2} \exp(i\phi_m)] \right|^2 \qquad (19)$$

where σ = total RCS

M = number of discrete scatterers

σ_m = RCS of the m^{th} scattering center

ϕ_m = phase of field scattered by the m^{th} center relative to that scattered by the first center, and where σ_m is evaluated for the desired polarization.

In examining the relations between the monostatic and bistatic RCS for a given aspect angle Θ, Kell expresses the individual scattering center's phase in eq. (19) as a two-term sum (Kell, 1965:986):

$$\phi_m = 2kz_m(\Theta)\mathrm{Cos}(\beta/2) + \xi_m \qquad (20)$$

where $z_m(\Theta)$ = distance between the m^{th} and the first phase center, projected on the bistatic bisector axis

ξ_m = residual phase contributions of the m^{th} center

The bistatic RCS for scattering centers that do not move with changes in bistatic angle can now be written as (Kell, 1965:986)

$$\sigma(\Theta) = \left| \sum_{m=1}^{M} (\sigma_m)^{1/2} \exp[i2kz_m(\Theta)\mathrm{Cos}(\beta/2) + i\xi_m] \right|^2 \qquad (21)$$

Kell uses eq. (21) to make a statement for monostatic-bistatic equivalence and the conditions required for its occurrence.

If for a chosen aspect angle, the following conditions hold:

1) The RCS may be written as a squared sum of fields from discrete scattering centers, and
2) The amplitude σ_m , position z_m, and residual phase ξ_m are insensitive to the bistatic angle β over the range of β considered, for those centers which are significant members in this sum;

it then follows that the bistatic cross section of aspect angle θ and bistatic angle β is equal to the monostatic cross section measured on the bisector at a frequency by the factor $\cos(\beta/2)$ [Kell, 1965:987].

Implementing Kell's method. The step-by-step process to employ Kell's method calls for first measuring the monostatic cross section as a function of aspect angle and at a frequency higher than the one desired for the bistatic data by a factor of $\sec(\beta/2)$. The reason Kell raises the frequency can be seen in eq. (18). As previously explained, phase changes are indicated by the factor $\cos(\beta/2)$ accompanying the wave number k. This can be considered a change in wavelength or frequency corresponding to a change in bistatic angle. The measured monostatic data is then translated along the aspect angle axis $\beta/2$ degrees and the measurement frequency is reduced by $\cos(\beta/2)$ (Kell, 1965:987).

Summary

It was demonstrated theoretically that the MBET provides a relationship between monostatic and bistatic RCS when physical optics approximations are valid. The utility of the MBET for small bistatic angles was shown in the work performed by Coleman.

Kell's method approaches the problem of equating bistatic RCS and monostatic RCS in much the same way as the MBET in that it uses the same scattering geometry and is in the high frequency regime. Unlike the MBET which approximates surface currents to determine RCS, the theoretical basis for Kell's method lies in the summation of the contributions from individual scattering centers. His mathematical formulation of this hypothesis is exact up to the point where he makes far field approximations and evaluates the bistatic RCS integral using stationary phase mehtods. According to Kell, the change in the contributions from the scattering centers with changing bistatic angle is due in large part to changes in the relative phase of each scattering center. For small bistatic angles, Kell reports phase will change by a factor of $\mathrm{Cos}(\beta/2)$. Kell noticed that the $\mathrm{Cos}(\beta/2)$ factor occurs with the wave number k. Viewing this as a change in frequency, Kell hypothesizes that monostatic RCS is equal to bistatic RCS when the frequency of the monostatic case is increased by a factor of $\mathrm{Sec}(\beta/2)$.

Kell's method could be tested theoretically by comparing computer predicted monostatic cross sections to bistatic RCS predictions.

III. Results

There are proven RCS prediction methods that can accurately approximate bistatic RCS as well as monostatic RCS for certain shapes. Kell's hypothesis can be tested by comparing data derived from bistatic prediction methods with that obtained from monostatic approximations at appropriately adjusted frequencies and aspect angles. Three simple shapes are used to prove the accuracy and limitations of Kell's hypothesis. These are the sphere, square flat plate, and right circular cylinder. An exact solution is used to predict the RCS of a sphere, physical optics methods are applied to approximate the RCS of a square flat plate, and, finally, the RCS of a right circular cylinder is obtained using geometrical theory of diffraction techniques.

Testing Kell's Hypothesis

Kell's hypothesis can be tested theoretically by comparing the predicted bistatic RCS to the predicted monostatic cross section at the bisector of the bistatic angle. The bistatic RCS is calculated for each target at designated angles of incidence with the bistatic angle varying from 0° to 60° in 1° increments for the square flat plate and the cylinder while the range of bistatic angles for the sphere is 0° to 90° in 1° increments. All bistatic RCS predictions are made at a constant frequency. Monostatic RCS predictions are made at aspect angles equal

to the designated angle of incidence plus half the bistatic angle. The monostatic RCS prediction frequency is increased by a factor of secant($\beta/2$) (β = bistatic angle) above the frequency used for the bistatic case.

The accuracy of Kell's theory can be determined by comparing the data obtained from each method. A plot of bistatic RCS and monostatic RCS versus bistatic angle at a given angle of incidence shows how closely Kell's equivalent monostatic RCS coincides with the bistatic RCS as bistatic angle increases.

Sphere

Approach. In the case of a perfectly conducting sphere, the exact solution for the bistatic cross section of a plane electromagnetic wave is taken from the Mie series. It is (Bowman, 1969:400)

$$\sigma(\theta,\phi) = \frac{4\pi}{k^2}\left[\,|S_1(\theta)|^2\mathrm{Cos}^2(\phi) + |S_2(\theta)|^2\mathrm{Sin}^2(\phi)\right] \qquad (22)$$

where,

$$S_1 = -i\sum_{n=1}^{\infty}\frac{(-1)^n\ 2n+1}{n(n+1)}\left[b_n\frac{\partial P_n^1(\mathrm{Cos}\theta)}{\partial\theta} - a_n\frac{P_n^1(\mathrm{Cos}\theta)}{\mathrm{Sin}\theta}\right] \qquad (23)$$

$$S_2 = i\sum_{n=1}^{\infty}\frac{(-1)^n(2n+1)}{n(n+1)}\left[b_n\frac{P_n^1(\mathrm{Cos}\theta)}{\mathrm{Sin}\theta} - a_n\frac{\partial P_n^1(\mathrm{Cos}\theta)}{\partial\theta}\right] \qquad (24)$$

θ = bistatic angle

ϕ = angle between plane of scattering and the plane containing the incident E field and the direction of incidence

and (Knott, 1985:90)

$$a_n = \frac{j_n(ka)}{h_n^{(1)}(ka)} \tag{25}$$

$$b_n = \frac{kaj_{n-1}(ka) - nj_n(ka)}{kah_{n-1}^{(1)}(ka) - nh_n^{(1)}(ka)} \tag{26}$$

with

$j_n(ka)$ = spherical Bessel function

$h_n^{(1)}(ka)$= spherical Hankel function of the first kind

$k = 2\pi/\lambda$ (the wave number)

a = sphere radius

For the monostatic case, eq. (22) reduces to (Bowman, 1969:401)

$$\sigma = \frac{4\pi}{k^2} \sum_{n=1}^{\infty} \frac{(1-)^n 2n+1}{n(n+1)} (b_n - a_n)^2 \tag{27}$$

The geometry describing scattering from a sphere is given in Figure 3.

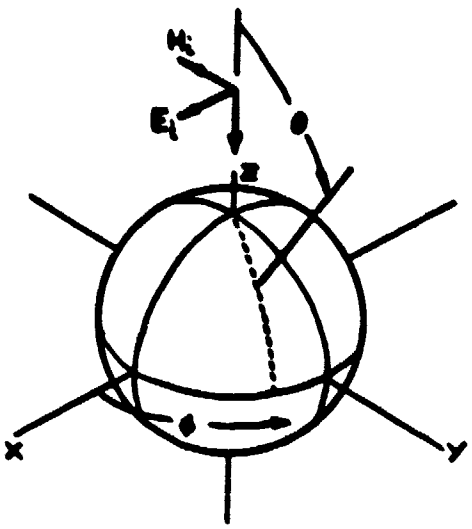

Figure 3. Scattering Geometry for a Sphere (Knott, 1985:89)

Two computer programs given in Appendix B were used to derive the RCS of various sized spheres. One program, a product of Ohio State University that is used on the Wright-Patterson AFB indoor radar range for calibration purposes, gives an exact solution for the radar cross section of a sphere for any number of bistatic angles. For this study, the bistatic angle was varied from 0° to 90° in increments of 1°. The second program is a modified version of the first program. It computes the monostatic RCS of a sphere over a range of discrete frequencies with each frequency increased by a factor of secant(β/2) over the previous frequency. β is the bistatic angle and ranges from 0° to 90° in increments of

1°. Varying the frequency in this way directly relates the equivalent monostatic RCS data in a one-to-one correspondence to the bistatic RCS obtained for each bistatic angle.

Figures 4 through 27 show the relationship between bistatic RCS and the RCS obtained using Kell's method. Six sphere sizes of ka equal to 1, 3, 5, 10, 30, and 50 at 10 GHz were examined using horizontal and vertical polarizations.

Near resonant size sphere results. A comparison of Figures 5 and 7 show there is a significant difference between vertically and horizontally polarized bistatic RCS and between bistatic and monostatic RCS for an electrically small sphere (ka = 1). The differences are caused by creeping waves. For a vertically polarized field as shown in Figure 4, boundary conditions for a perfectly conducting surface require the tangential component of the surface electric field to be zero in the x-y plane.

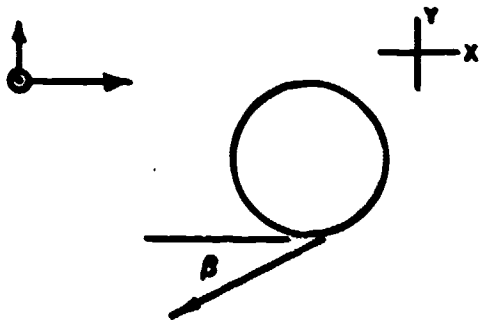

Figure 4. Creeping Wave Scattering in the x-y Plane

Therefore, vertically polarized creeping waves contribute to the monostatic RCS, but as the bistatic angle increases in the x-y plane, creeping waves no longer scatter in the x-y plane and the bistatic RCS decreases.

For horizontal polarization, Figure 7 demonstrates the creeping wave continues to contribute as the bistatic angle increases. In the case of ka = 1 (Figure 7), the phase of the creeping wave is relatively insensitive to changes in bistatic angle. This allows the creeping wave contribution to equal that of the monostatic case at bistatic angles greater than 45°.

The effects of creeping waves can also be seen in the RCS data for spheres ka = 3 (Figures 9 and 11) and ka = 5 (Figures 13 and 15). The horizontally polarized creeping wave continues to contribute to the RCS, however, creeping wave phase is becoming more sensitive to changes in bistatic angle as the sphere becomes larger. Bistatic and monostatic RCS are in agreement to approximately 35° of bistatic angle for ka = 3 and only 8° of bistatic angle for ka = 5. For the case of vertical polarization, the bistatic and monostatic RCS begin to diverge at 1 to 2 degrees of bistatic angle for ka=3,5.

This data demonstrates Kell's relationship cannot account for creeping waves that are polarization dependent and, therefore, is not suitable for electrically small targets.

Page 28 Blank

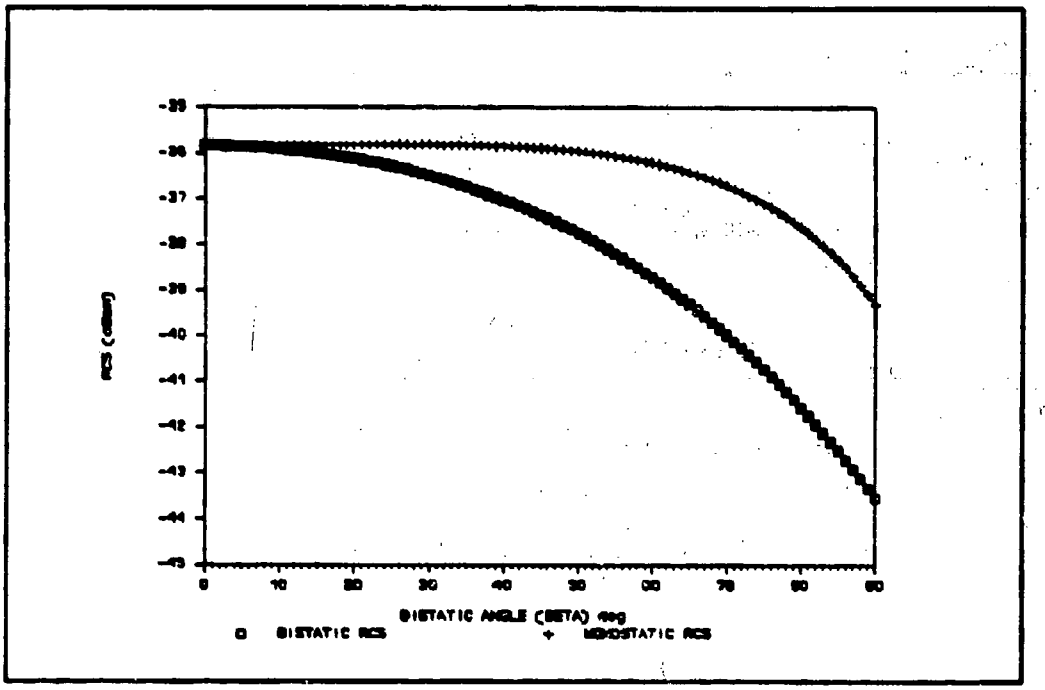

Figure 5. Sphere (ka = 1; Vertical Polarization): Bistatic RCS and Equivalent Monostatic RCS

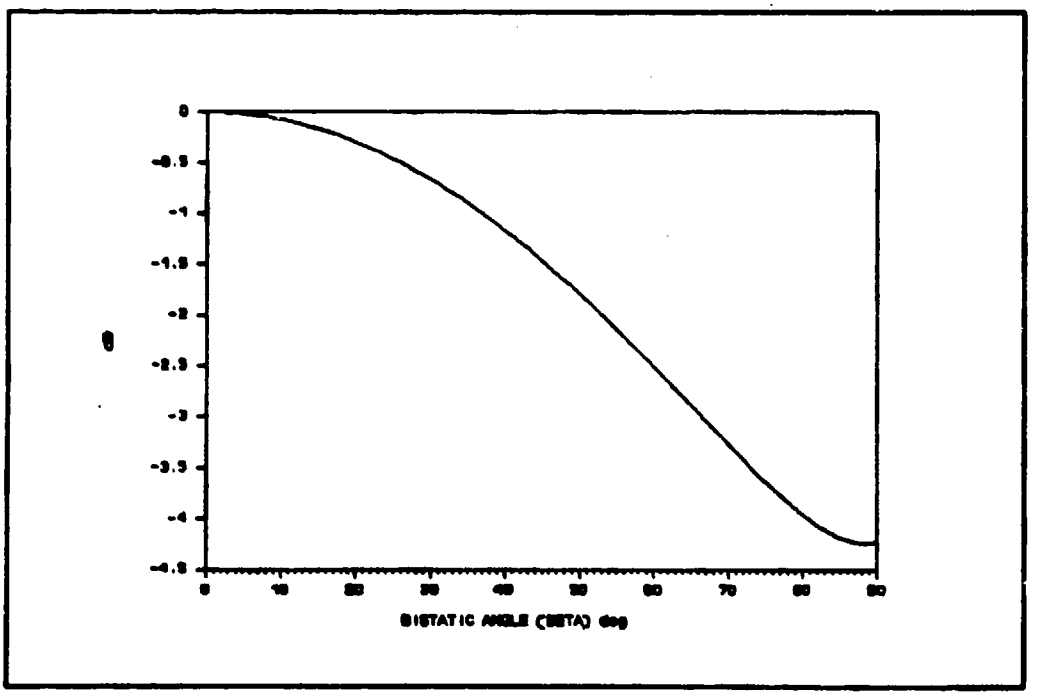

Figure 6. Sphere (ka=1; Vertical Polarization): Difference in RCS (Bistatic - Monostatic)

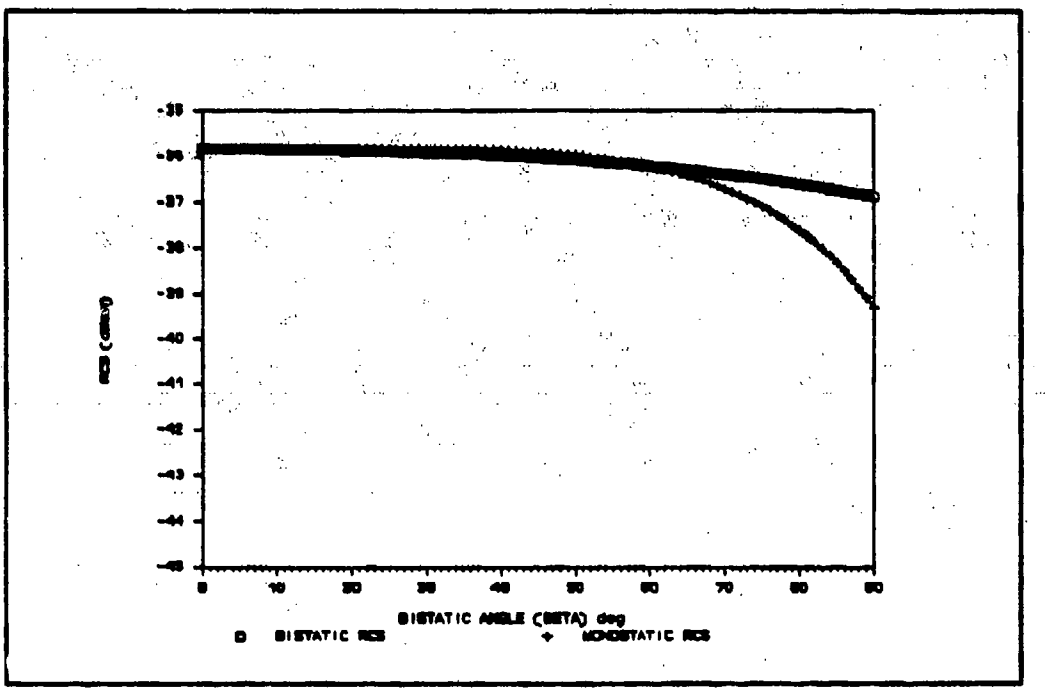

Figure 7. Sphere (ka=1; Horizontal Polarization): Bistatic RCS and Equivalent Monostatic RCS

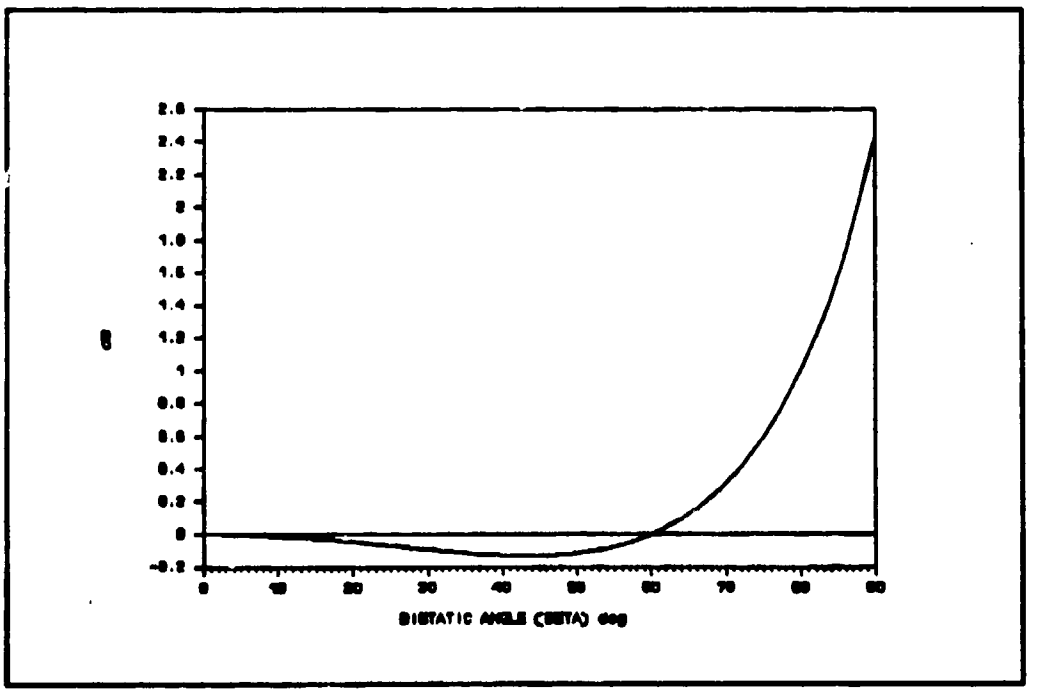

Figure 8. Sphere (ka=1; Horizontal Polarization): Difference in RCS (Bistatic - Monostatic)

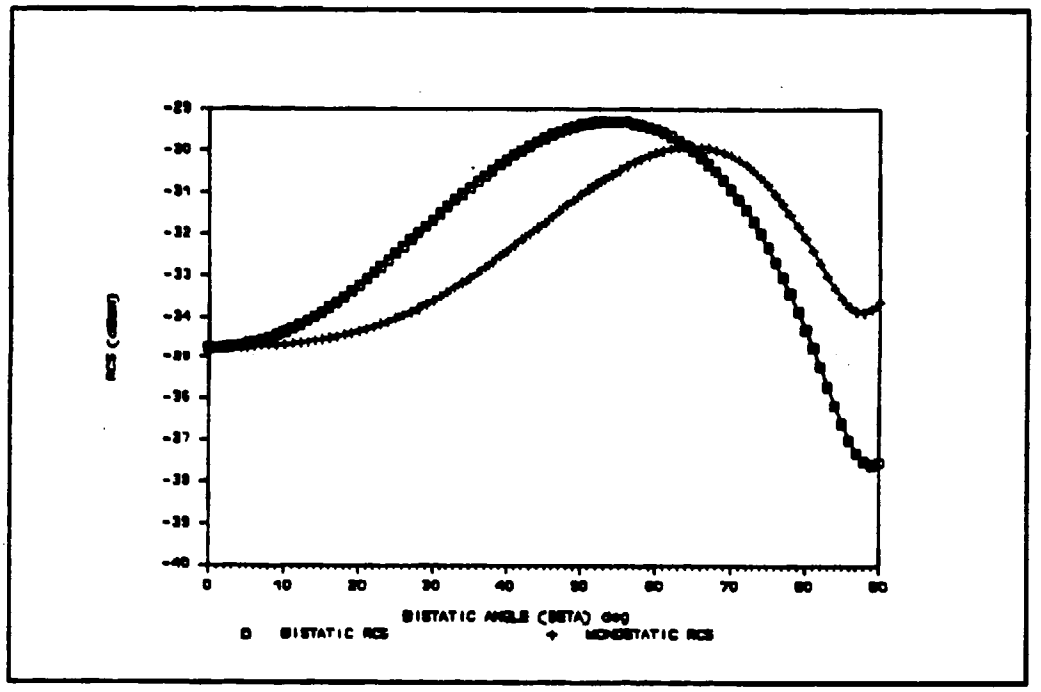

Figure 9. Sphere (ka=3; Vertical Polarization): Bistatic RCS and Equivalent Monostatic RCS

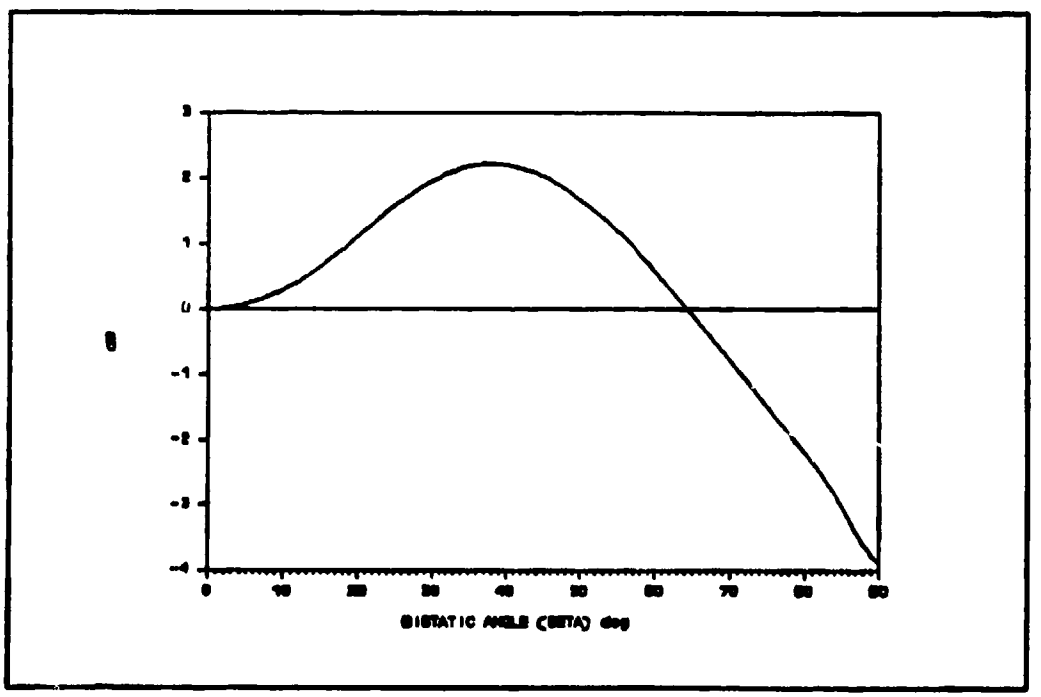

Figure 10. Sphere (ka=3; Vertical Polarization): Difference in RCS (Bistatic - Monostatic)

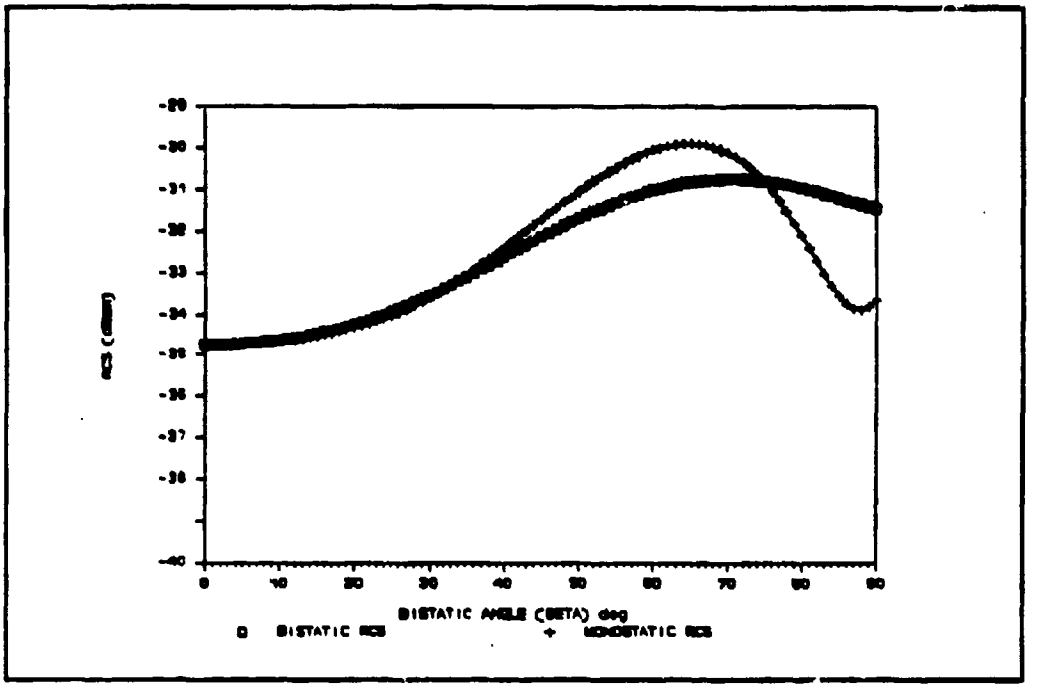

Figure 11. Sphere (ka=3: Horizontal Polarization): Bistatic RCS and Equivalent Monostatic RCS

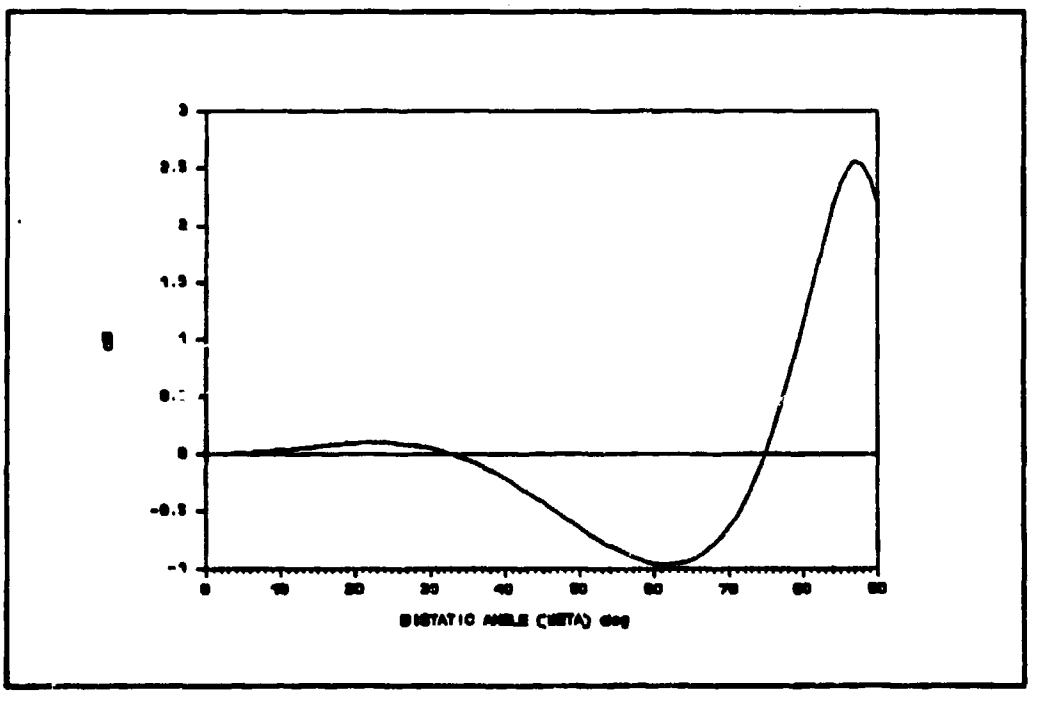

Figure 12. Sphere (ka=3; Horizontal Polarization): Difference in RCS (Bistatic - Monostatic)

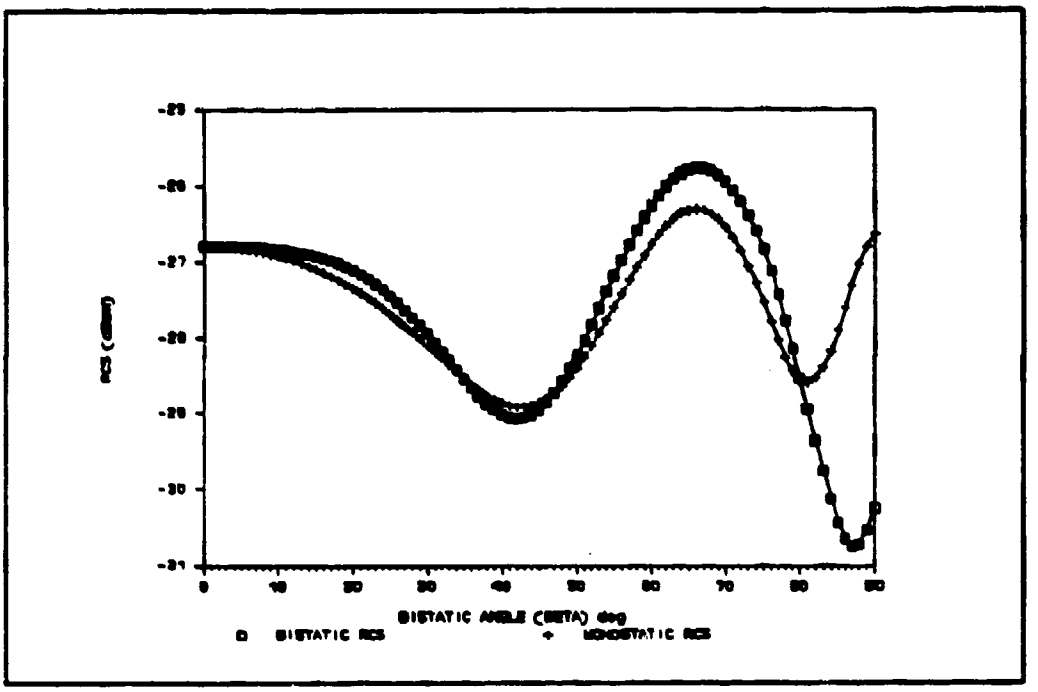

Figure 13. Sphere (ka=5; Vertical Polarization): Bistatic RCS and Equivalent Monostatic RCS

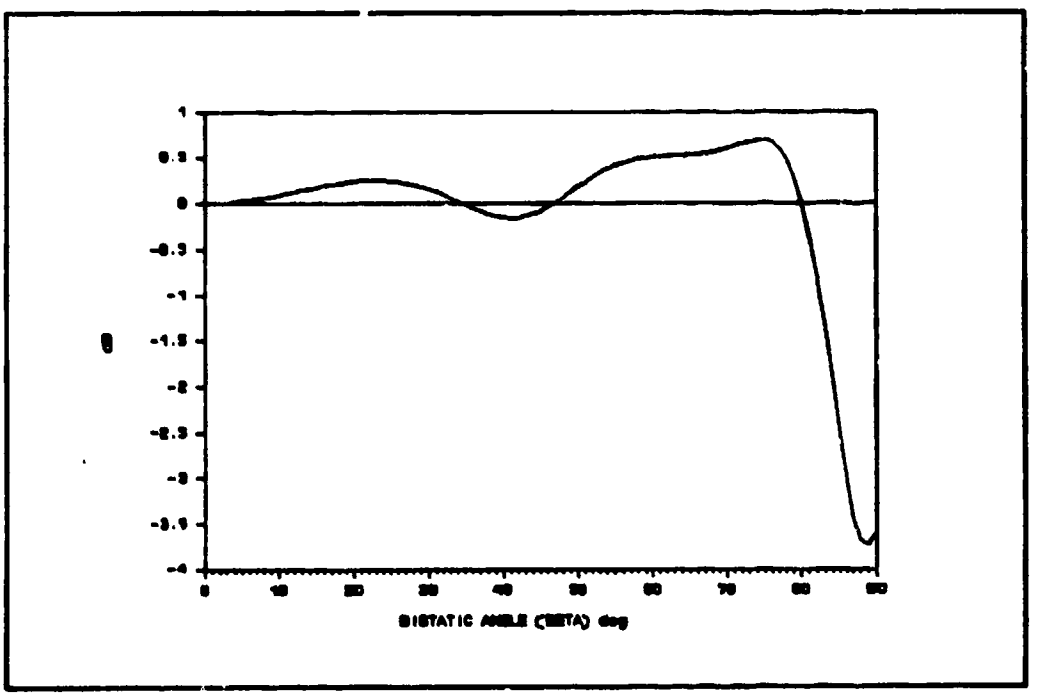

Figure 14. Sphere (ka=5; Vertical Polarization): Difference in RCS (Bistatic - Monostatic)

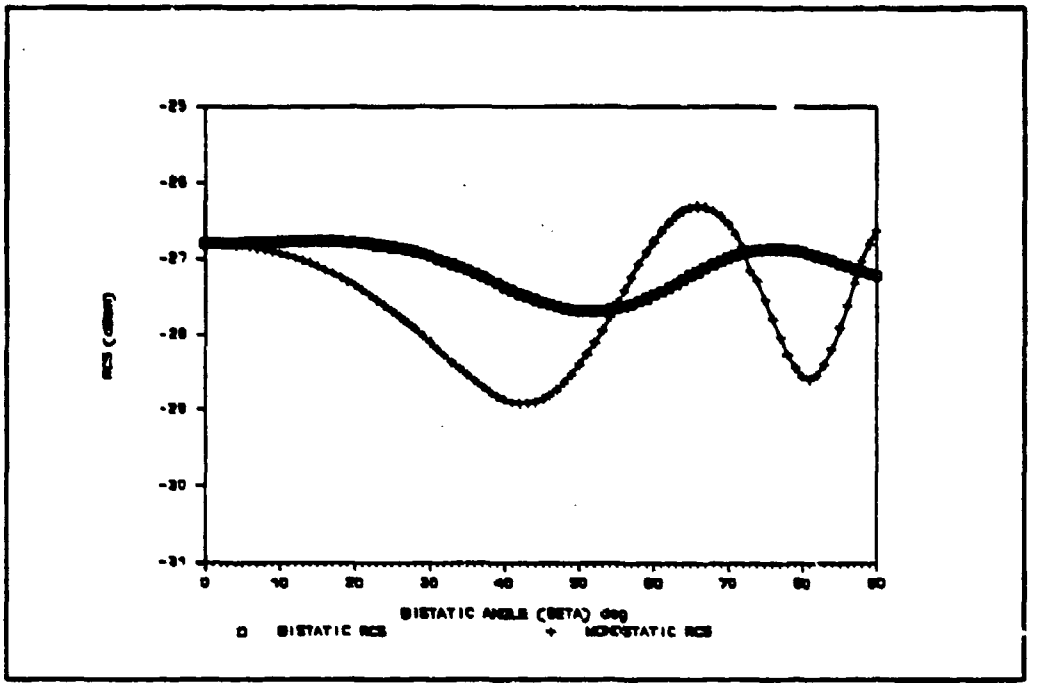

Figure 15. Sphere (ka=5; Horizontal Polarization): Bistatic RCS and Equivalent Monostatic RCS

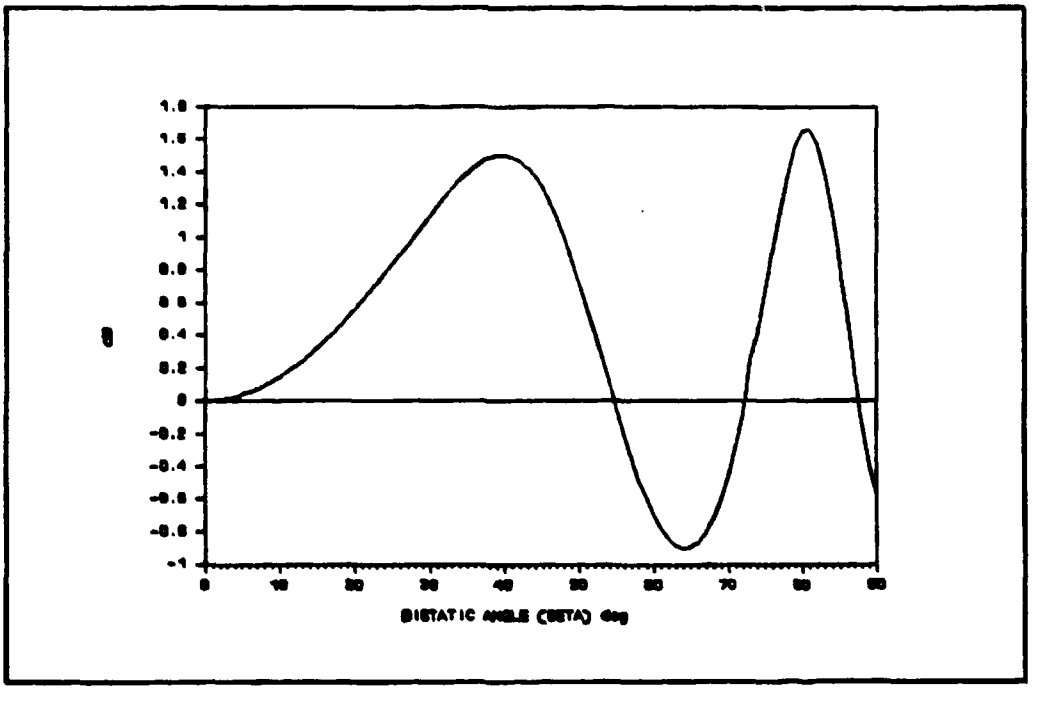

Figure 16. Sphere (ka=5; Horizontal Polarization): Difference in RCS (Bistatic - Monostatic)

Large sphere results. The equivalent monostatic cross section values are very close to those predicted for the bistatic case. Much of the slight differences between the two cases are caused by creeping waves. This can be seen in Figures 17, 19, 21, 23, 25, and 27. Attenuation due to the larger electrical path lengths of these larger spheres causes the reduction in creeping wave effects. Looking at Figures 18, 20, 22, 24, 26, and 28, Kell's method is very good well beyond 10° for doubly curved surfaces with no surface discontinuities and at high frequencies.

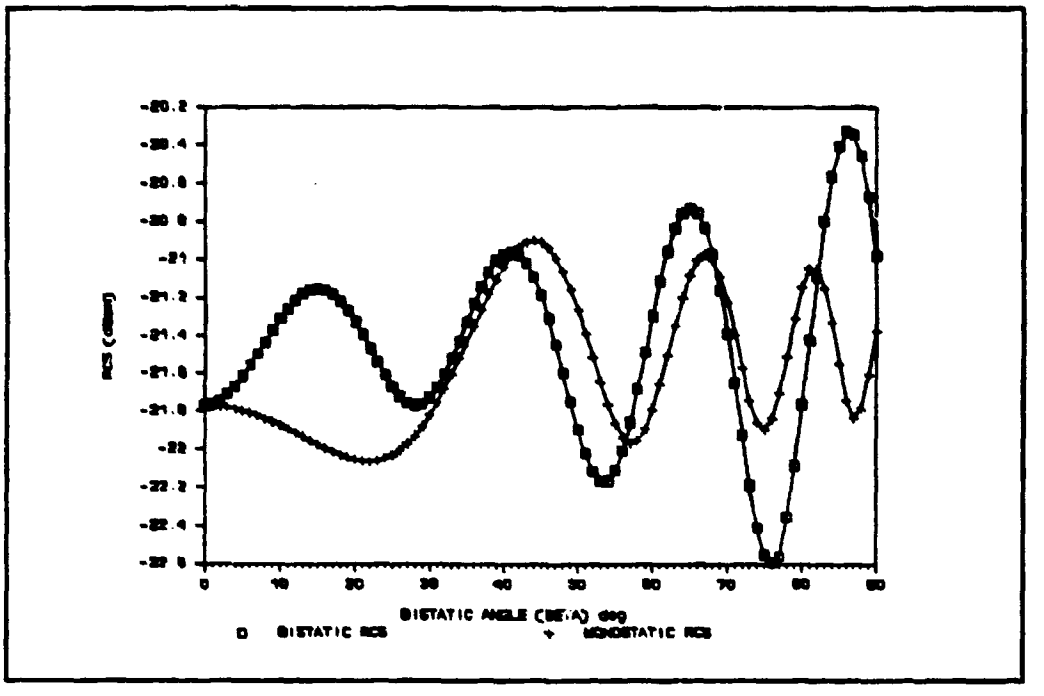

Figure 17. Sphere (ka=10; Vertical Polarization): Bistatic RCS and Equivalent Monostatic RCS

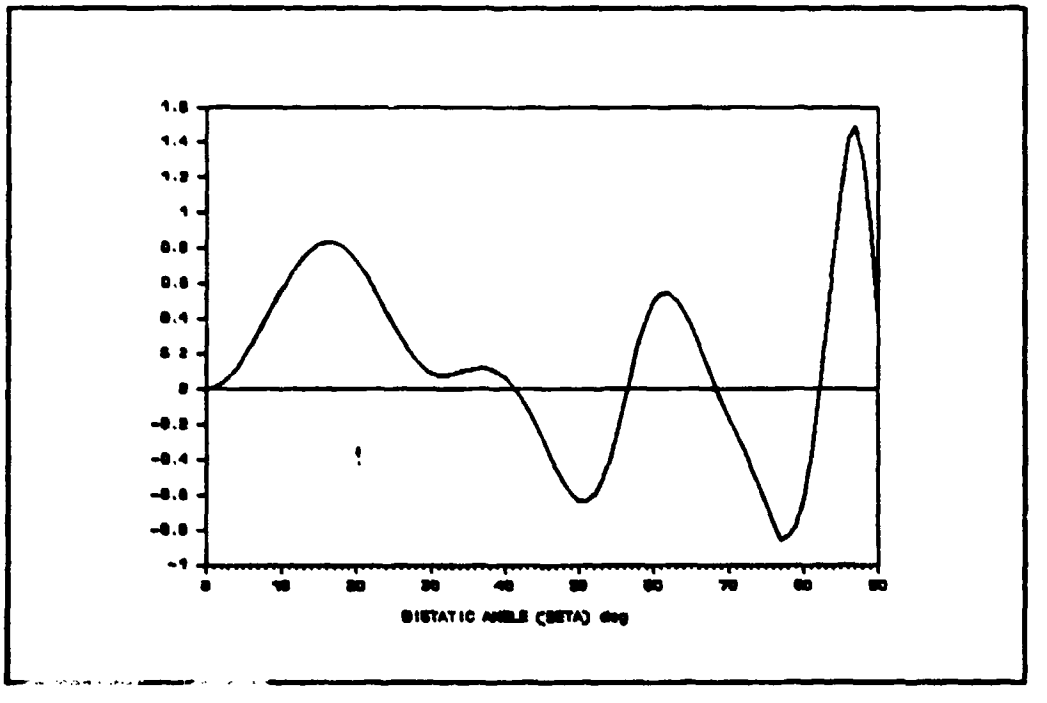

Figure 18. Sphere (ka=10; Vertical Polarization): Difference in RCS (Bistatic - Monostatic)

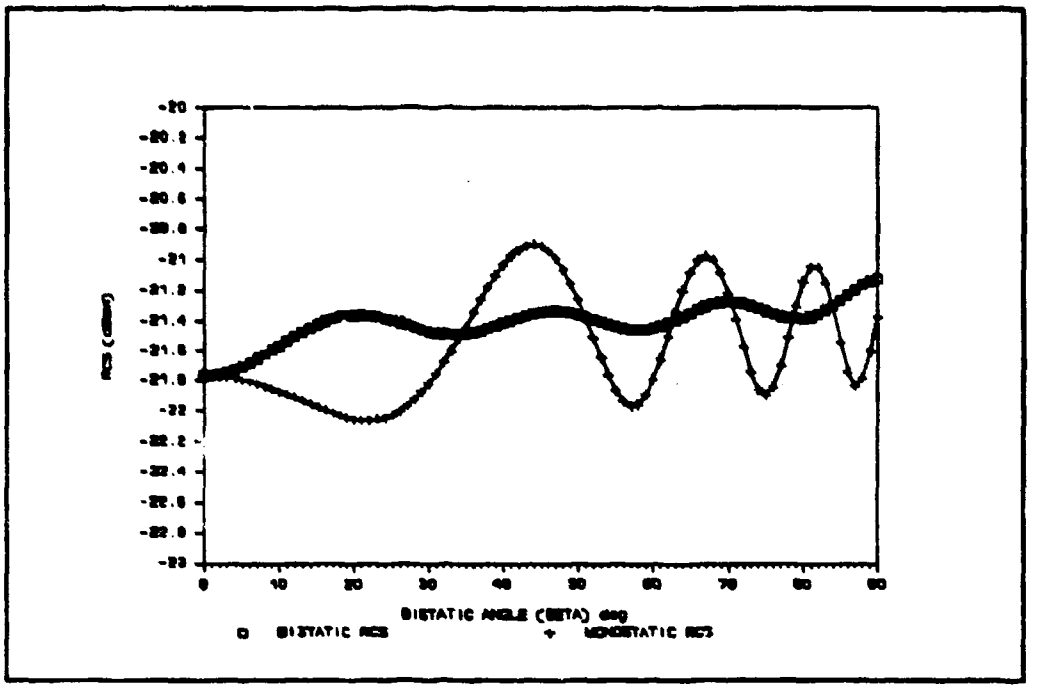

Figure 19. Sphere (ka=10; Horizontal Polarization) Bistatic RCS and Equivalent Monostatic RCS

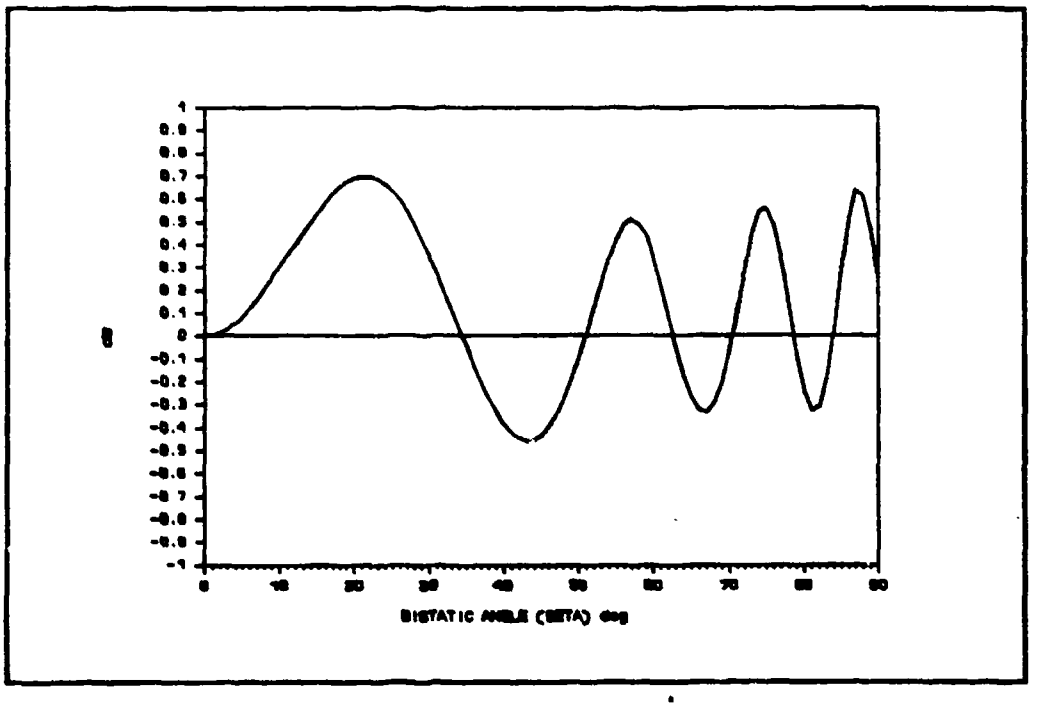

Figure 20. Sphere (ka=10; Horizontal Polarization): Difference in RCS (Bistatic - Monostatic)

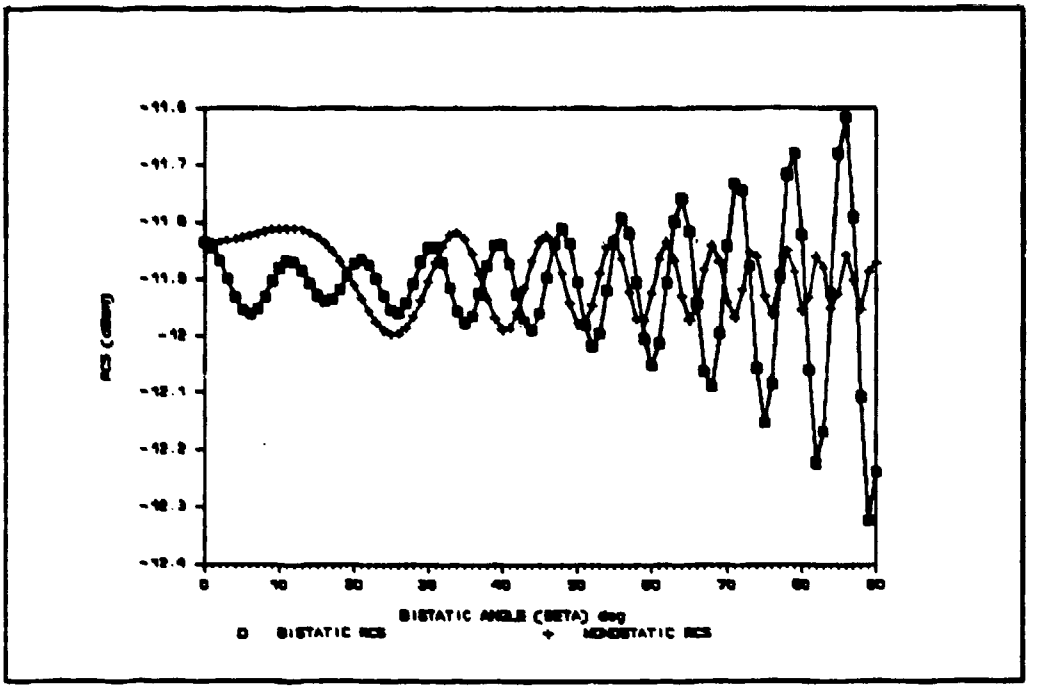

Figure 21. Sphere (ka=30; Vertical Polarization): Bistatic RCS and Equivalent Monostatic RCS

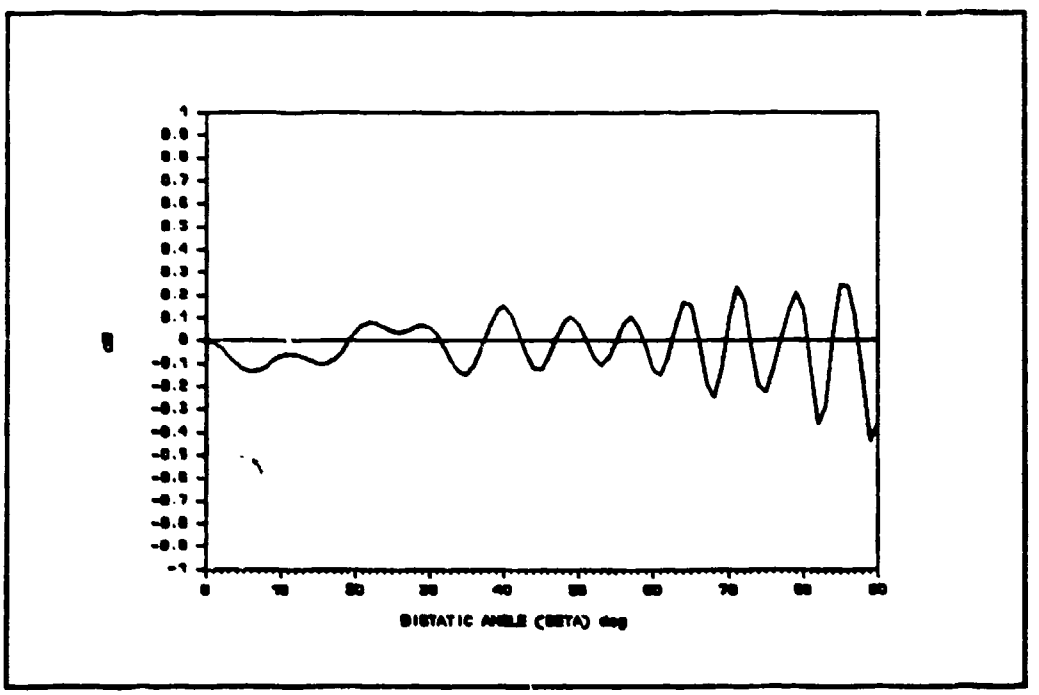

Figure 22. Sphere (ka=30; Vertical Polarization): Difference in RCS (Bistatic - Monostatic)

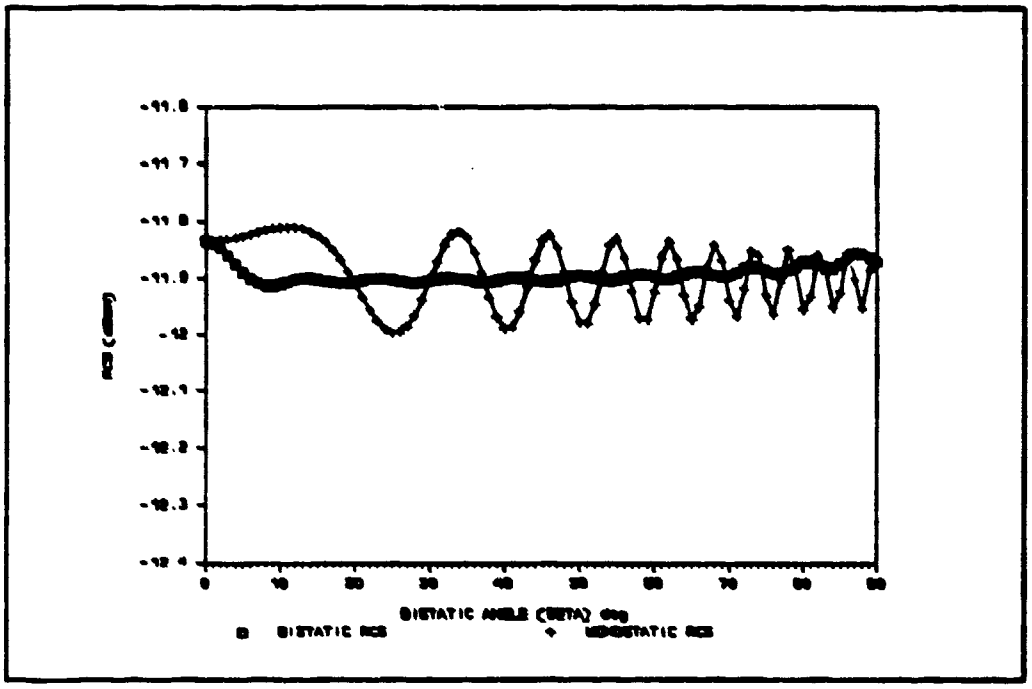

Figure 23. Sphere (ka=30; Horizontal Polarization): Bistatic RCS and Equivalent Monostatic RCS

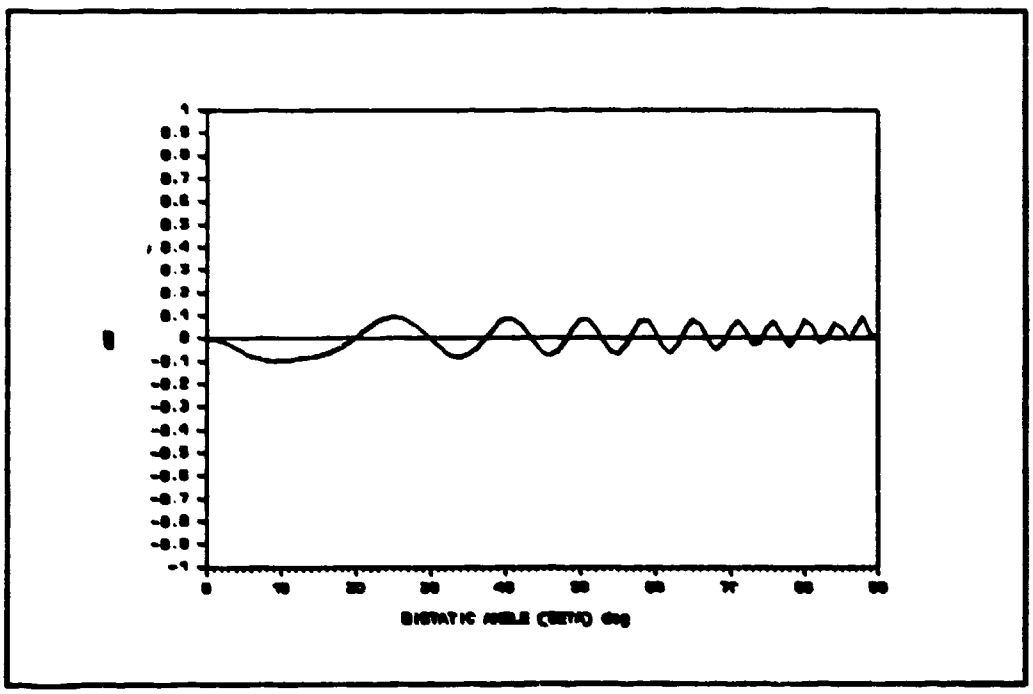

Figure 24. Sphere (ka=30; Horizontal Polarization): Difference in RCS (Bistatic - Monostatic)

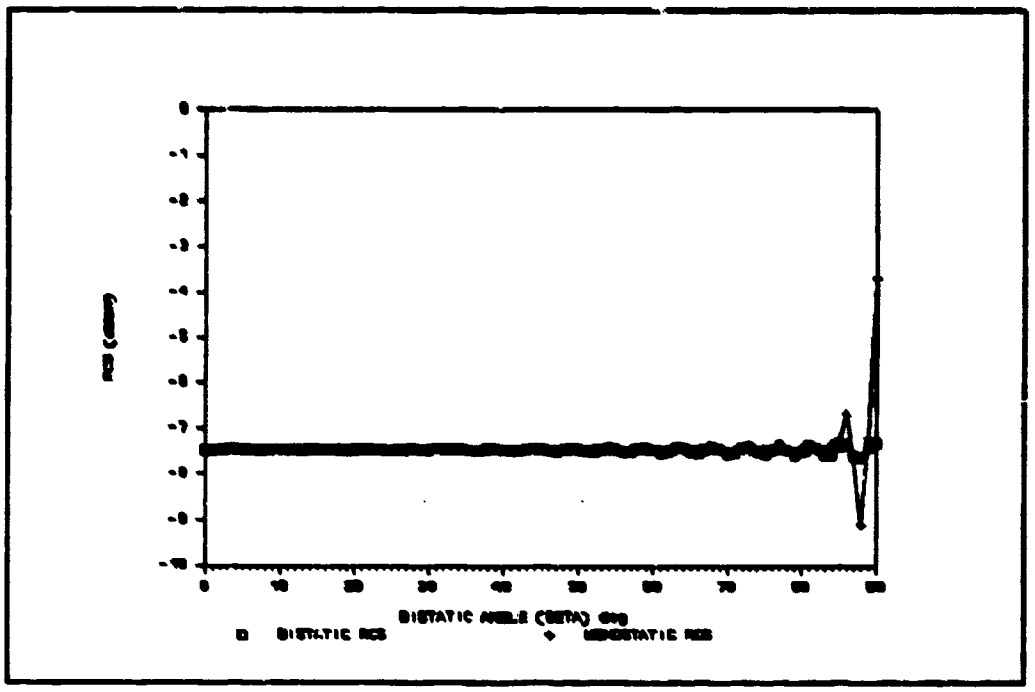

Figure 25. Sphere (ka=50; Vertical Polarisation): Bistatic RCS and Equivalent Monostatic RCS

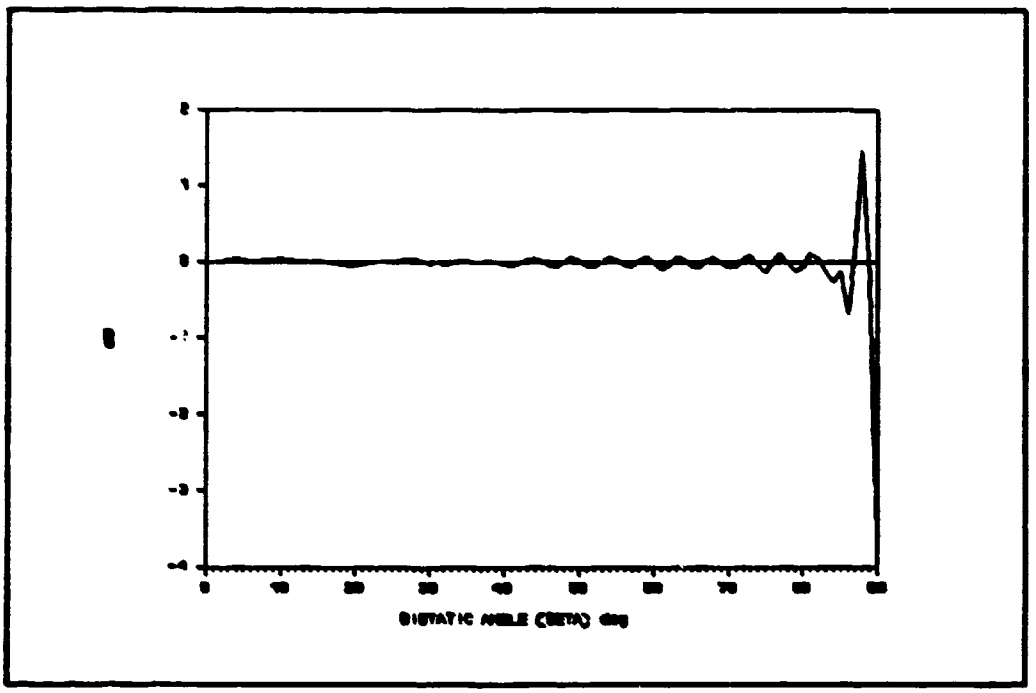

Figure 26. Sphere (ka=50; Vertical Polarisation): Difference in RCS (Bistatic - Monostatic)

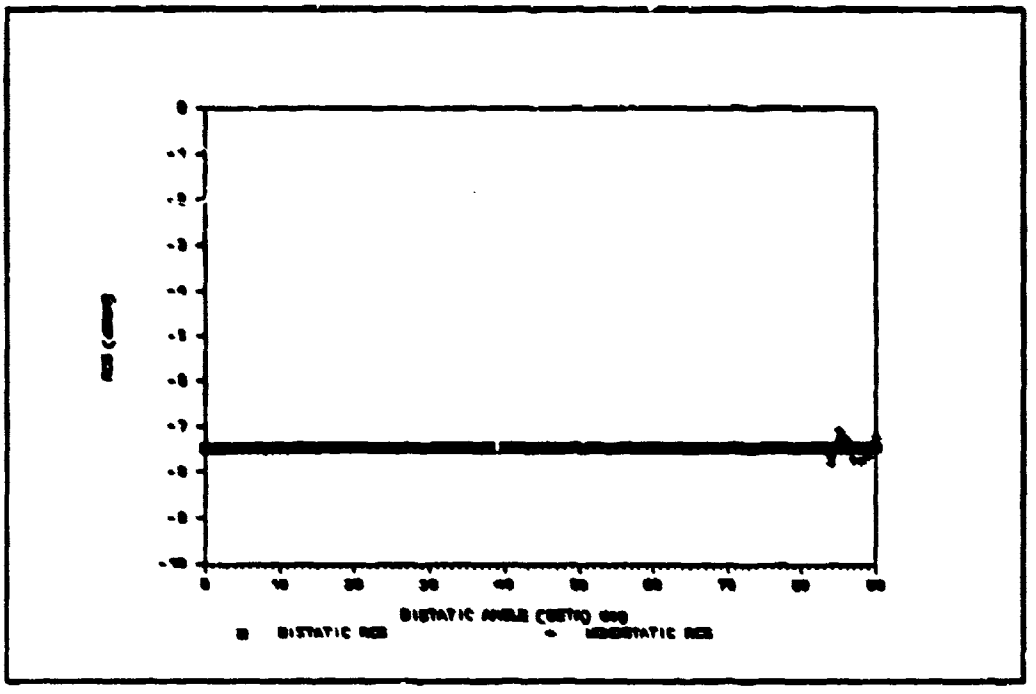

Figure 27. Sphere (ka=50; Horizontal Polarisation): Bistatic RCS and Equivalent Monostatic RCS

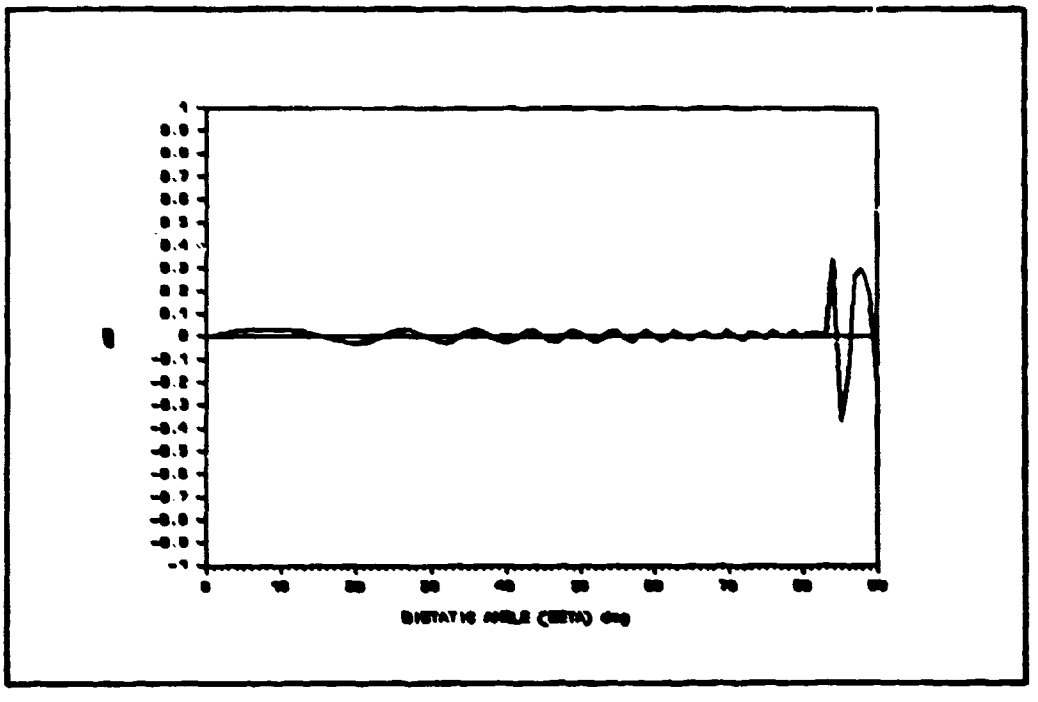

Figure 28. Sphere (ka=50; Horizontal Polarisation): Difference in RCS (Bistatic - Monostatic)

Flat Plate

Approach. Using the geometry given in Figure 29, the bistatic RCS for a perfectly conducting square flat plate is expressed as

$$\sigma = 4\pi \left[\frac{a^2}{\lambda} \cos(\theta+\beta) \frac{\sin[(ka/2)(\sin\theta + \sin(\theta+\beta))]}{(ka/2)(\sin\theta + \sin(\theta+\beta))}\right]^2 \quad (28)$$

where

θ = angle of incidence

β = bistatic angle

a = length of side

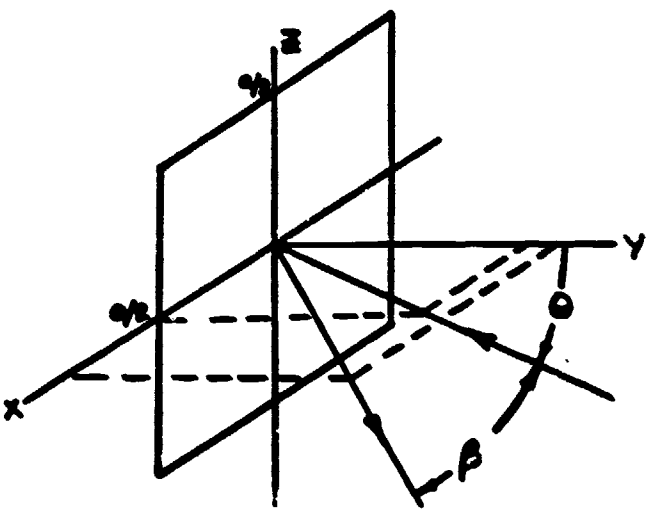

Figure 29. Bistatic Scattering Geometry for a Square Flat Plate

The equivalent monostatic cross section uses a different geometry, shown in Figure 30, because Kell's method requires the monostatic aspect angle bisect the bistatic angle. This changes eq. (28) to

$$\sigma = 4\pi \left[\frac{a^2}{\lambda} \cos(\Theta+(\beta/2)) \frac{\sin[ka\sin(\Theta+(\beta/2))]}{ka\sin(\Theta+(\beta/2))}\right]^2 \qquad (29)$$

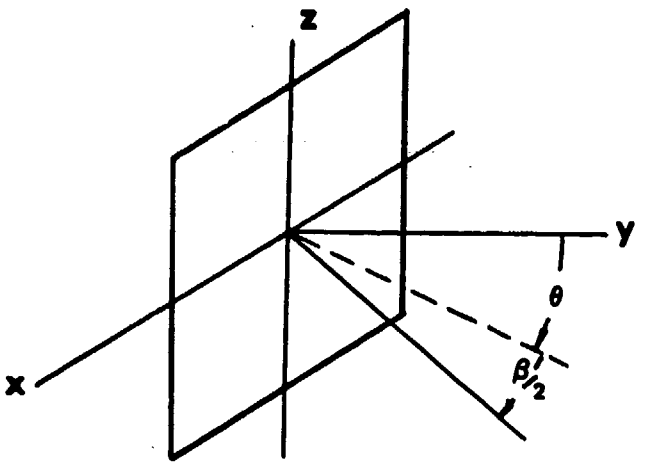

Figure 30. Equivalent Monostatic Scattering Geometry for a Square Flat Plate

The derivation of eqs.(28) and (29) can be found in appendix C. These are physical optics approximations. Using physical optics to compute the RCS of a flat plate limits the size of the angle of incidence that can be accurately modeled to about 40° from broadside (Knott, 1985:174). This is because physical optics does not account for edge effects (Skinner and Jost, 1988:8).

Only one polarization is used, $\bar{E}$ field in the x-z plane. Because edge effects are not considered and the plate is square as opposed to rectangular, Kell's method can be adequately described with one polarization.

Flat plate results. It can be seen in Figures 31 through 42 that Kell's method degrades as the angle of incidence moves away from broadside. Figure 31, broadside incidence, shows Kell's method holds beyond 20° of bistatic angle. When the angle of incidence is between 8° and 24° from broadside, Figures 33, 35, and 37, the lobe maximums are in close agreement to about 16° of bistatic angle. The nulls, however, are significantly different. The large differences in nulls cause the oscillation between 0° and 20° of bistatic angle in the plots showing the difference between bistatic and equivalent monostatic RCS, Figures 34, 36, and 38.

The agreement between bistatic and equivalent monostatic RCS breaks down before 10° of bistatic angle as the angle of incidence from broadside becomes large. From Figures 39 and 41, significant differences begin to occur at the first null as was seen at smaller angles of incidence; the second lobes, however, do not agree.

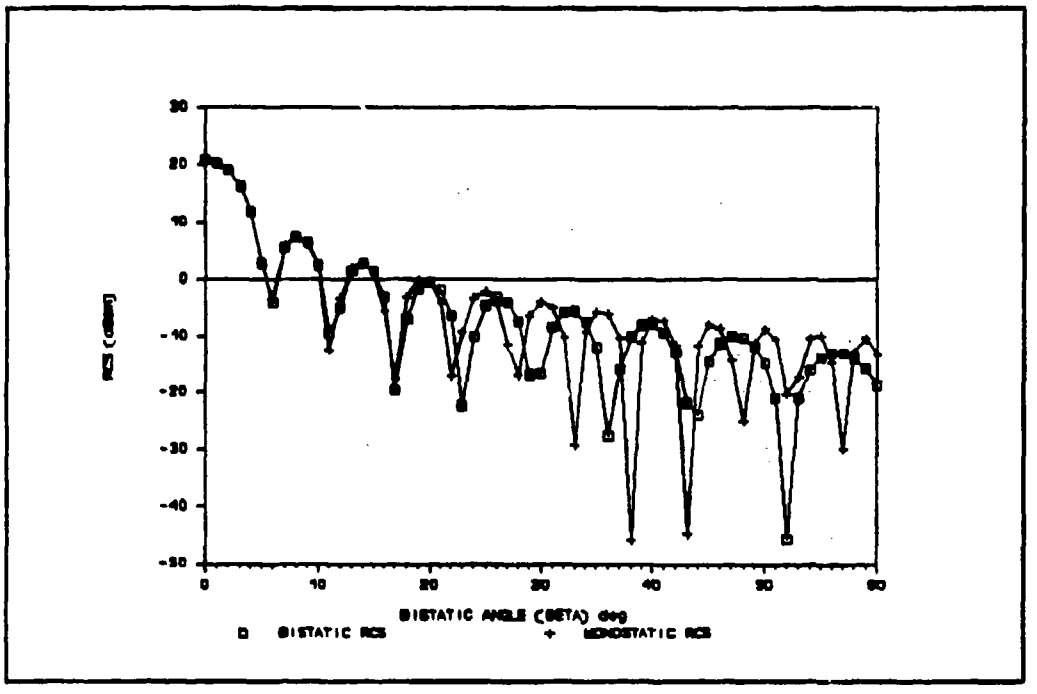

Figure 31. Square Flat Plate (Θ = 0°): Bistatic RCS and Equivalent Monostatic RCS

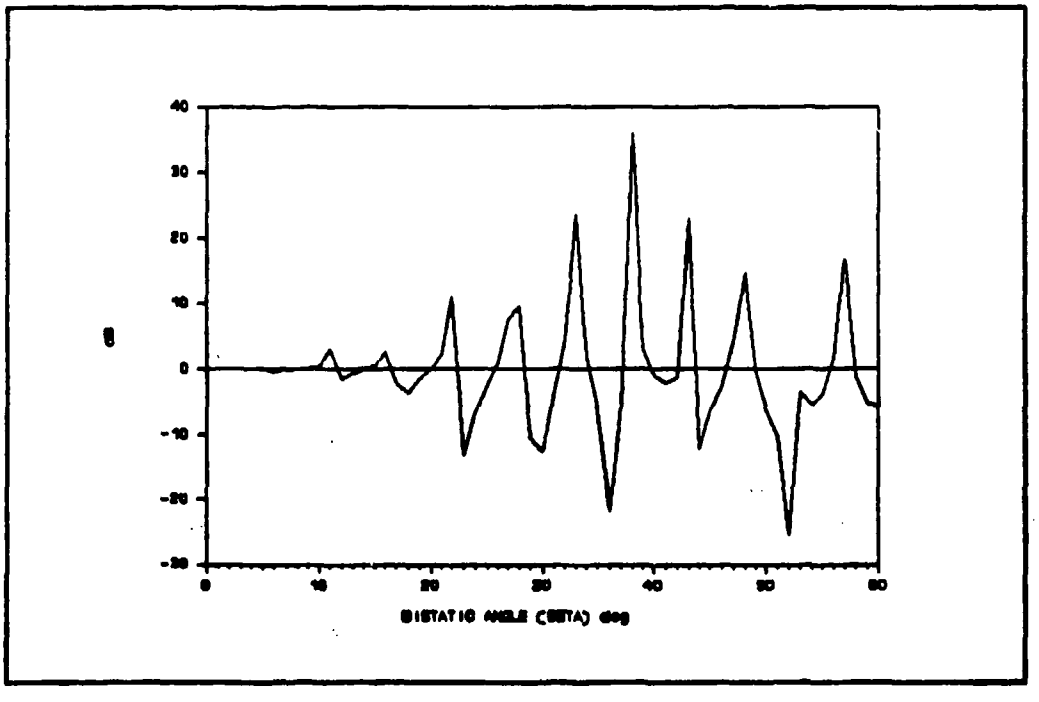

Figure 32. Square Flat Plate (Θ = 0°) Difference in RCS (Bistatic - Monostatic)

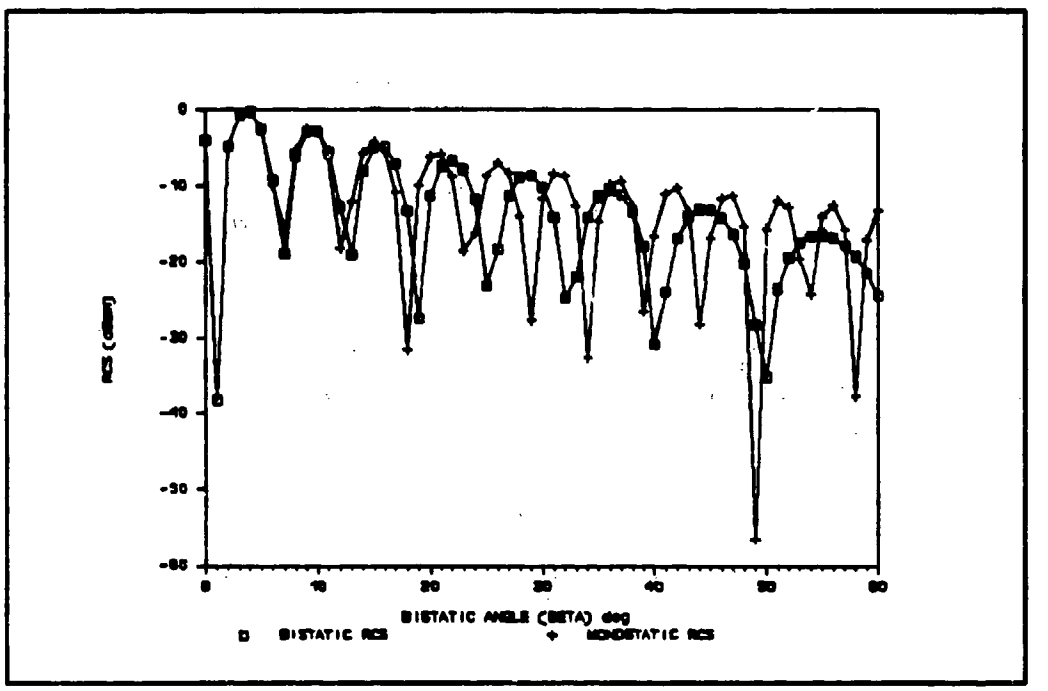

Figure 33. Square Flat plate (Θ = 8°): Bistatic RCS and Equivalent Monostatic RCS

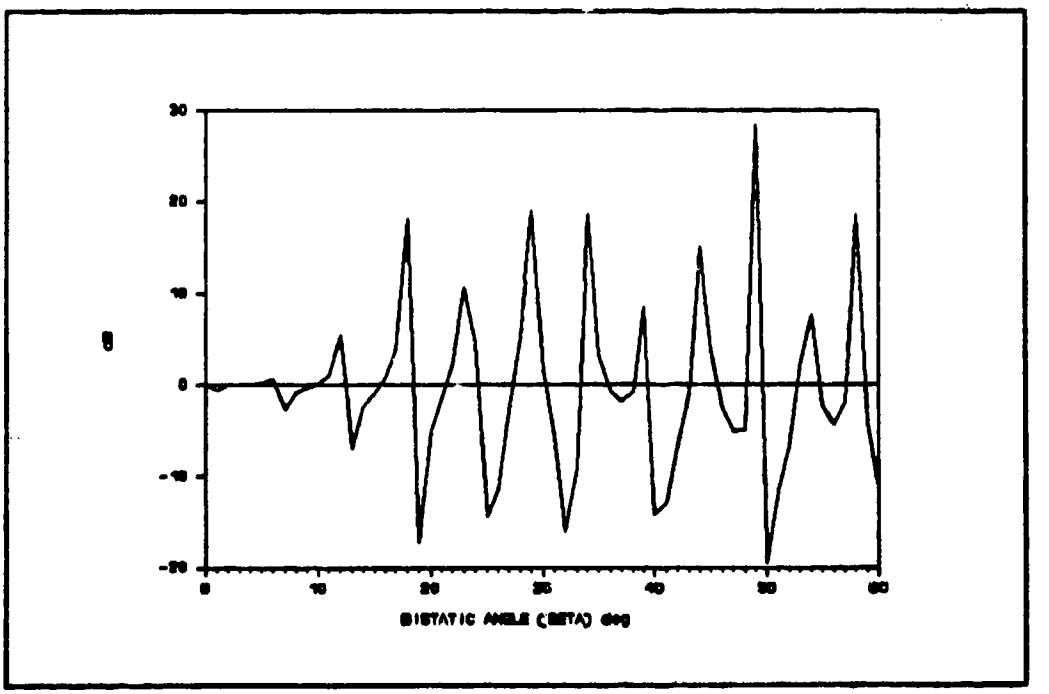

Figure 34. Square Flat Plate (Θ = 8°): Difference in RCS (Bistatic - Monostatic)

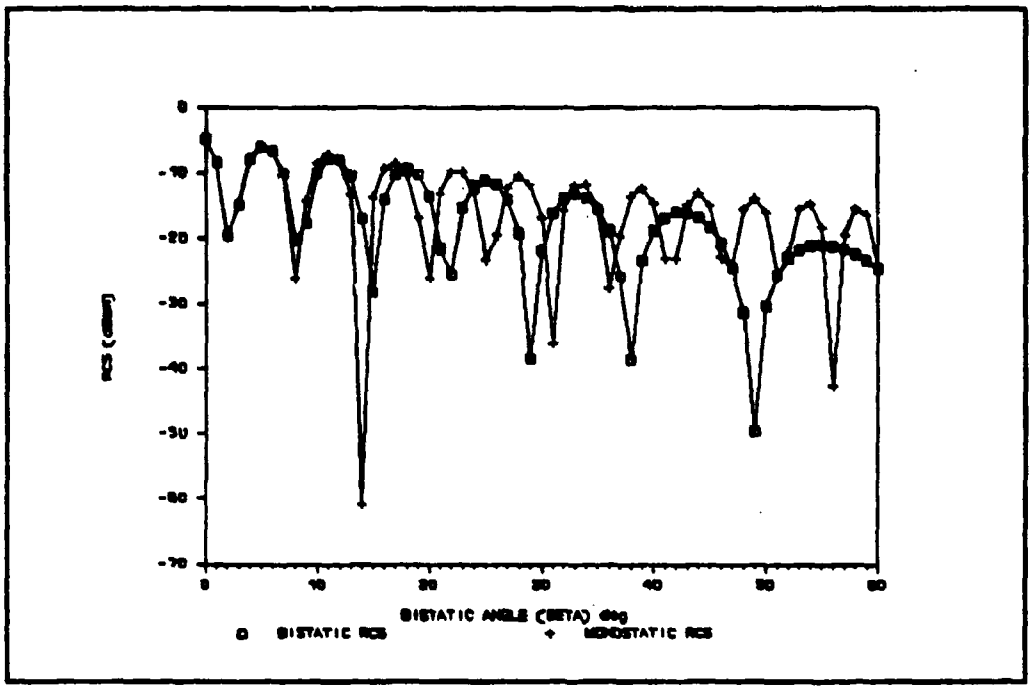

Figure 35. Square Flat Plate (Φ = 16°): Bistatic RCS and Equivalent Monostatic RCS

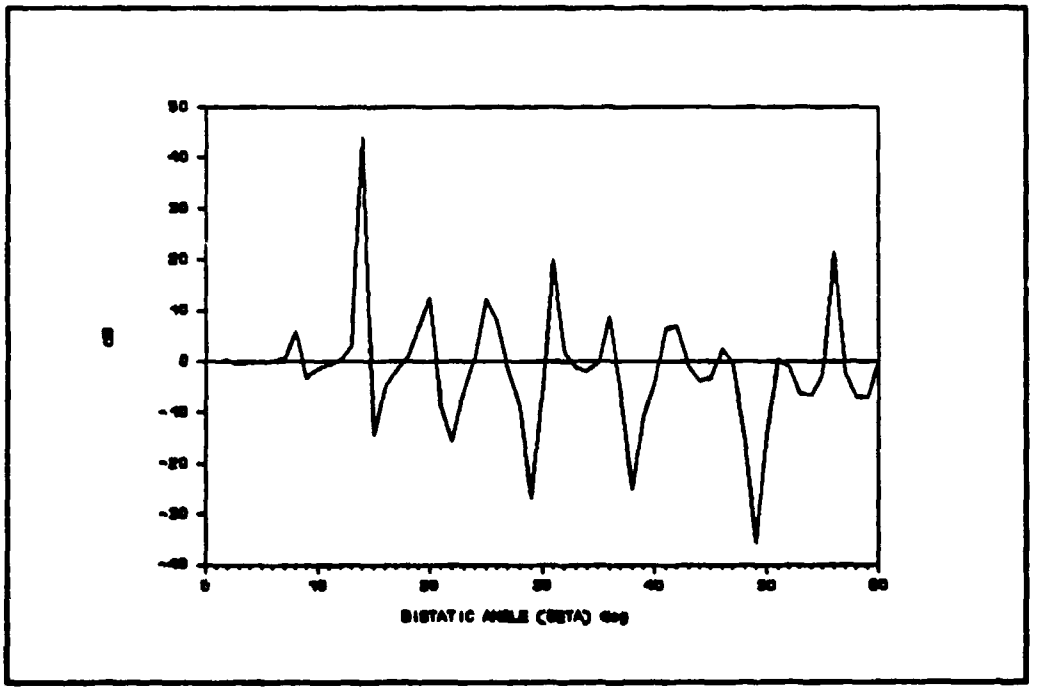

Figure 36. Square Flat Plate (Φ = 16°): Difference in RCS (Bistatic - Monostatic)

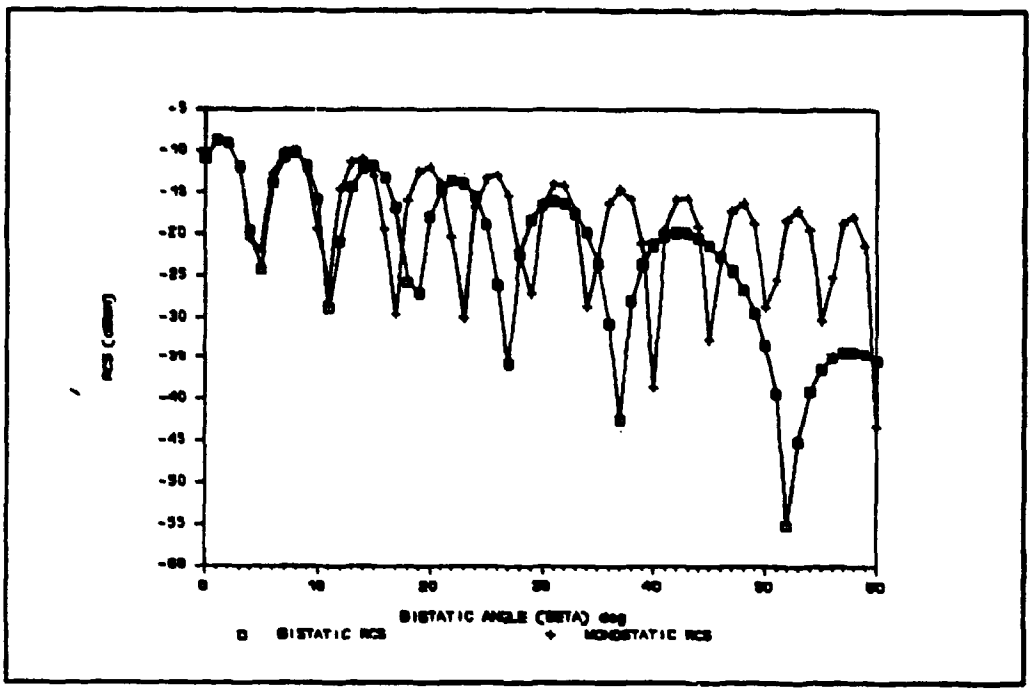

Figure 37. Square Flat Plate (Θ = 24°): Bistatic RCS and Equivalent Monostatic RCS

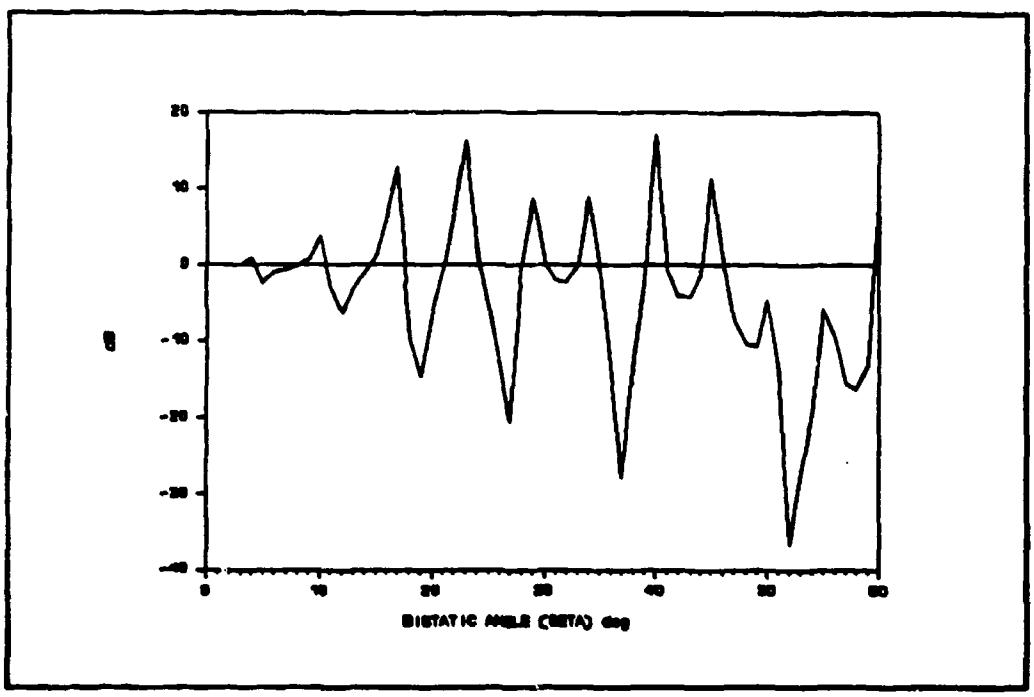

Figure 38. Square Flat Plate (Θ = 24°): Difference in RCS (Bistatic - Monostatic)

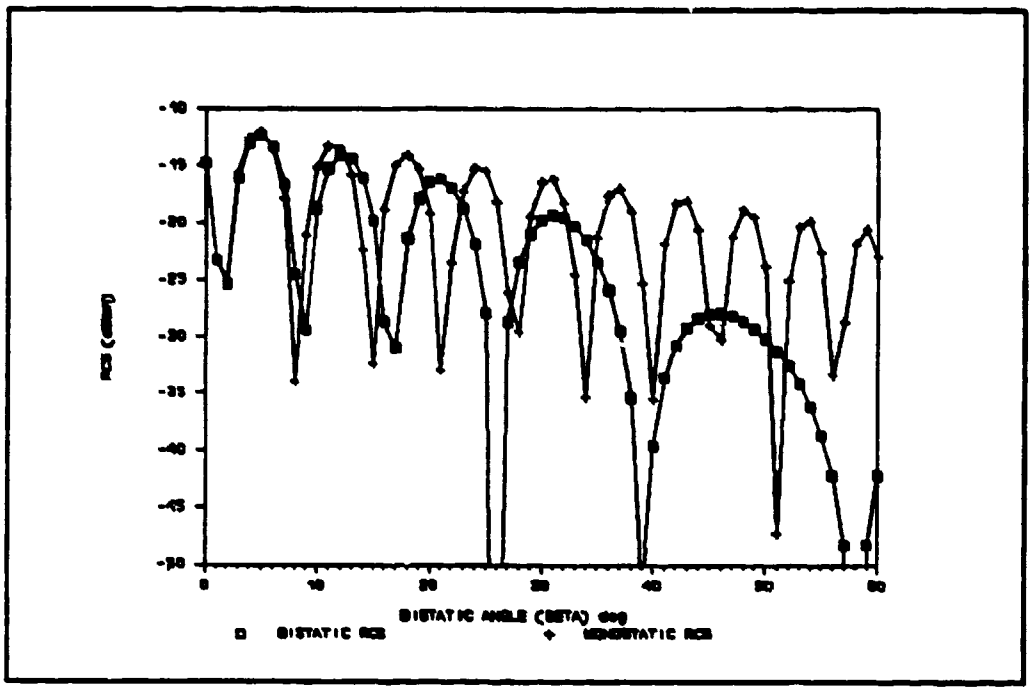

Figure 39. Square Flat Plate (Φ = 32°): Bistatic RCS and Equivalent Monostatic RCS

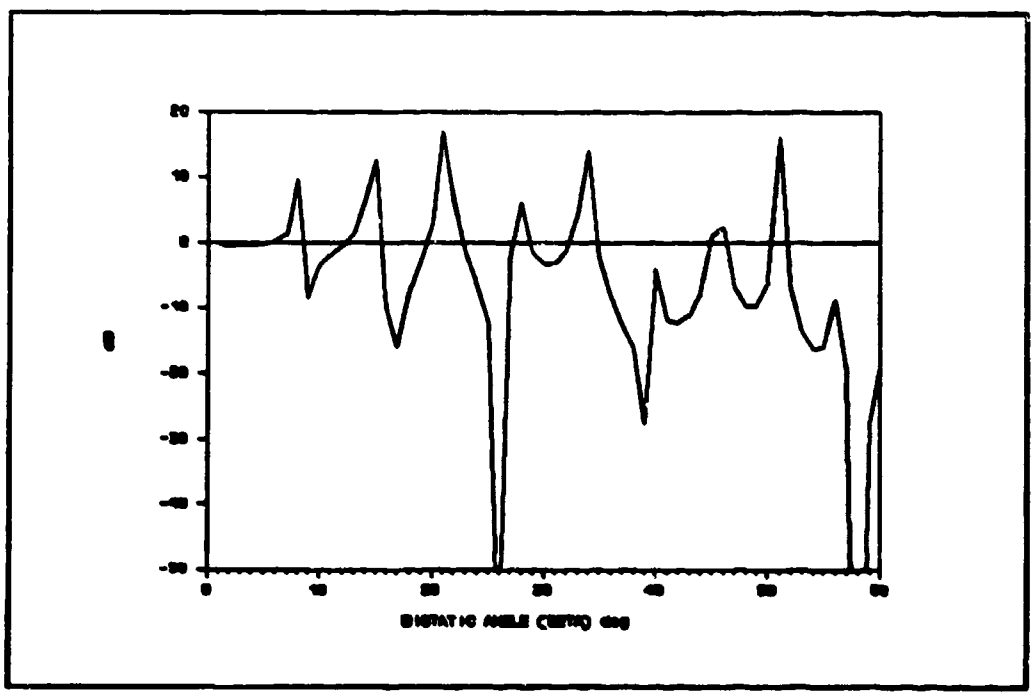

Figure 40. Square Flat Plate (Φ = 32°): Difference in RCS (Bistatic - Monostatic)

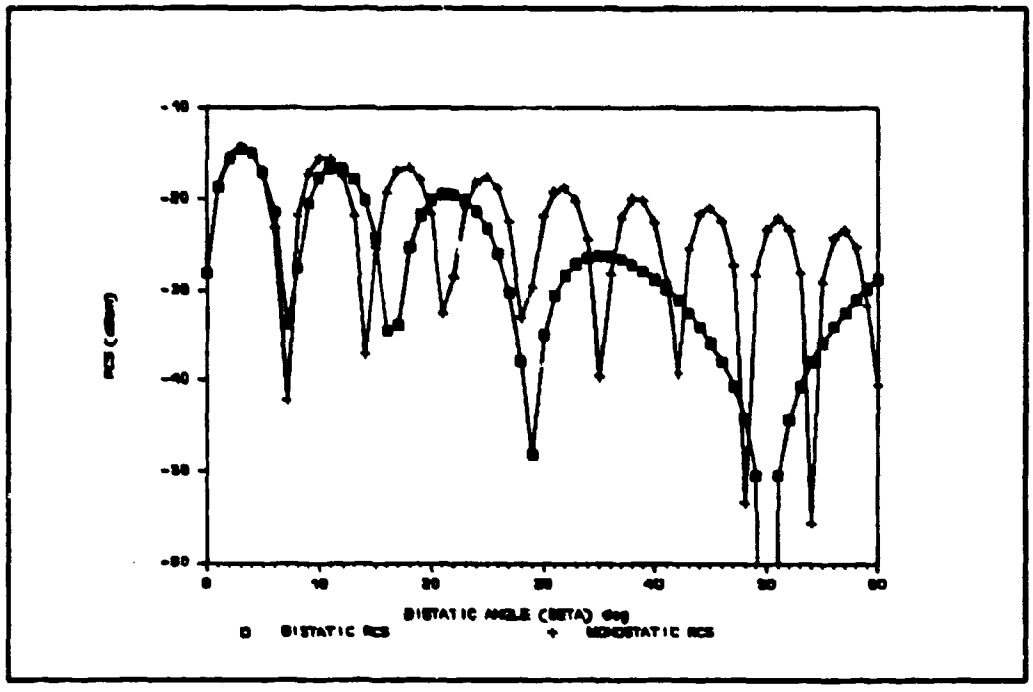

Figure 41. Square Flat Plate (θ = 40°): Bistatic RCS and Equivalent Monostatic RCS

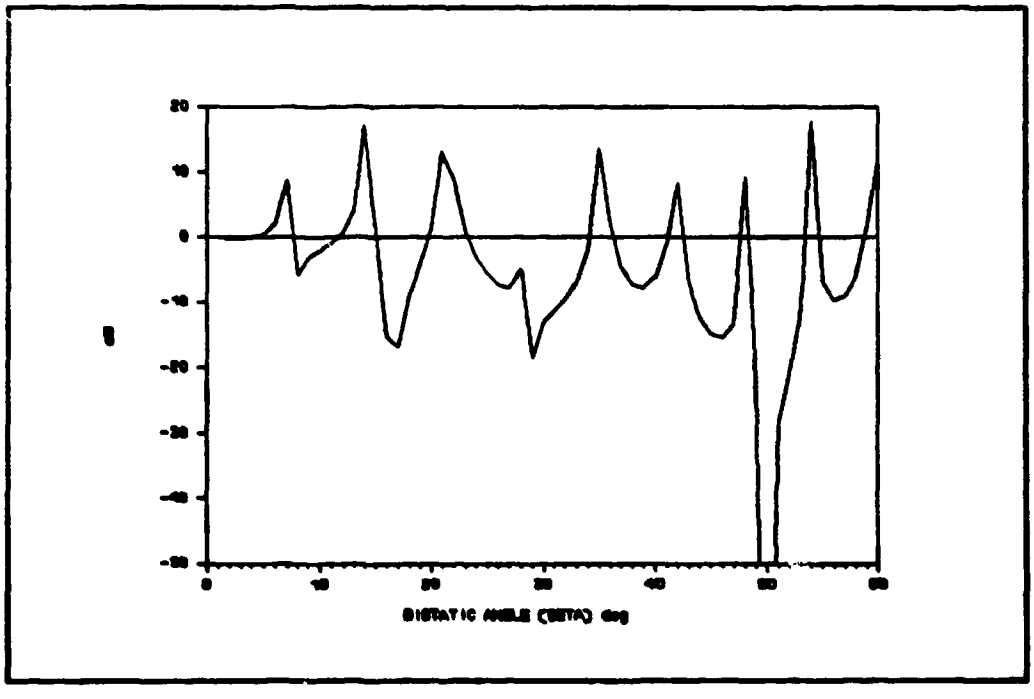

Figure 42. Square Flat Plate (θ = 40°): Difference in RCS (Bistatic - Monostatic)

Cylinder

Approach. The RCS of a perfectly conducting right circular cylinder is dominated by diffraction at most aspect angles. For this reason, the geometrical theory of diffraction (GTD) is used to calculate its cross section (Anderson, 1965:3-21). According to GTD, the illuminated edges of the cylinder shown in Figure 43 as S_1, S_2, and S_3 are the major contributors to the cylinder's RCS (Anderson, 1965:3-21).

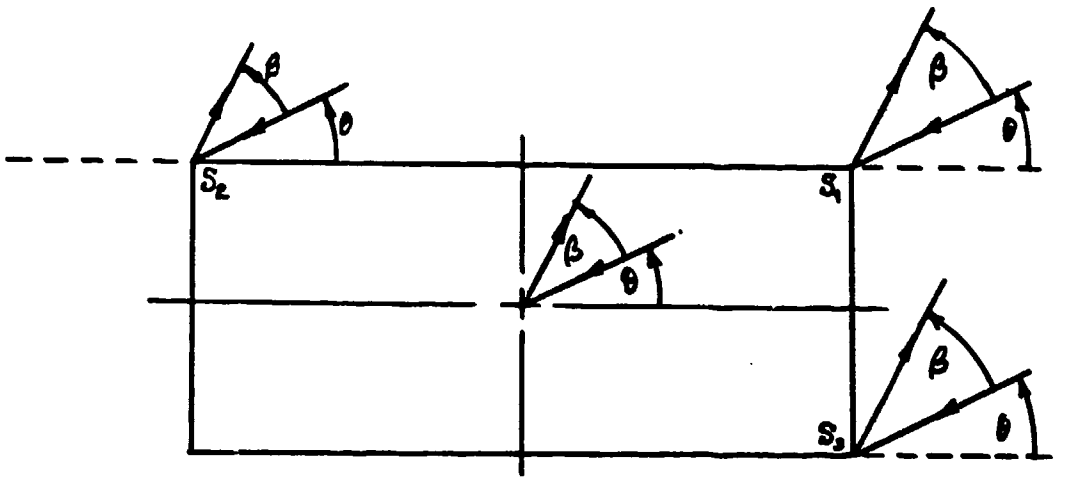

Figure 43. Cylinder Geometry

The directions of incidence and reflection are constrained to lie in the x-y plane. The electrical polarization is vertical when in the z direction and horizontal when in the x-y plane (Anderson, 1965:3-21).

The RCS of a perfectly conducting right circular cylinder is expressed in eq. (30) (Anderson, 1965:3-22).

$$\sigma = 4\pi \left| P_1 e^{j\rho_1} + P_2 e^{j\rho_2} + P_3 e^{j\rho_3} \right|^2 \qquad (30)$$

where

$$P_1 e^{j\rho_1} = \mp\frac{2}{3} \frac{e^{i\pi/4} \mathrm{Sin}(2\pi/3)}{(2\pi k)^{1/2}} \left[\frac{a}{\mathrm{Sin}\theta + \mathrm{Sin}(\theta+\beta)}\right]^{1/2}$$

$$\times \exp\{-i2k[a(\mathrm{Sin}\theta + \mathrm{Sin}(\theta+\beta)) + h(\mathrm{Cos}\theta + \mathrm{Cos}(\theta+\beta))]\}$$

$$\times \{[\mathrm{Cos}(2\pi/3) - \mathrm{Cos}(2\beta/3)]^{-1} \mp [\mathrm{Cos}(2\pi/3) - \mathrm{Cos}(2(\pi+2\theta+\beta)/3)]^{-1}\} \qquad (31a)$$

$$P_2 e^{j\rho_2} = \mp\frac{2}{3} \frac{e^{i\pi/4} \mathrm{Sin}(2\pi/3)}{(2\pi k)^{1/2}} \left[\frac{a}{\mathrm{Sin}\theta + \mathrm{Sin}(\theta+\beta)}\right]^{1/2}$$

$$\times \exp\{-i2k[a(\mathrm{Sin}\theta + \mathrm{Sin}(\theta+\beta)) - h(\mathrm{Cos}\theta + \mathrm{Cos}(\theta+\beta))]\}$$

$$\times \{[\mathrm{Cos}(2\pi/3) - \mathrm{Cos}(2\beta/3)]^{-1} \mp [\mathrm{Cos}(2\pi/3) - \mathrm{Cos}(2(2\theta+\beta)/3)]^{-1}\} \qquad (31b)$$

$$P_3 e^{j\rho_3} = \mp\frac{2}{3} \frac{e^{-i\pi/4} \mathrm{Sin}(2\pi/3)}{(2\pi k)^{1/2}} \left[\frac{a}{\mathrm{Sin}\theta + \mathrm{Sin}(\theta+\beta)}\right]^{1/2}$$

$$\times \exp\{i2k[a(\mathrm{Sin}\theta + \mathrm{Sin}(\theta+\beta)) - h(\mathrm{Cos}\theta + \mathrm{Cos}(\theta+\beta))]\}$$

$$\times \{[\mathrm{Cos}(2\pi/3) - \mathrm{Cos}(2\beta/3)]^{-1} \mp [\mathrm{Cos}(2\pi/3) - \mathrm{Cos}(2(\pi-2\theta-\beta)/3)]^{-1}\} \qquad (31c)$$

θ = angle of incidence in degrees from end-on

β = bistatic angle

h = half the cylinder's length

a = cylinder's radius

k = $2\pi/\lambda$ (wave number)

Analytic singularities occur at $\Theta = 0°$ and $\Theta = 90°$ in eqs. (31a)-(31c). Therefore, at $\Theta = 0°$, the RCS is computed using eq. (32) (Anderson, 1965:3-24).

$$\sigma = \pi[ka^2\mathrm{Cos}(\beta/2)]^2 \qquad (32)$$

At $\Theta = 90°$, because only edges S_1 and S_2 are illuminated, eq. (30) reduces to (Anderson, 1965:3-24)

$$\sigma = 4kah^2\mathrm{Cos}(\beta/2) \qquad (33)$$

The derivations of eqs. (31a,c,b), (32),and (33) are given in appendix D. Computer data generated from eqs. (31)-(33) Was compared to measured data for the monostatic and bistatic case ($\beta = 10°$). The predicted monstatic case was within 3-dB of the measured data between 4° and 86° of end-on while the predicted bistatic case was within 5-dB over the same range of aspect angles.

Cylinder results. It's obvious something is amiss when viewing Figures 44 and 45 in which the angle of incidence is end-on. The disparity arises from how the two cross sections are calculated. In the bistatic case, eq. (32) is used for all bistatic angles. The equivalent monostatic case calls for eq. (32) when the monostatic angle of incidence is equal to 0°, but when beta does not equal 0° it uses eq. 30. In doing this, the bistatic RCS is calculated

as if the target is a disc which allows the use of the physical optics approximation given by eq. (32). The equivalent monostatic RCS is calculated the same way when the angle of incidence is end-on, but once the equivalent monostatic angle of incidence is no longer exactly end-on the target becomes a cylinder and GTD approximations are applied. In short, scattering for the equivalent monostatic case is being modeled as either purely specular or purely diffraction. Neither of these conditions is likely at small angles from end-on. For this reason, no conclusions can be drawn regarding the accuracy of Kell's method when either the angle of incidence or bistatic bisector are end-on.

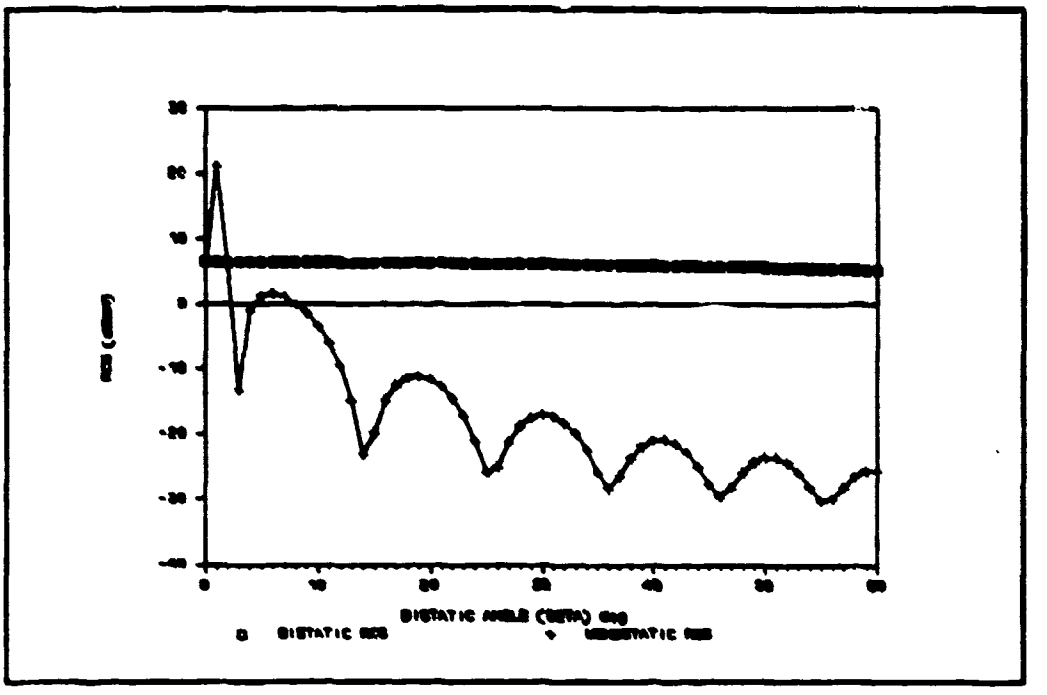

Figure 44. Cylinder (Φ = 0°;Vertical Polarization): Bistatic RCS and Equivalent Monostatic RCS

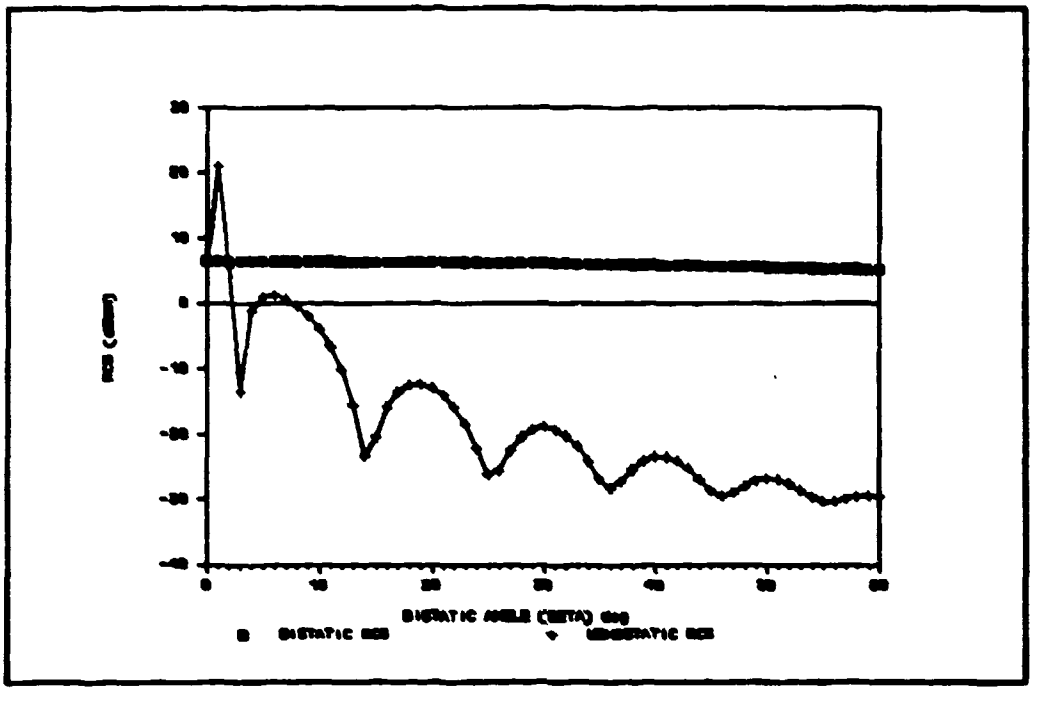

Figure 45. Cylinder (Φ = 0°; Horizontal Polarization): Difference in RCS (Bistatic - Monostatic)

It can be seen in Figures 47-65 that Kell's method is polarization dependent. Vertically polarized cross sections are smooth curves while horizontal polarization produces rapid fluctuation with deep nulls. This results from the fact that the scattered fields from a right-circular cylinder are polarization dependent.This is demonstrated in Figure 46.

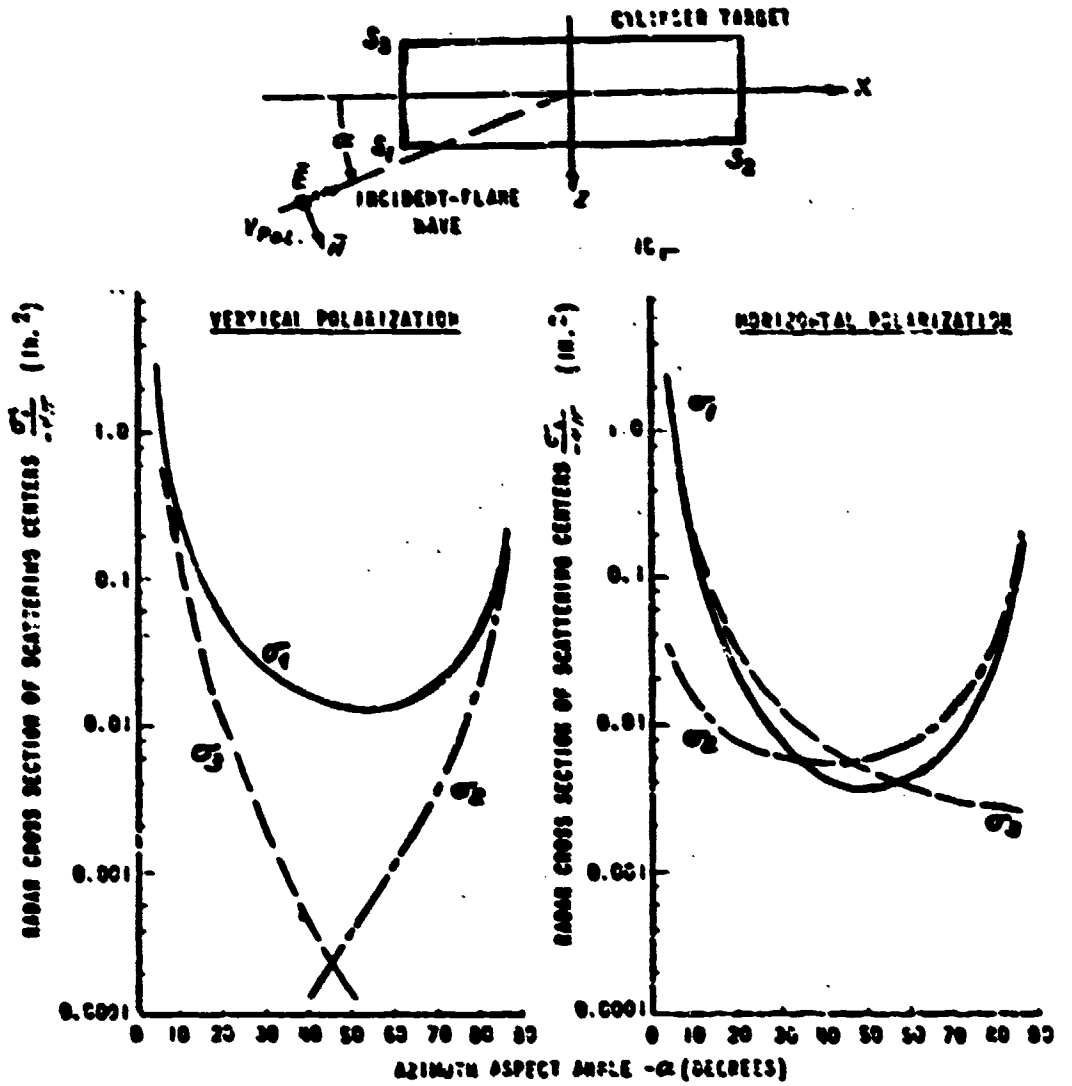

Figure 46. GTD Applied to Right-Circular Cylinder to Show Contributions from Illuminated Edges (Anderson, 1965:3-28)

The plots shown in Figure 46 depict the RCS magnitude of each of the major scattering centers with respect to aspect angle. The vertically polarized RCS is dominated by the return from S_1 except at end-on and broadside. Therefore, the fluctuations in the cylinder's vertically polarized RCS are governed by changes in phase from S_1 as the aspect angle changes. This results in relatively smooth curves which can be seen in Figures 47, 51, 55, 59, and 63.

When the polarization is in the horizontal direction, Figure 46 shows that the RCS is no longer dominated by one scattering center but is a combination of two or three scattering centers at all aspect angles. With each change in aspect angle there will be a change in the phase of the scattered fields from each scattering center. Combining the phases from each scattering center produces an overall phase that is sensitive to aspect angle changes. This results in rapid fluctuations in RCS which can be seen in Figures 49, 53, 57, 61, and 65. Because of the sensitivity to aspect angle, the equivalent monostatic case does not track the bistatic case well.

Kell's relationship holds up better for vertical polarization because the relative phase between the cylinder's scattering centers is less sensitive to changes in aspect angle than the horizontal case.

When the angle of incidence from end-on is 30°, Figures 49-52, the vertically polarized cross sections are in close agreement through 10° of bistatic angle as before. The lobes of the horizontally polarized cross sections have about a 1-2 dB difference to about 10° of bistatic angle, however, the nulls are significantly different at 5° bistatic angle.

Another observation can be made regarding Figures 47-65: as the angle of incidence approaches broadside the bistatic angle for which the bistatic and equivalent monostatic RCS agree becomes larger. This concurs with the data obtained for the square flat plate. For both vertical and horizontal polarizations near broadside, the contribution from scattering center S_3 is negligible while S_1 and S_2 have similar diffraction coefficients and phase. This results in low sensitivity to changes in aspect angle and good agreement between bistatic and equivalent monostatic RCS.

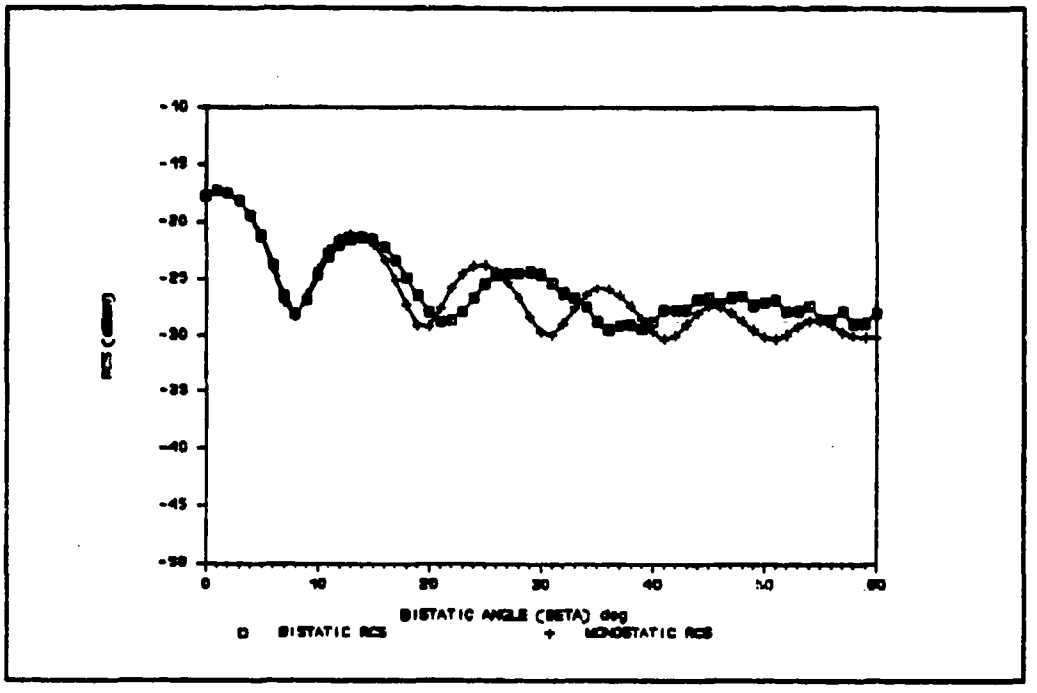

Figure 47. Cylinder (θ = 15°; Vertical Polarization): Bistatic RCS and Equivalent Monostatic RCS

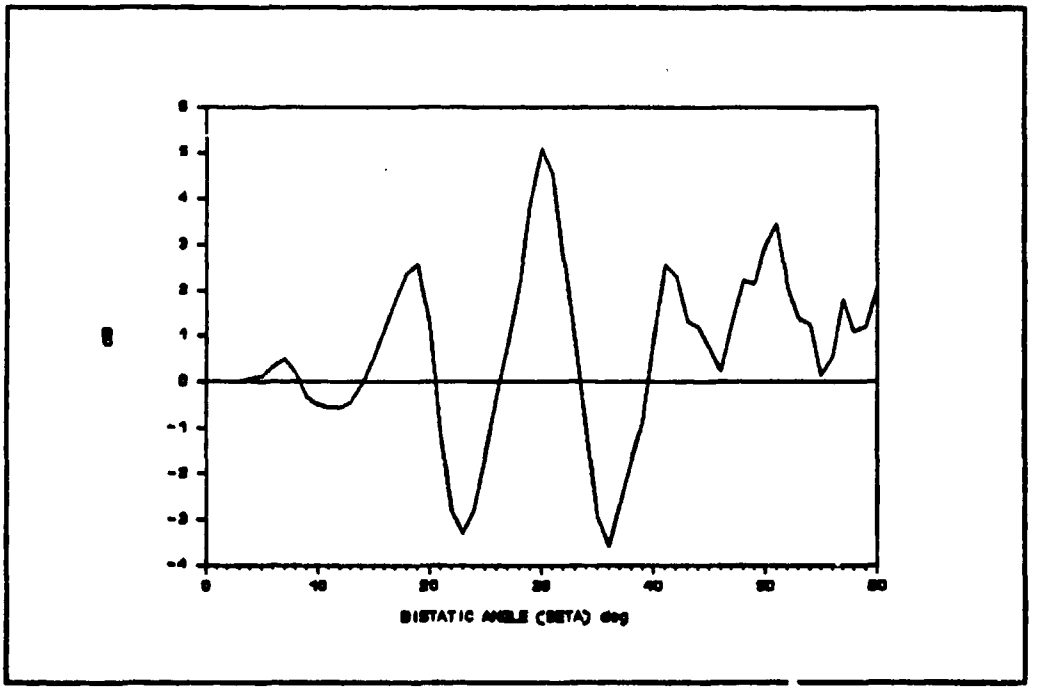

Figure 48. Cylinder (θ = 15°; Vertical Polarization): Difference in RCS (Bistatic - Monostatic)

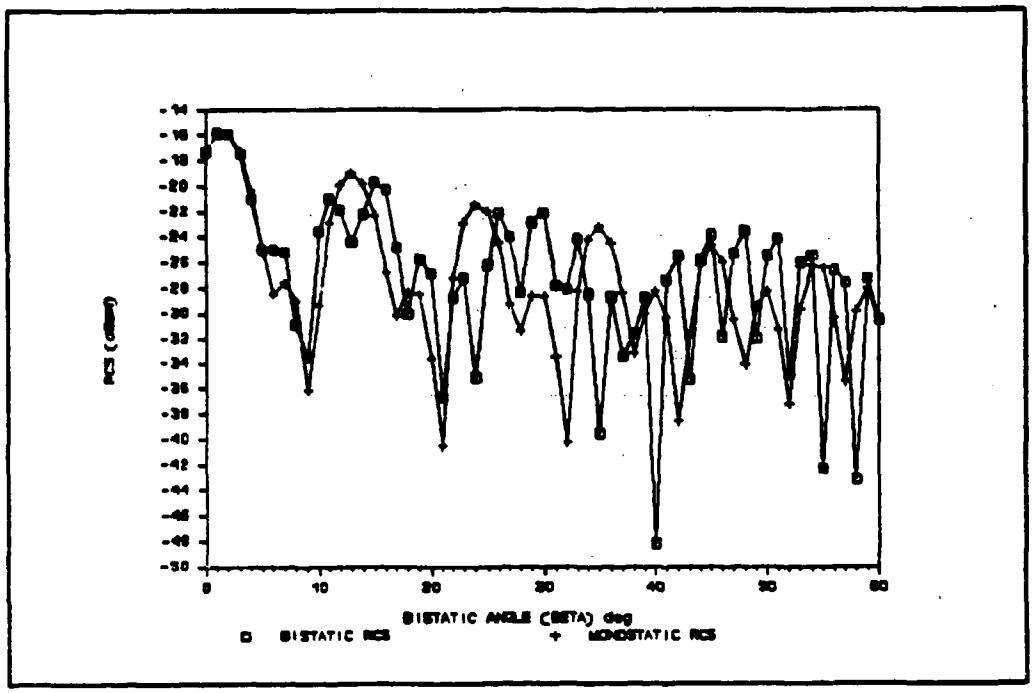

Figure 49. Cylinder (Θ=15°; Horizontal Polarization): Bistatic RCS and Equivalent Monostatic RCS

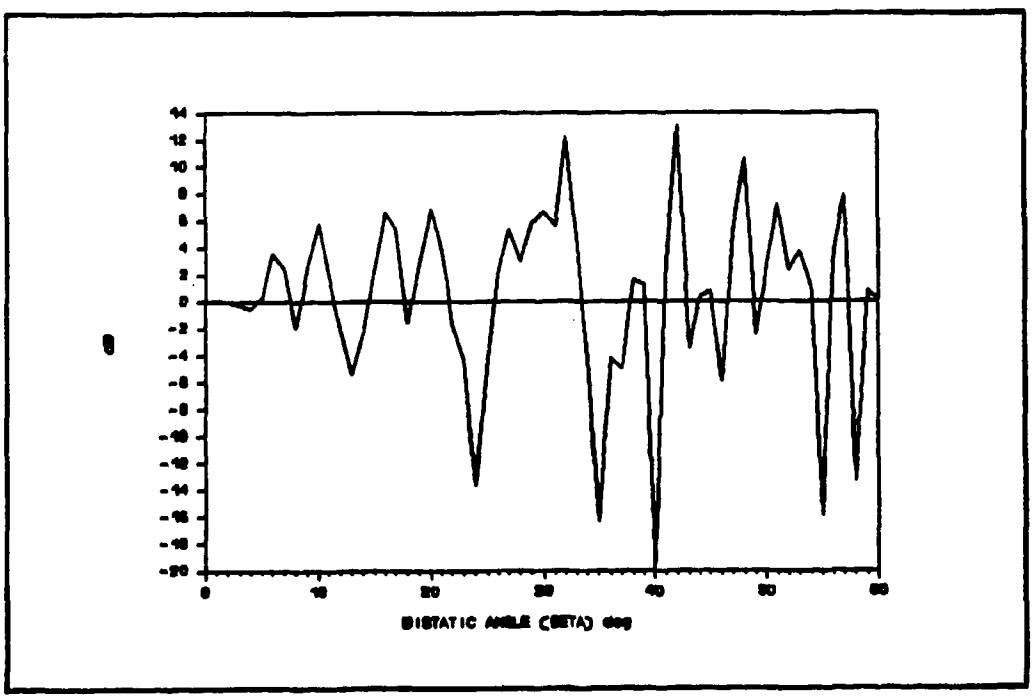

Figure 50. Cylinder (Θ=15°; Horizontal Polarization): Difference in RCS (Bistatic - Monostatic)

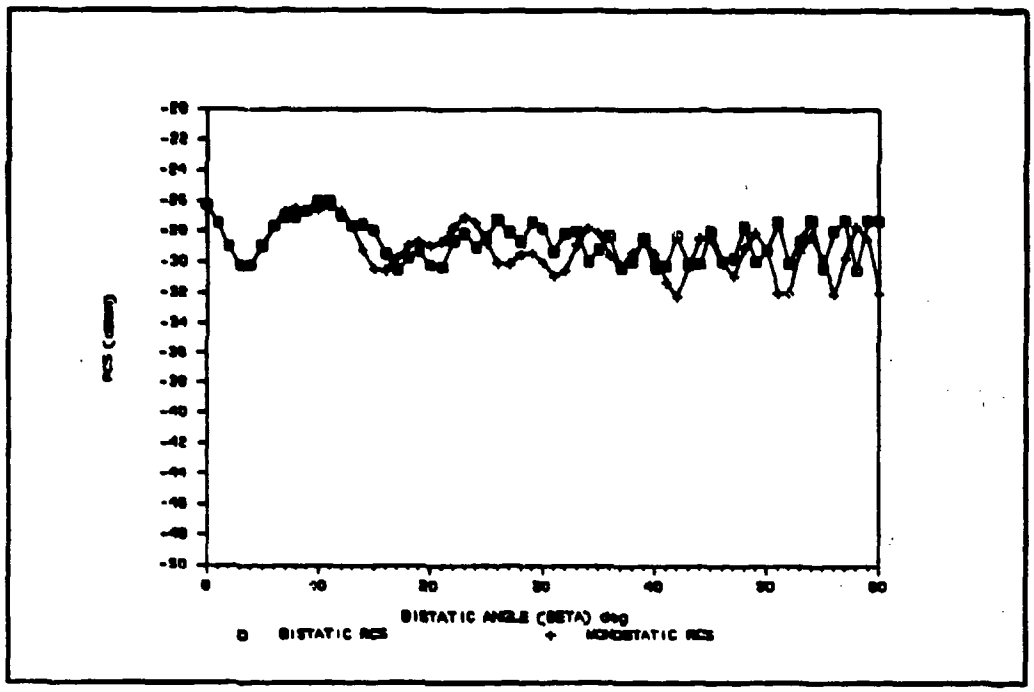

Figure 51. Cylinder (Φ = 30°; Vertical Polarization): Bistatic RCS and Equivalent Monostatic RCS

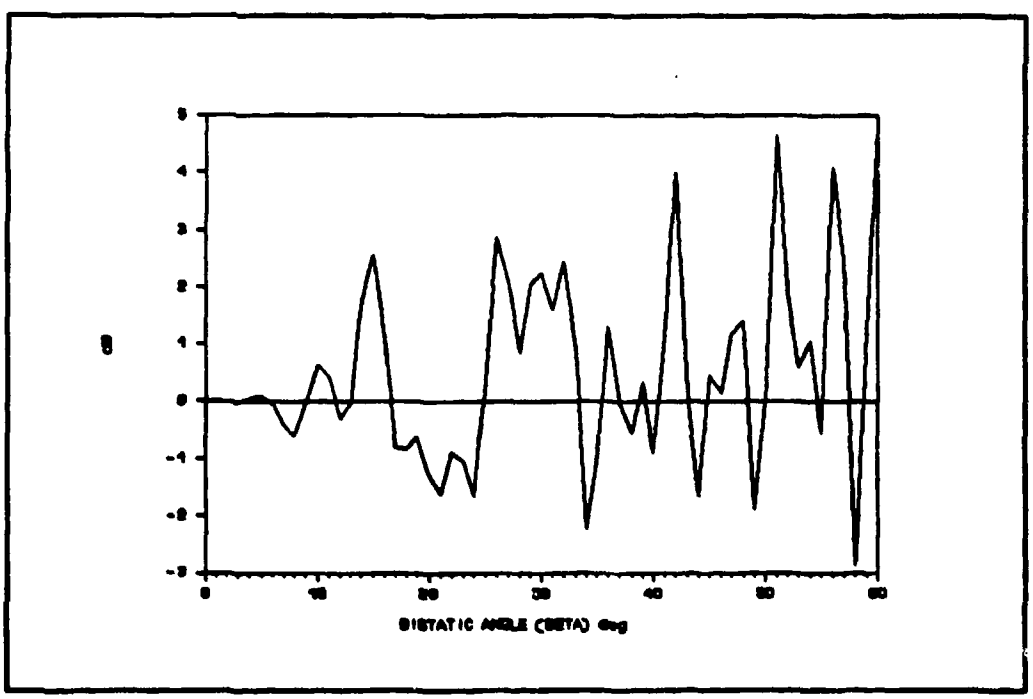

Figure 52. Cylinder (Φ = 30°; Vertical Polarization): Difference in RCS (Bistatic - Monostatic)

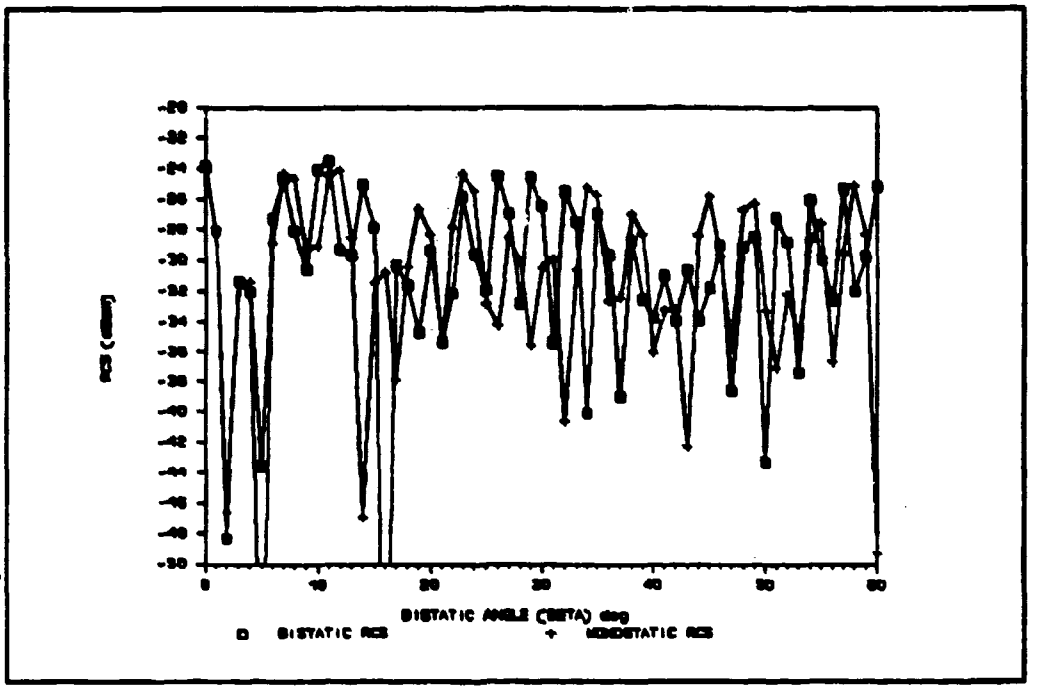

Figure 53. Cylinder (θ= 30°; Horizontal Polarization): Bistatic RCS and Equivalent Monostatic RCS

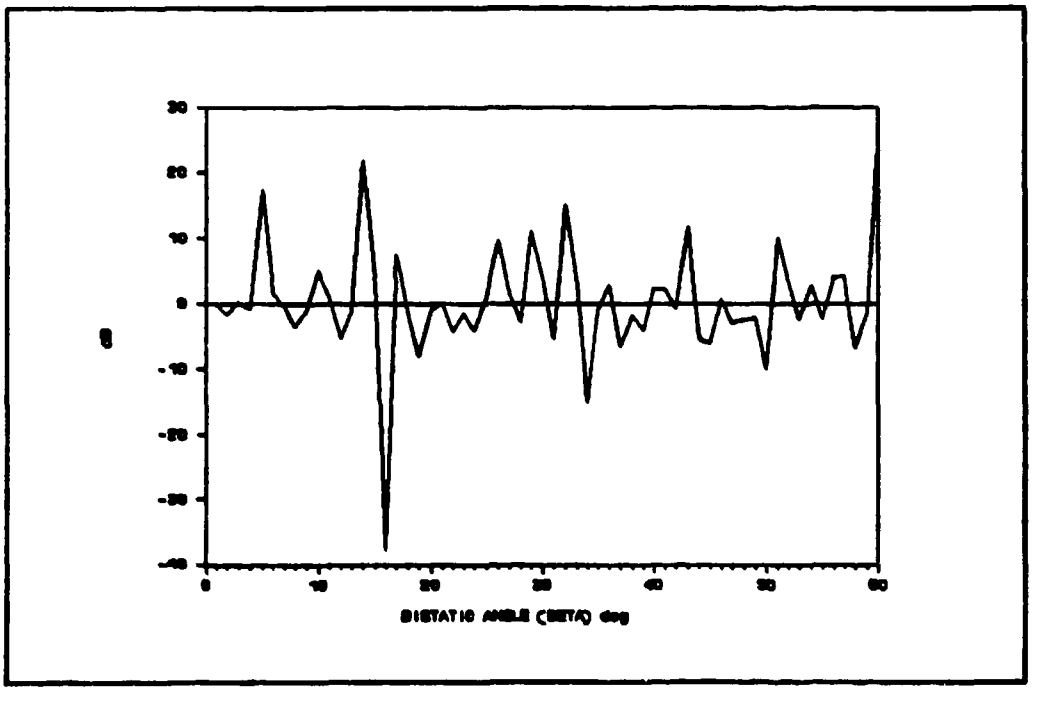

Figure 54. Cylinder (θ=30°; Horizontal Polarization): Difference in RCS (Bistatic - Monostatic)

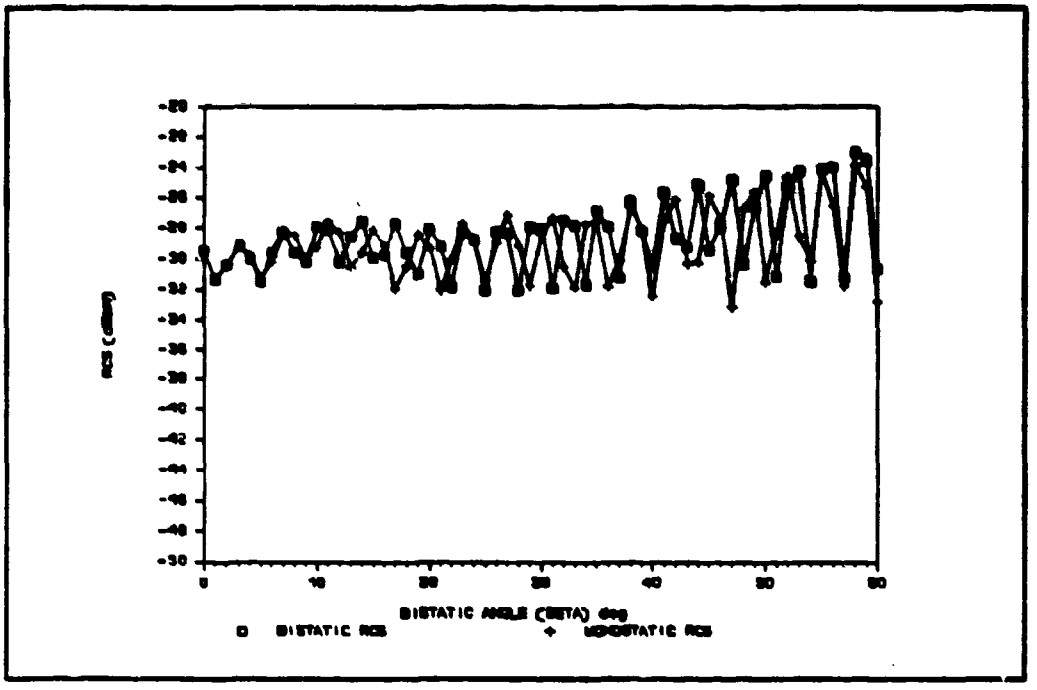

Figure 55. Cylinder (Φ = 45°; Vertical Polarization): Bistatic RCS and Equivalent Monostatic RCS

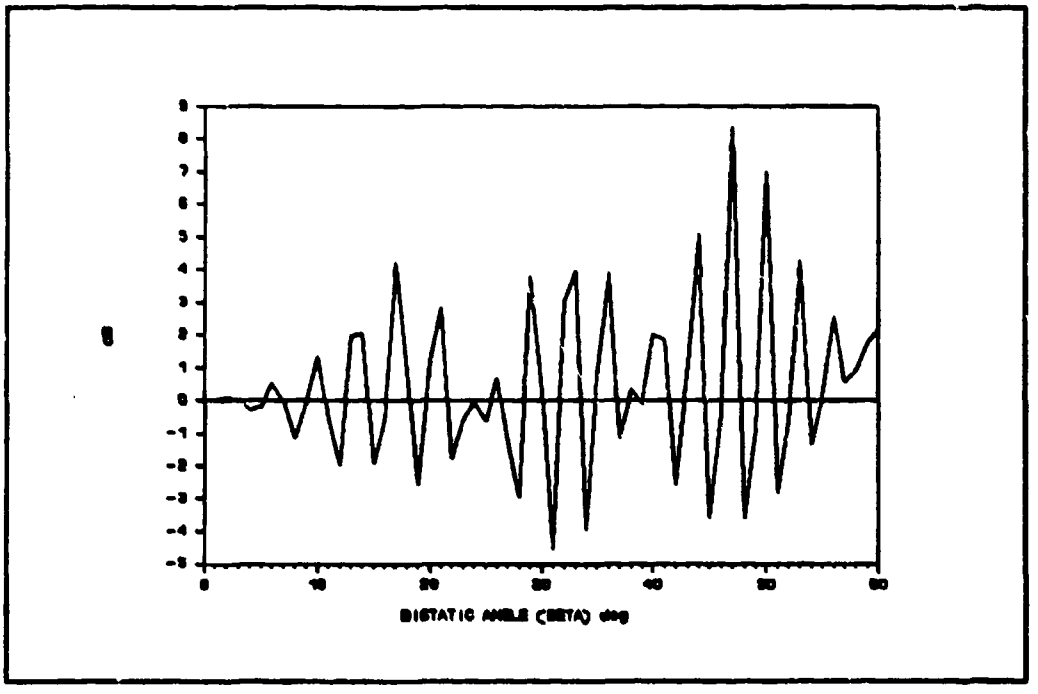

Figure 56. Cylinder (Φ = 45°; Vertical Polarization): Difference in RCS (Bistatic - Monostatic)

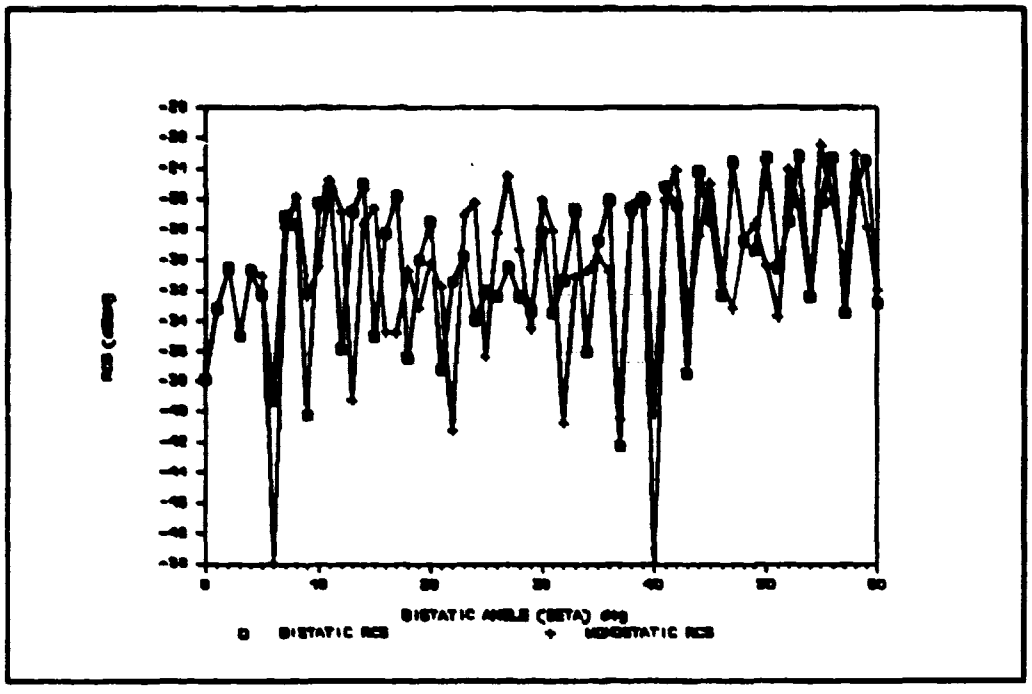

Figure 57. Cylinder (Θ=45°;Horizontal Polarization): Bistatic RCS and Equivalent Monostatic RCS

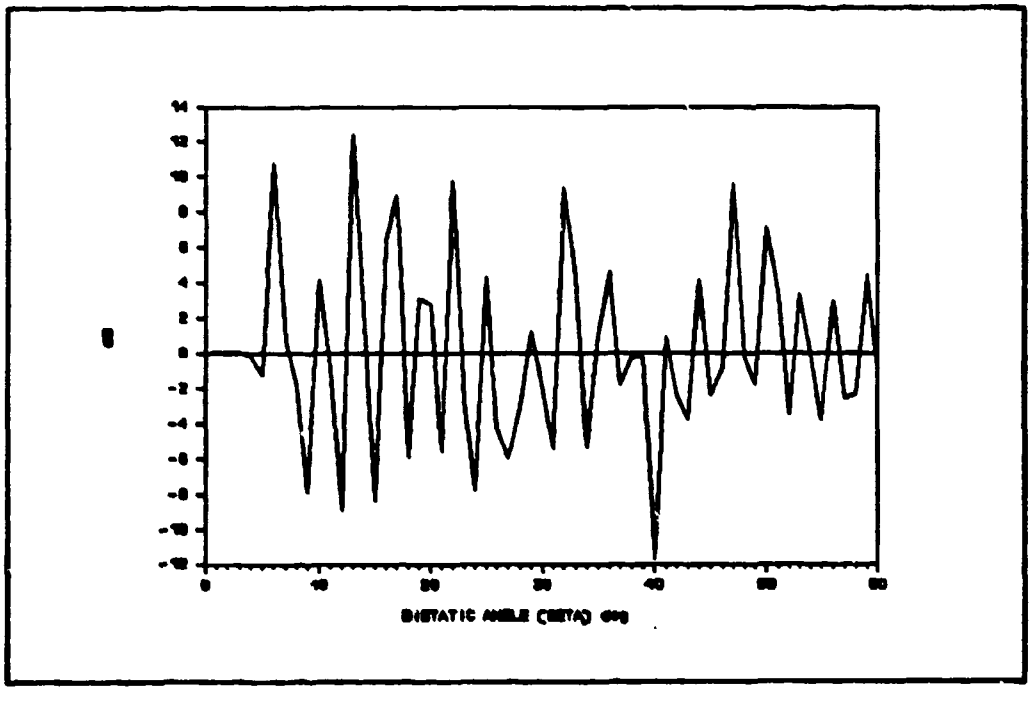

Figure 58. Cylinder (Θ=45°; Horizontal Polarization): Difference in RCS (Bistatic - Monostatic)

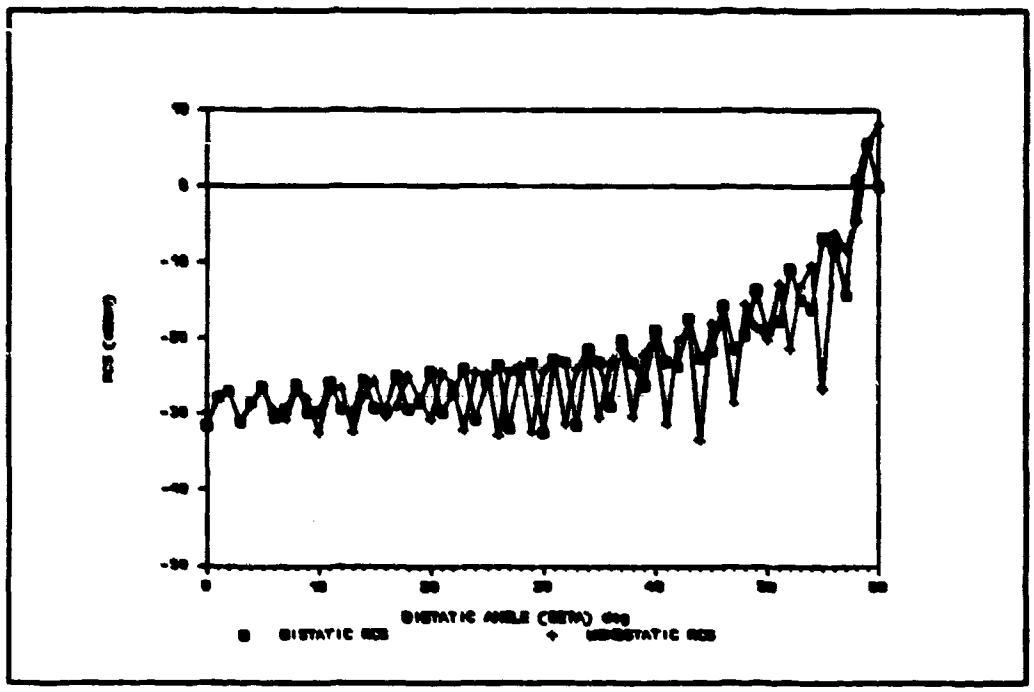

Figure 59. Cylinder (Θ = 60°; Vertical Polarization): Bistatic RCS and Equivalent Monostatic RCS

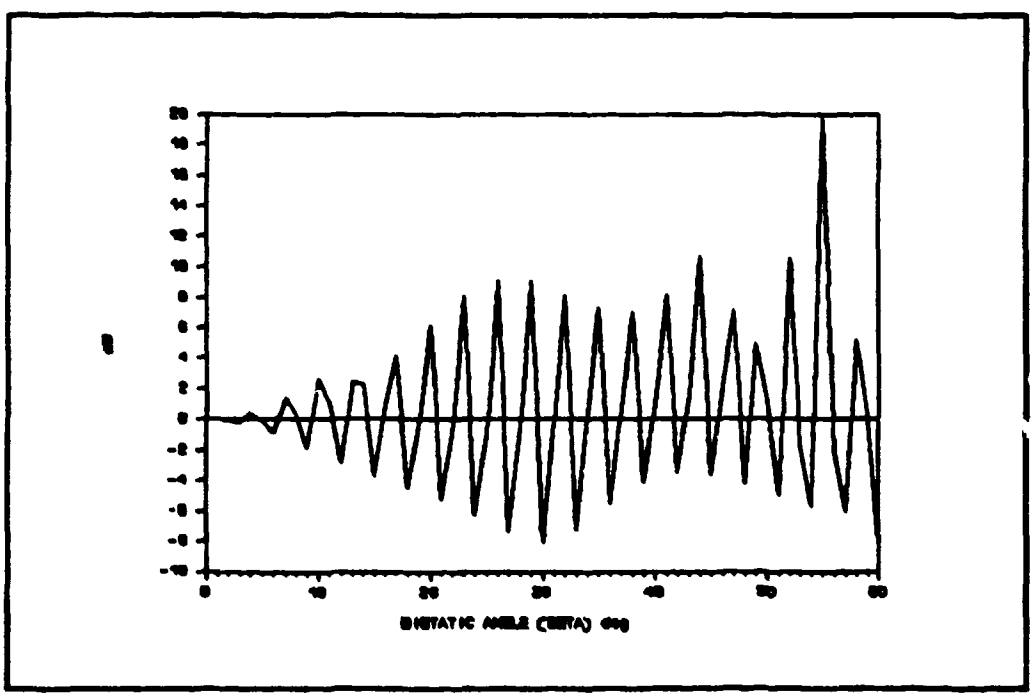

Figure 60. Cylinder (Θ = 60°; Vertical Polarization): Difference in RCS (Bistatic - Monostatic)

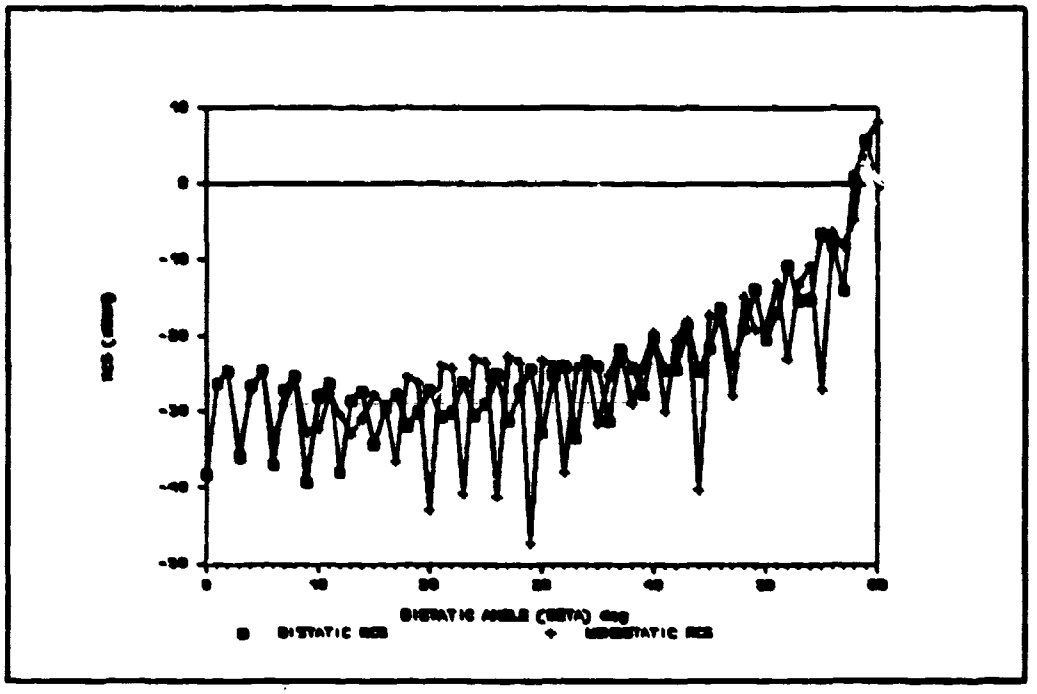

Figure 61. Cylinder (Θ=60°;Horizontal Polarization): Bistatic RCS and Equivalent Monostatic RCS

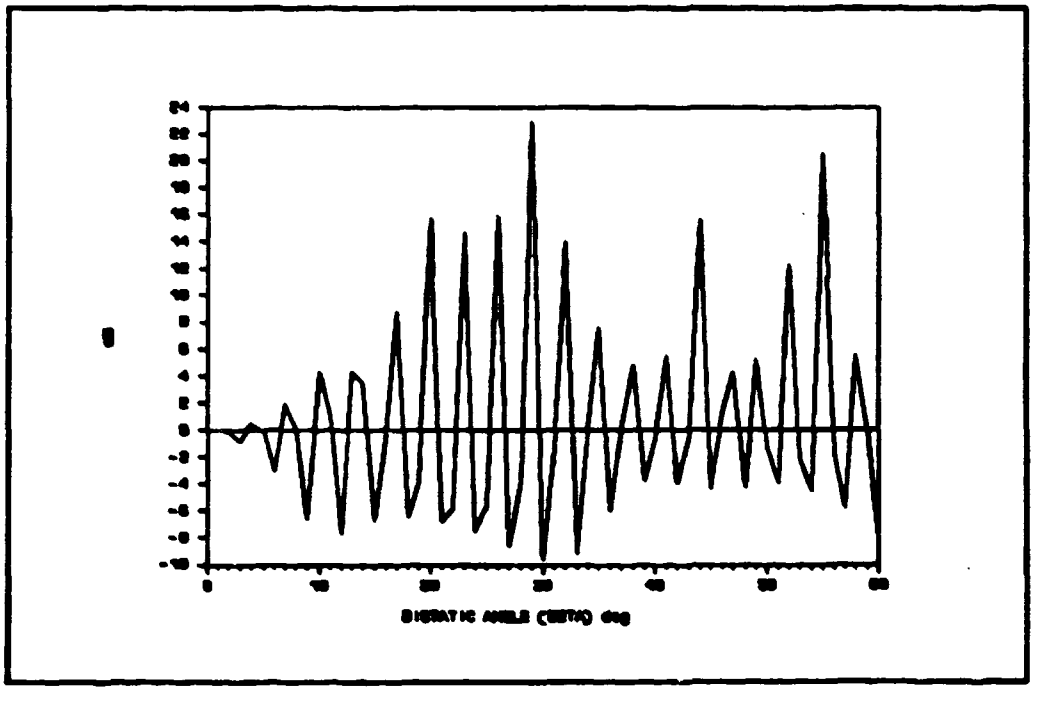

Figure 62. Cylinder (Θ=60°; Horizontal Polarization): Difference in RCS (Bistatic - Monostatic)

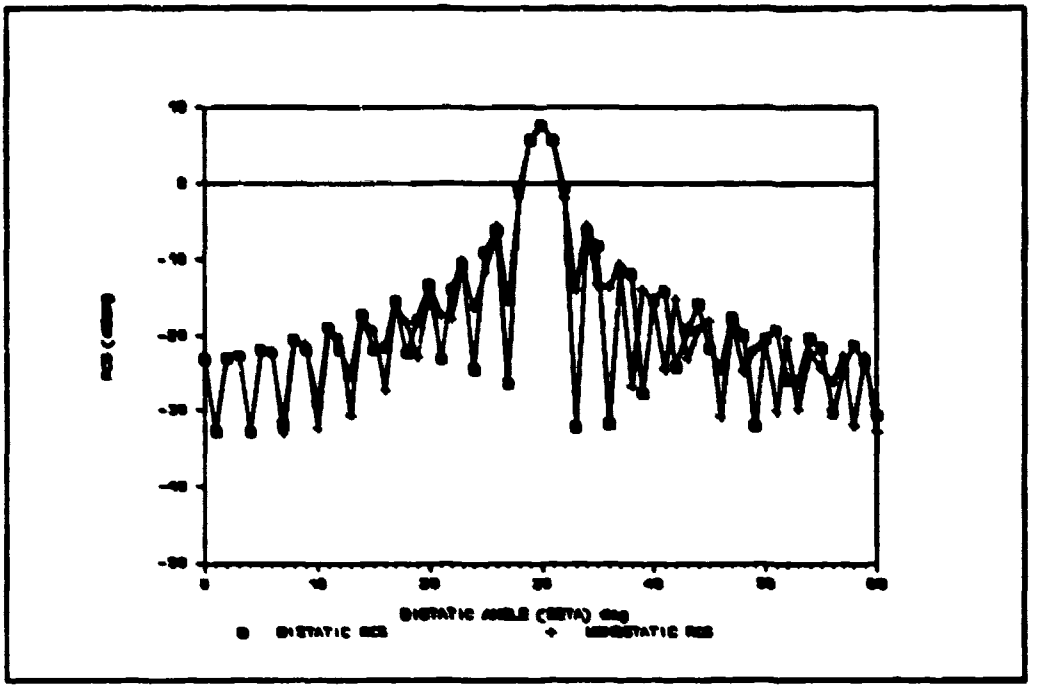

Figure 63. Cylinder (θ = 75°; Vertical Polarization): Bistatic RCS and Equivalent Monostatic RCS

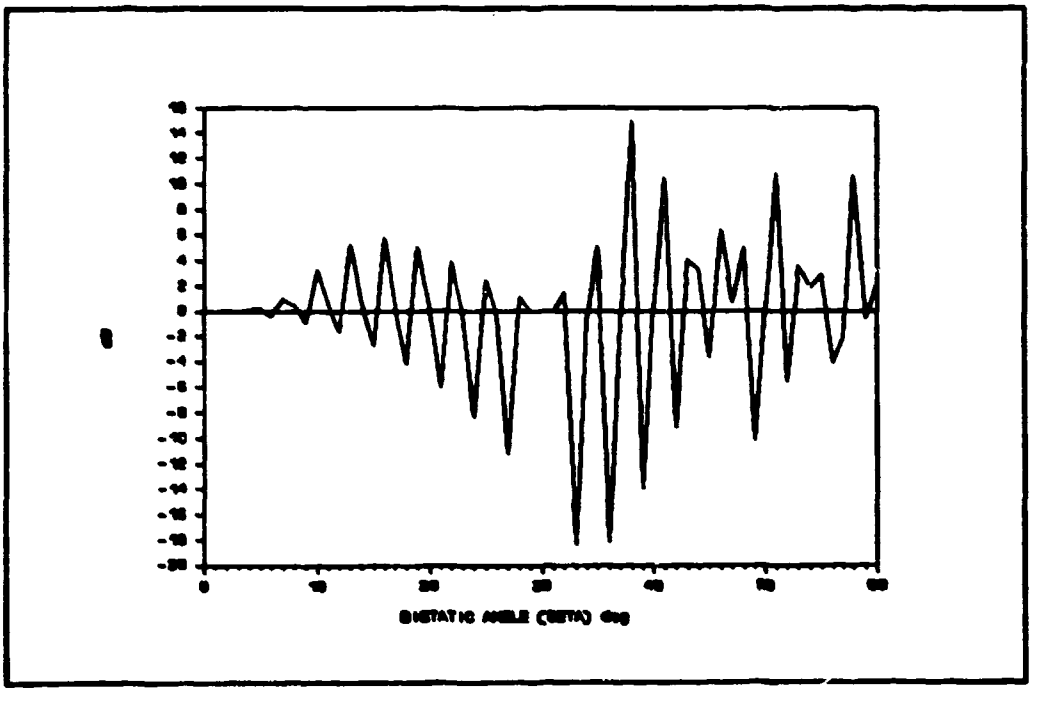

Figure 64. Cylinder (θ = 75°; Vertical Polarization): Difference in RCS (Bistatic - Monostatic)

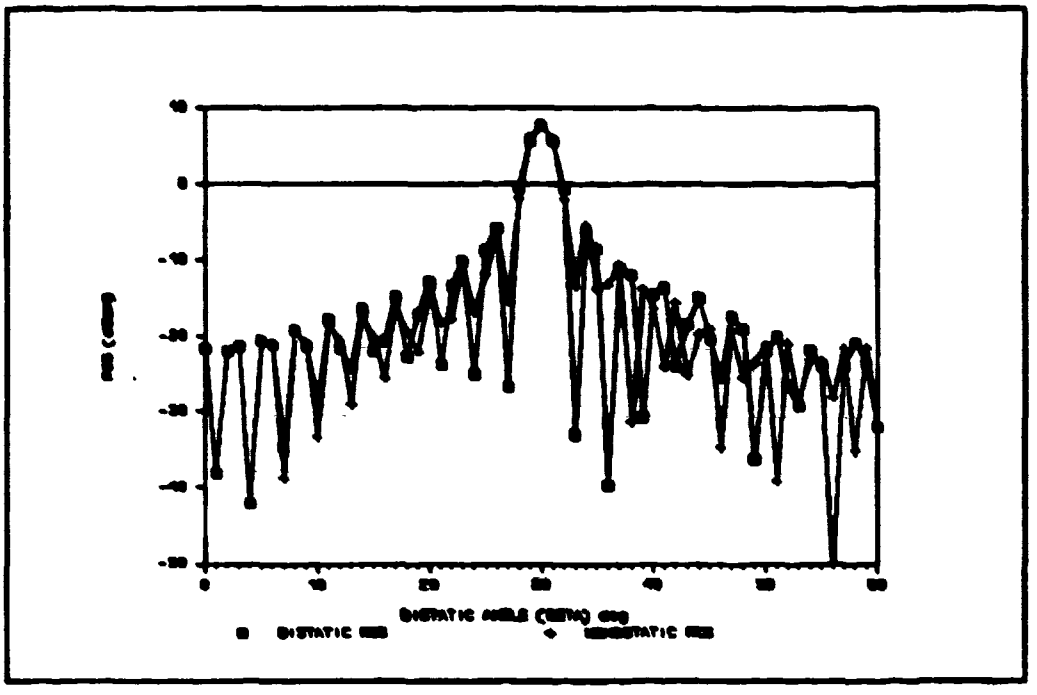

Figure 65. Cylinder (Θ=75°; Horizontal Polarization): Bistatic RCS and EQuivalent Monostatic RCS

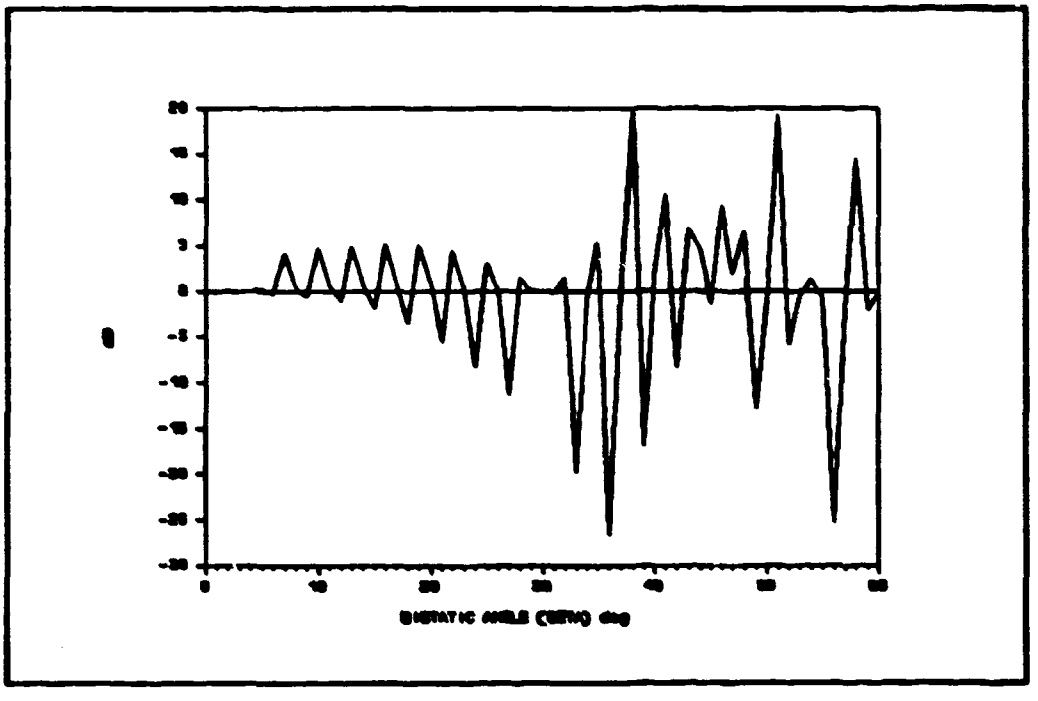

Figure 66. Cylinder (Θ=75°; Horizontal Polarization): Difference in RCS (Bistatic - Monostatic)

It can be seen in Figures 67 and 68 that the same problems occurring at end-on also occurred at broadside. The only difference between the two is that broadside bistatic RCS uses eq. (33) while end-on uses eq. (32). There is little difference, though, in these equations and the overall effect is the same.

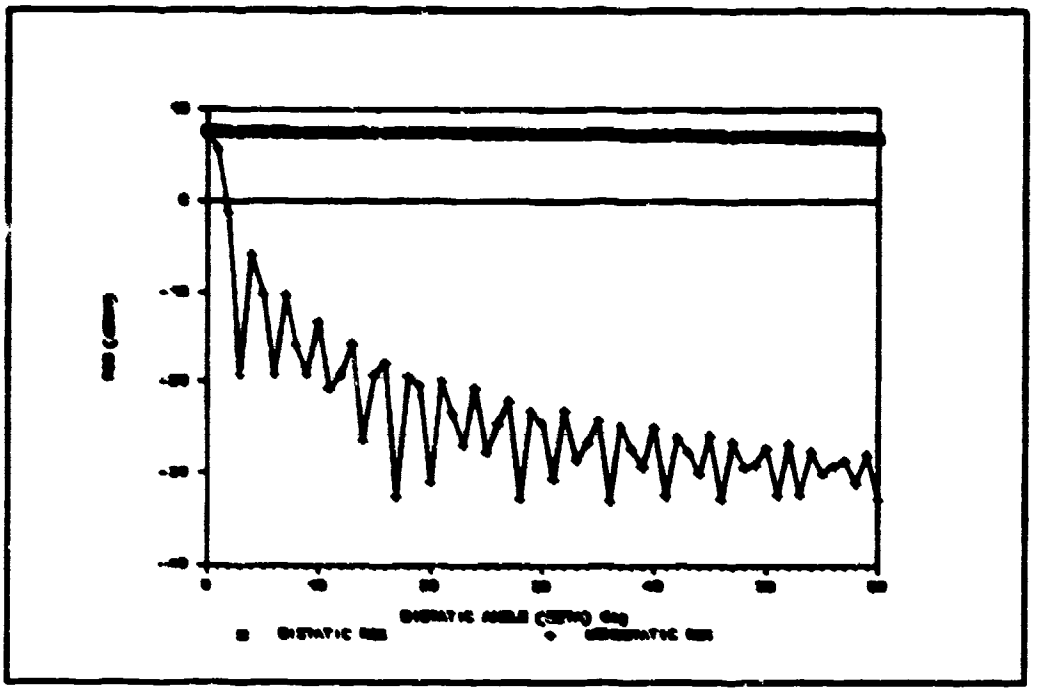

Figure 67. Cylinder (Θ = 90°; Vertical Polarisation): Bistatic RCS and Equivalent Monostatic RCS

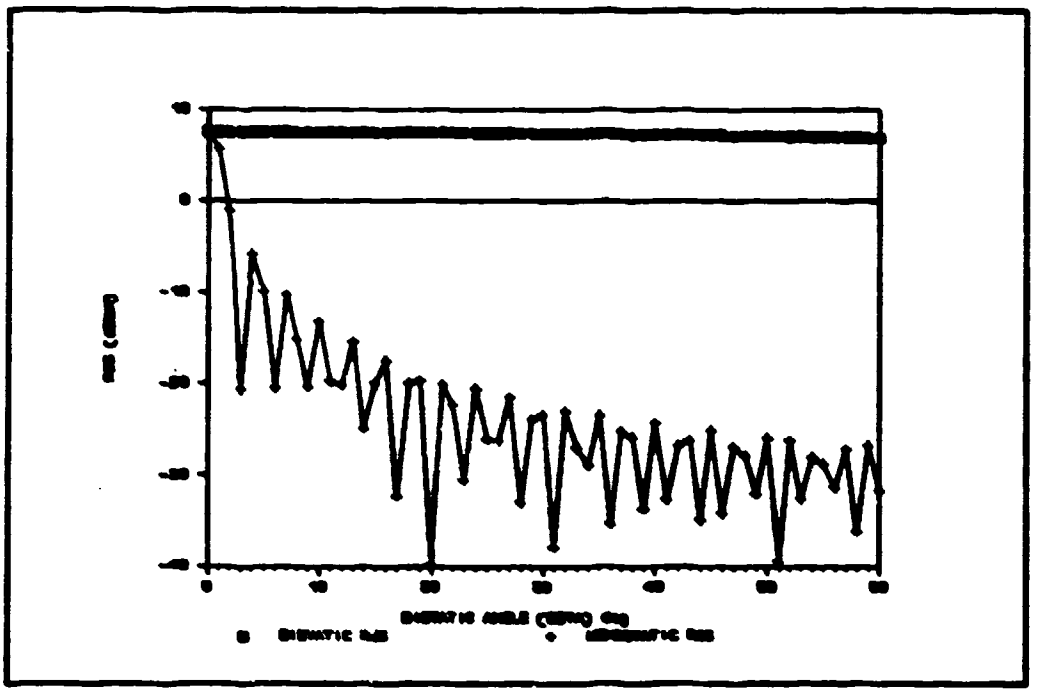

Figure 68. Cylinder (Θ=90°; Horizontal Polarisation): Bistatic RCS and Equivalent Monostatic RCS

IV. Conclusion

The purpose of this study was to investigate the applicability of Robert Kell's method under varying conditions. The mathemathical formulation of Kell's relationship was first examined. This was done by presenting the proof for the monostatic-bistatic equivalence theorem (MBET), the foundation of Kell's method, and research supporting the MBET. It was brought out that the MBET is a physical optics approximation and, therefore, it is limited by physical optics requirements. The mathematical formulation of Kell's method was then presented. With this formulation it was shown Kell's method does not rely on approximations of the scattered fields but upon the scattering centers of the target. The accuracy of Kell's method is dependent upon the behavior of the individual scattering centers relative to each other as the bistatic angle changes.

Kell's method was theoretically applied to three shapes of varying complexity to determine some of its limitations. The sphere was used to show how well Kell's method predicted bistatic RCS for electrically small targets as compared to large targets. Also, the effects of creeping waves were examined. A square flat plate was analyzed to investigate the effects angle of incidence have upon the accuracy of Kell's method. Finally, a right circular cylinder was

studied to determine what success Kell's method would have predicting the bistatic RCS of a target containing surface discontinuities.

Conclusions

This investigation was conducted to determine the applicability of Kell's method as certain parameters were changed. These parameters are bistatic angle, electrical size of the target, angle of incidence, and surface continuity. The following conclusions were reached.

Bistatic Angle. Kell claims his relationship works best when the scattering centers are insensitive to changes in bistatic angle. The scattering centers of an electrically large sphere are insensitive to changes in bistatic angle relative to one another at high frequencies. As a result Kell's relationship proved to be quite accurate for spheres at high frequencies beyond bistatic angles of 80°. The scattering center of the flat plate and circular cylinder are least sensitive to changes in bistatic angle at high frequencies near broadside incidence. Under these condition, Kell's relationship was accurate (less than 2-dB difference between bistatic and equivalent monostatic RCS) to 20° of bistatic angle for the square flat plate and 30° for the cylinder.

Electrical size. The sphere was the target shape used to predict the accuracy of Kell's method when the electrical size of the target is varied. It can be seen in the data

that good accuracy, less than 1-dB difference for both horizontal and vertical polarization did not occur until the sphere became large (ka = 10). Much of the inaccuracy for smaller spheres can be attributed to the inability of Kell's method to account for creeping waves which have small effect on the RCS of electrically large spheres.

Angle of incidence. It can be seen in both the flat plate and cylinder data that the bistatic angles for which the bistatic and equivalent monostatic RCS agree decreases as the angle of incidence increases from broadside. For the flat plate some of the degradation in agreement between the bistatic and equivalent monostatic RCS is attributable to the inability of physical optics to accurately model RCS as the angle of incidence from broadside becomes larger than 45°. In the case of the cylinder using horizontal polarization, the difference between bistatic and monostatic RCS is due to the interaction of the diffracted fields from the scattering centers. As the aspect angle approaches end-on to the cylinder the diffracted field becomes more sensitive to changes in aspect angle and Kell's relationship loses accuracy.

Surface continuity. The agreement between bistatic and monostatic RCS becomes polarization dependent when surface discontinuities in the form of 90° wedges are present. The relative phase between scattering centers was sensitive to changes in aspect angle when horizontal polarization was

utilized. This resulted in poor agreement between the bistatic and equivalent monostatic RCS. Because one scattering center dominated the RCS when vertical polarization was employed, the relative phase between scattering centers was insensitive to changes in aspect angle giving better agreement between the bistatic and equivalent monostatic cases. Overall, Kell's relationship produced better agreement between bistatic and monostatic RCS when the surface was electrically large and free of any surface discontinuities such as a sphere's than when significant discontinuities such as 90° wedges are present.

Recommendations for Further Study

Other avenues of study to determine the limits of Kell's method include:

1. A comparison of measured bistatic RCS data with measured monostatic RCS data at appropriately adjusted frequencies is a required step in the process of verifying Kell's relationship. Initially, electrically large, simple, and continuous shapes should be measured. These shapes reduce higher order effects and their RCS is not affected by diffraction from discontinuities. The complexity of the shape can then be increased to include edges such as on plates, discontinuous surfaces such as the mating of a spheroid and cylinder, and multiple reflections like those found in a hollow cylinder or corner reflector. Also, various materials and polarizations could be measured using

the same approach.

2. Using the approach this study followed, either more rigorous computer modeling of the simple shapes used in this investigation or computer modeling of shapes resembling aircraft such as cylinders with hemispherical or spheroidal end-caps could be examined. The RATSCAT has some bistatic RCS measurement data of such shapes. Comparing their data with data derived using Kell's relationship using computer modeling would give a good indication of the accuracy of Kell's relationship.

3. Study the corresponding behaviors of the monostatic and bistatic RCS keeping the bisector of the bistatic angle oriented at a constant aspect angle to the target as the bistatic angle increases. This approach could be used to study the accuracy of Kell's relationship when viewing a particular surface discontinuity or to present the data provided in a study such as this one in a different light.

Appendix A

The following derivation presents the mathematical formulation Kell employed in an effort to relate bistatic RCS to monostatic RCS.

Radar cross section can be expressed in terms of the Poynting vector (Kerr, 1951:33):

$$\sigma = 4\pi R^2 \frac{|\bar{S}^s|}{|\bar{S}^i|} \tag{34}$$

σ = radar cross section

$\bar{S}^s$ = back scattered Poynting vector

$\bar{S}^i$ = incident Poynting vector

For $|\bar{E}| = |\bar{H}|(\mu_o/\epsilon_o)^{(1/2)}$ and taking the time average value of $\bar{S}$, eq. (34) becomes

$$S_{av} = (1/2)|\bar{E}||\bar{H}| \tag{35}$$

and, therefore,

$$\sigma = 4\pi R^2 \frac{[(\mu_o/\epsilon_o)^{(1/2)}|\bar{H}^s|^2]/2}{[(\mu_o/\epsilon_o)^{(1/2)}|\bar{H}^i|^2]/2} \tag{36}$$

Reducing and assuming far field gives the starting point for Kell's formulation:

$$\sigma = 4\pi \lim_{R_o \to \infty} R_o \frac{|\bar{H}_R|^2}{|\bar{H}_i|^2} \tag{37}$$

where $\bar{H}_R = \bar{H}^s$ = reradiated magnetic field

R_o = distance to observer

Solve for $\bar{H}_R$ using the Stratton-Chu equation (Stratton, 1941:466):

$$\bar{H}_R = \frac{1}{4\pi}\int_V (i\omega\epsilon\bar{M} + \bar{J} \times \nabla\psi + -\frac{1}{\mu m}\nabla\psi)dV$$

$$- \frac{1}{4\pi}\oint_S [(\hat{n} \times \bar{H}_s) \times \nabla\psi + (\hat{n} \times \bar{H}_s)\nabla\psi$$

$$-i\omega\epsilon(\hat{n} \times \bar{E}_s)\psi]\, da \qquad (38)$$

$\bar{M}$ = magnetic current density

$\bar{J}$ = electric current density

m = magnetic charge

$\bar{H}_s$ = magnetic vector on target surface

$\bar{E}_s$ = electric vector on target surface

ψ = free space Green's function (e^{ikr_o}/r_o; r_o = distance from elemental area to observer)

If we assume there are no sources within the target volume then Stratton's equation can be reduced to give the right hand side of Kell's equation (2) given below (Kell, 1965:983):

$$f_\zeta \bar{H}_R = - \frac{1}{4\pi}\int_S [(\hat{n} \times \bar{H}_s) \times \frac{\nabla e^{ikr_o}}{r_o} + (\hat{n} \times \bar{H}_s)\frac{\nabla e^{ikr_o}}{r_o}$$

$$-i\omega\epsilon(\hat{n} \times \bar{E}_s)(e^{ikr_o})/r_o]\, da \qquad (39)$$

H_R = magnetic vector amplitude of reradiated field

ζ = phase of reradiated field relative to chosen reference

da = element of area on surface of target

$\hat{n}$ = unit vector normal to target surface and pointing inward

Figure 69 relates the target to the incident and scattered fields.

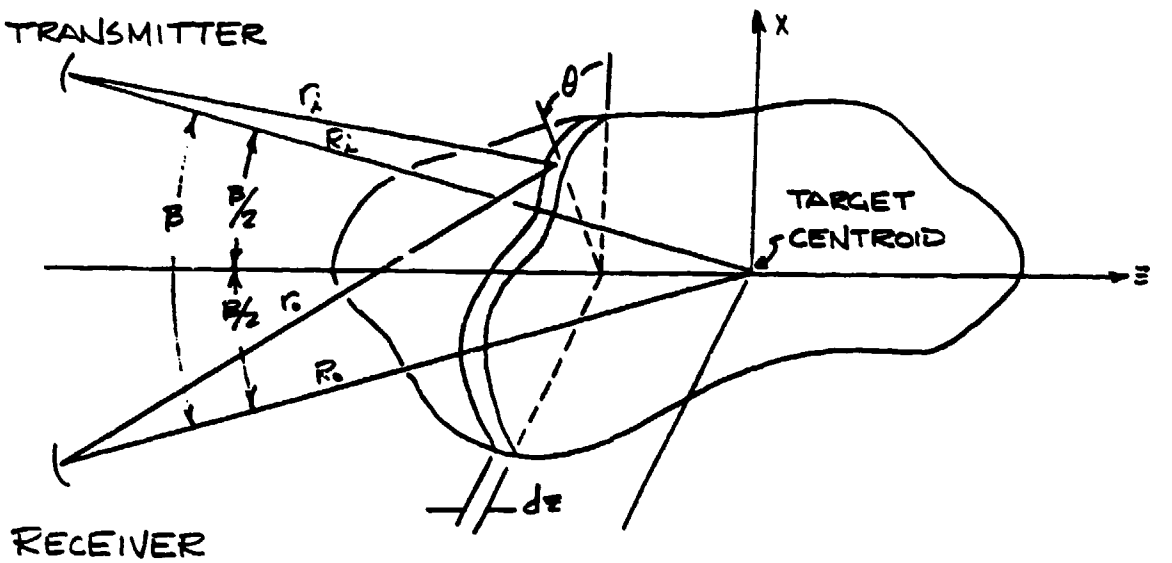

Figure 69. Bistatic Coordinate System with Antennas in the x-z Plane (Kell, 1965:984)

Kell gives the relation between r_i, r_o, R_i, R_o, z and β as

$$(r_i+r_o) = 2z\cos(\beta/2) + 2(R_i+R_o) \qquad (40)$$

This is incorrect. The correct relationship is

$$(r_i+r_o) = 2z\cos(\beta/2) + (R_i+R_o) \text{ as } R_i \text{ and } R_o \rightarrow \infty \qquad (41)$$

Kell normalizes the surface fields by dividing by the absolute magnetude of the incident field. He then accounts for illumination phase delay at each elemental area by dividing by $e^{i(kr_i+\phi)}$. This is summarized in eqs (42) and (43).

For $\frac{|\bar{E}_s|}{|\bar{E}_i|} e^{-i(kr_i+\phi)} = \bar{e}_s$ and $\frac{|\bar{H}_s|}{|\bar{H}_i|} e^{-i(kr_i+\phi)}$

$$|\bar{E}_s| = \bar{e}_s |\bar{E}_i| \exp\{i(kr_i+\phi)\} \quad (42)$$

$$|\bar{H}_s| = \bar{h}_s |\bar{H}_i| \exp\{i(kr_i+\phi)\} \quad (43)$$

where

$\bar{e}_s$ = normalized electric vector

$\bar{h}_s$ = normalized magnetic vector

ϕ = phase difference between the incident field (either electric or magnetic) and the local field at da

Using far field approximations

$$(44) \quad \frac{\nabla e^{ikr_o}}{r_o} = \frac{ik}{r_o} (e^{ikr_o}) \hat{r}_o$$

And recognizing

$$|\bar{E}_i| = |\bar{H}_i| (\mu_o/\epsilon_o)^{(1/2)} \quad (45)$$

Equations (42)-(45) can be substituted into (39) to give

$$\hat{r}_o \bar{H}_R = -\frac{1}{4\pi} \int_S [(\hat{n} \times \bar{h}_s |\bar{H}_i| e^{i(kr_i+\phi)}) \times \hat{r}_o (ike^{ikr_o})/r_o$$

$$+ (\hat{n} \cdot \bar{h}_s |\bar{H}_i| e^{i(kr_i+\phi)}) \hat{r}_o (ike^{ikr_o})/r_o$$

$$- i\omega(\mu_o/\epsilon_o)^{1/2} (\hat{n} \times \bar{e}_s |\bar{H}_i| e^{i(kr_i+\phi)}) (e^{ikr_o})/r_o] da \quad (46)$$

Rearranging the above equation gives

$$\hat{r}_o \bar{H}_R = -\frac{1}{4\pi}|\bar{H}_i| \int_S [(\hat{n} \times \bar{h}_s e^{i(kr_i+\phi)}) \times \hat{r}_o(ike^{ikr_o})/r_o$$

$$+ (\hat{n}\cdot\bar{h}_s e^{i(kr_i+\phi)})\hat{r}_o(ike^{ikr_o})/r_o$$

$$- i\omega(\mu_o/\epsilon_o)^{1/2}(\hat{n} \times \bar{e}_s e^{i(kr_i+\phi)})(e^{ikr_o})/r_o]da \quad (47)$$

Knowing that $\omega(\mu_o/\epsilon_o)^{1/2} = k$ and making the far field approximation $r_o \sim R_o$, eq. (47) can be written

$$\hat{r}_o \bar{H}_R = \frac{|\bar{H}_i|}{2R_o\pi} \int_S [i(\hat{n} \times \bar{h}_s e^{ik(r_i+r_o)}) \times \hat{r}_o(\hat{e}^{i\phi})$$

$$+ i(\hat{n}\cdot\bar{h}_s e^{ik(r_i+r_o)})(\hat{e}^{i\phi})\hat{r}_o$$

$$- i(\hat{n} \times \bar{e}_s e^{ik(r_i+r_o)}\hat{e}^{i\phi}] da \quad (48)$$

Using the relationship given in eq. (41), the phase term in eq. (48) can be rewritten as

$$e^{ik(r_i+r_o)} = e^{i2kz\cos(\beta/2)} \; e^{ik(R_i+R_o)} \quad (49)$$

By writing the imaginary expression i as $e^{i\pi/2}$ and using eq. (49), eq. (48) becomes

$$\hat{r}_o \bar{H}_R = \frac{|\bar{H}_i|}{2R_o\lambda} e^{ik(R_i+R_o)} e^{i\pi/2} \int_S [(\hat{n} \times \bar{h}_s) \times \hat{r}_o(\hat{e}^{i\phi})$$

$$+ (\hat{n}\cdot\bar{h}_s)(e^{i\phi})\hat{r}_o - (\hat{n} \times \bar{e}_s)\hat{e}^{i\phi}]$$

$$\times e^{ik2z\cos(\beta/2)} da \quad (50)$$

Any specific geometry will be dependent on ϕ and z, therefore, eq. (50) can be rewritten using $p(\phi,z)$, a

conversion factor relating the surface element da, to the differential coordinate product dΘdz to yield Kell's eq. (6) with one difference, the $e_i/2$ term:

$$\hat{f}_o \bar{H}_R = -\frac{\bar{H}_i}{2R_o\lambda} e^{ik(R_i+R_o)} e^{i\pi/2} \iint [(\hat{n} \times \bar{h}_s) \times \hat{f}_o(e^{i\phi}) + (\hat{n}\cdot\bar{h}_s)(e^{i\phi})\hat{f}_o - (\hat{n} \times \bar{e}_s)e^{i\phi}] \times p(\Theta,z)\, e^{ik2z\cos(\beta/2)}\, d\Theta dz \qquad (51)$$

Using eq. (51) in (37) yields

$$\sigma = \frac{\pi}{\lambda^2} e^{ik(R_i+R_o)} e^{i\pi/2} \iint [(\hat{n} \times \bar{h}_s) \times \hat{f}_o(e^{i\phi}) + (\hat{n}\cdot\bar{h}_s)(e^{i\phi})\hat{f}_o - (\hat{n} \times \bar{e}_s)e^{i\phi}] \times p(\Theta,z)\, e^{ik2z\cos(\beta/2)}\, d\Theta dz \qquad (52)$$

By allowing the magnitude squared of $e^{ik(R_i+R_o)} e^{i\pi/2}$ to equal 1 and integrating eq. (52) with respect to Θ, the RCS is given by

$$\sigma = \frac{\pi}{\lambda^2} \left| \int I(z)\, e^{i2kz\cos(\beta/2)} dz \right|^2 \qquad (53)$$

where

$$I(z) = \int [(\hat{n} \times \bar{h}_s) \times \hat{f}_o(e^{i\phi}) + (\hat{n}\cdot\bar{h}_s)(e^{i\phi})\hat{f}_o - (\hat{n} \times \bar{e}_s)e^{i\phi}]\, p(\Theta,z)\, e^{ik2z\cos(\beta/2)}\, d\Theta \qquad (54)$$

The following comments can be made regarding eq. (53):

a) It has the form of physical optics.

b) The difference between eq. (53) and physical optics lies in the fact that eq. (53) is exact. However, the I(z) term in eq. (53) is not precisely known.

c) I(z) is a composite of surface geometry, illuminating and observing ray geometry, and surface wave propagation effects.

d) The analytic continuity of I(z) significantly effects σ since eq. (53) may be subdivided into a sum of integrals, each subintegral taken over a range of z withing which its integrand is continuous.

e) Approximations of I(z) yield contributions dependent only on the integral's endpoints.

f) The endpoints are the scattering centers.

From this logic, Kell proposes that RCS can be computed from discrete scattering centers as shown below:

$$\sigma = \left| \sum_{m=1}^{M} (\sigma_m)^{1/2} e^{i\phi_m} \right|^2 \qquad (55)$$

M = number of scattering centers

σ_m = RCS of m^{th} scattering center

ϕ_m = phase of field scattered by m^{th} center relative to the phase of the first scattering center

According to Kell, eq. (55) is used to determine the relation between monostatic and bistatic RCS for a given aspect angle Φ. Expanding the phase term in eq. (55)

$$\phi_m = 2kz_m\text{Cos}(\beta/2) + \xi_m \qquad (56)$$

where z_m = distance between 1st and m^{th} scattering center

ξ_m = residual phase contributions (creeping waves, etc.)

Substituting eq. (56) into (55):

$$\sigma = \left| \sum_{m=1}^{M} (\sigma_m)^{1/2} \, e^{i2kz_m\text{Cos}(\beta/2)} \right|^2 \qquad (57)$$

Kell uses eq. (57) to make a statement for monostatic-bistatic equivalence and the conditions required for its occurrence:

> If for a chosen aspect angle, the following conditions hold:
>
> 1) The RCS may be written as a squared sum of fields from discrete scattering centers, and
> 2) The amplitude $(\sigma_m)^{1/2}$, position z_m, and residual phase ξ_m are insensitive to the bistatic angle β over the range of β considered, for those centers which are significant members in this sum;
>
> it then follows that the bistatic cross section of aspect angle θ and bistatic angle β is equal to the monostatic cross section measured on the bisector at a frequency lower by the factor $\text{Cos}(\beta/2)$ [Kell,1965:987].

Appendix B

This appendix presents the computer programs used to calculate the bistatic and equivalent monostatic RCS of a sphere. These programs were developed by Ohio State University in 1978. They were then modified by AFWAL for use on the indoor radar range at Wright-Patterson AFB. The first program, BISPH.FOR, computes the bistatic RCS. MONOSPH.FOR is a modification to BISPH.FOR. It calculates monostatic RCS at a frequency adjusted by a factor of Sec(β/2) (β = bistatic angle) to give a one-to-one correspondence between bistatic RCS and monostatic RCS.

```
C      ================<<< BISPH.FOR >>>====================
C
C     THIS PROGRAM GENERATES SPHERE CALIBRATION DATA FOR
C     THE SWEPT FREQUENCY SYSTEM
C
C     OUTPUT---MAGNITUDE:  10LOG(RCS)-40; RCS IN SQUARE CM
C                  PHASE:  RADIANS; FROM SPHERE CENTER
C
C     MODIFICATIONS:  THIS PROGRAM WAS MODIFIED FOR USE ON A
C                     PDP-11/23.  OUTPUT IN NOW STORED IN ONE
C                     2-DIMENSIONAL ARRAY YM.  THE PHASE IS
C                     GIVEN IN RADIANS.  OUTPUT GOES TO AN
C                     UNFORMATTED FILE.
C
      COMMON BUFF,NDIM,ANST,AINC
      COMPLEX ETH,EPH
      character*20output_file
      REAL KA
      DIMENSION AM(2000),PH(2000)
      INTEGER*2 INFILE(15)
      BYTE BUFF(35000)
      LOGICAL VHP,LBK
      DATA PI/3.141593/
      DATA LT,LF/-1,0/
      CONST=2.*PI*1.E9/300.E6
      RTD=180./PI
C
C
C ====DEFINE RANGE GEOMETRY
C     SPHERICAL SCATTERING
```

```
C
      WRITE(5,*) 'INPUT T FOR VER POL AND F FOR HOR POL'
      ACCEPT *, VHP
      WRITE(6,*) 'INPUT ANTENNA START SEPARATION IN DEGREES'
      ACCEPT *, ASD
      asdp=asd
      write(6,*) 'INPUT ANTENNA STOP SEPARATION IN DEGREES'
      accept *, asd1
      THB=180.-ASD
      THBp=thb
      PHB=-90.
      IF(VHP) PHB=180.
      write(6,*) 'ANTENNA SEPARATION INCREMENT >= 1 DEG'
      accept *,dela
      nba=(asd1-asd)/dela+1.01
C
      WRITE(6,*) 'INPUT SPHERE DIAMETER IN INCHES'
      ACCEPT *,SDI
      WRITE(6,*) 'INPUT MIN FREQ. (GHZ):  '
      ACCEPT *, FMIN
      ANST=FMIN*1000.
      WRITE(6,*) 'INPUT MAX FREQ. (GHZ):  '
      ACCEPT *, FMAX
      WRITE(6,*) 'FREQUENCY INCREMENT (GHZ):  '
      ACCEPT *, DELF
      write(6,*) 'Type in output filename'
      read(5,15) output_file
15    format(a20)
      NF=(FMAX-FMIN)/DELF+1.1
      NDIM=NF
C
      SRCM=SDI*2.54/2.
      SRM=SRCM/100.
      AREACM=4.*PI*SRCM**2
      AINC=DELF*1000.
      CKA=CONST*SRM
      FREQ=FMIN-DELF
C
C====START OF LOOP====
C
C
C=============================================================
C
      FUNCTION CATAN2(Z)
      COMPLEX Z
      RZ=REAL(Z)
      FIZ=AIMAG(Z)
      CATAN2=ATAN2(FIZ,RZ)
      RETURN
      END
C
C=============================================================
C
```

```
      SUBROUTINE GPS(VHP,KA,EV,ETH,EPH)
      COMPLEX ETH,EPH,ETHT,EPHT,ETHI,EPHI
      REAL KA
      LOGICAL VHP
      IF(VHP) THEN
      THT=180.
      PHT=180.
      CALL FIELD(1.,KA,THT,PHT,ETHT,EPHT,IER)
      ETH=ETHT
      THI=180.-2*EV
      PHI=180.
      CALL FIELD(1.,KA,THI,PHI,ETHI,EPHI,IER)
      ETH=ETH+ETHI
      ELSE
      THT=180.
      PHT=-90.
      CALL FIELD(1.,KA,THT,PHT,ETHT,EPHT,IER)
      EPH=EPHT
      THI=180.-2.*EV
      PHI=90.
      CALL FIELD(1.,KA,THI,PHI,ETHI,EPHI,IER)
      EPH=EPH+EPHI
      ENDIF
      RETURN
      END
C
C=======================================================================
C
C     BISTATIC-BACKSCATTERED FIELD OF A SPHERE
C
      SUBROUTINE FIELD(TIMCON,KA,THE,PHI,GTHE,GPHI,IER)
C
C        TIMCON=TIME CONVENTION=+1.0 FOR HARRINGTON (-JWT)
C                               -1.0 FOR STRATTON (+JWT)
C
      COMPLEX J,GTHE,GPHI,SGTHE,SGPHI,BN,CN
      DIMENSION SJ(150),SY(150),DSJ(150),DSY(150),DP(150)
      DOUBLE PRECISION TPCERR,ANGDIF,P(151),DEF
      DOUBLE PRECISION U,DCOS,DSIN,V
      REAL KA
C
C=====DEFINE CONSTANTS
C     J=SQRT(-1)
C     TPCERR=TOTAL % CHANGE ERROR ALLOWABLE BETWEEN
C            SUCCESSIVE ITERATIONS TO DEVINE CONVERGENCE
C     TPCMAG=TOTAL % CHANGE IN MAGNITUDE ACTUALLY
C            OCCURRING BETWEEN SUCCESSIVE LOOPS.
C
      DATA PI,J/3.141593,(0.,1.)/
      DATA TPCERR,ANGDIF/1.0D-20,1.0D-2/
C
C=====INITIALIZE VARIABLES
C
```

```
      GTHE=CMPLX(0.,0.)
      GPHI=CMPLX(0.,0.)
      SGTHE=CMPLX(0.,0.)
      SGPHI=CMPLX(0.,0.)
C
      MO=150
      CALL SPHEBES(KA,SJ,SY,DSJ,DSY,MO,MAX)
C
C=====ELIMINATE ZERO ORDER TERMS FROM THE ARRAYS
C
      MAX=MAX-1
      DO 5 L=1,MAX
      LL=L+1
      SJ(L)=SJ(LL)
      SY(L)=SY(LL)
      DSJ(L)=DSJ(LL)
      DSY(L)=DSY(LL)
5     CONTINUE
C
      CHKTHE=ABS(180.-THE)
      IF (CHKTHE .LT. ANGDIF) GOTO 20
      IF (ABS(THE) .LT. ANGDIF) GOTO 15
      U=DCOS(DBLE(THE*PI/180.))
      V=DSIN(DBLE(THE*PI/180.))
      MAXN=MAX+1
      M=1
      DEF=-1.D0
      CALL POLY2(DEF,U,M,MAXN,P)
      DO 10 N=1,MAX
      DP(N)=(FLOAT(N+1)*U*P(N)-FLOAT(N-M+1)*P(N+1)
     &*V/1.-U**2)
      P(N)=P(N)/V
10    CONTINUE
      GOTO40
15    DO 16 N=1,MAX
      FN=FLOAT(N)
      DP(N)=.5*FN*(FN+1.)
      P(N)=(-1.)*DP(N)
16    CONTINUE
      GOTO 40
20    DO 30 N=1,MAX
      FN=FLOAT(N)
      P(N)=0.5*FN*(FN+1)*(-1.)**N
      DP(N)=P(N)
30    CONTINUE
C
40    DO 50 N=1,MAX
      AN=(-1.)*FLOAT(2*N+1)/FLOAT(N**2+N)
      BN=AN*(SJ(N)+KA*SDJ(N)/(SJ(N)+KA*DSJ(N)-J*
     &(SY(N)+KA*DSY(N)))
      CN=AN*SJ(N)/(SJ(N)-J*SY(N))
      GTHE=GTHE+BN*DP(N)-CN*P(N)
      GPHI=GPHI+BN*P(N)-CN*DP(N)
```

```
      AA=CABS(GTHE-SGTHE)
      BB=CABS(GTHE)
      CC=CABS(GPHI-SGPHI)
      DD=CABS(GPHI)
      IF (BB .NE. 0.) GOTO 44
      AA=0.
      BB=1.
44    IF (DD .NE. 0.) GOTO 45
      CC=0.
      DD=1.
45    TPCMAG=AA/BB+CC/DD
      IER=N
      IF (TPCMAG .LE. TPCERR) GOTO 60
      SGTHE=GTHE
      SGPHI=GPHI
50    CONTINUE
      IER=0
C
60    GTHE=TIMCON*GTHE*J*COS(PHI*PI/180.)/KA
      GPHI=TIMCON*BPHI*J*SIN(PHI*PI/180.)/KA
      RETURN
      END
C
C=============================================================
C
      SUBROUTINE SPHEBES(X,BJ,BY,BP,YP,IDM,MAX)
C
C     X=ARGUMENT
C     BJ=SPHERICAL BESSEL FUNCTION ARRAY
C     BY=SPHERICAL NEUMAN FUNCTION ARRAY
C     BP=PRIMED BESSEL FUNCTION ARRAY
C     YP=PRIMED NEUMAN FUNCTION ARRAY
C     IDM=MAX NUMBER OF ORDERS TO BE COMPUTED
C     MAX=MAX NUMBER OF ORDERS ACTUALLY COMPUTED
C
C     COMPUTATION IS STOPPED WHEN THE VALUE OF A NEUMAN
C     FUNCTION MAGNITUDE IS GREATER THAN FMAX WHICH IS
C     DEFINED INTERNALLY TO THE PROGRAM.
C
      DIMENSION BJ(1),BY(1),BP(1),YP(1)
      FMAX=1.E35
      FMIN=1.E-38
      SX=SIN(X)/X
      CX=COS(X)/X
      FF1=SX
      FF2=SX/X-CX
      YY1=-CX
      YY2=-(CX/X+SX)
      BY(1)=YY1
      BY(2)=YY2
      BYB=YY1
      BYC=YY2
      I=2
```

```
20      BYA=BYB
        BYB=BYC
        BYC=(2.*I-1.)*BYB/X-BYA
        L=I+1
        IF (L .LE. IDM) BY(L)=BYC
        AY1=ABS(BYC)
        I=I+1
        IF (AY1 .LT. FMAX) GOTO 20
        MAX=I-1
        BJB=0.
        BJA=FMIN
        I=MAX
50      I=I-1
        BJC=BJB
        BJB=BJA
        BJA=(2.*I+3)*BJB/X-BJC
        L=I+1
        IF (L .LE. IDM) BJ(L)=BJA
        IF (I .GT. 0) GOTO 50
        ALF=BJ(2)/FF2
        IF (ABS(FF1) .GT. ABS(FF2)) ALF=BJ(1)/FF1
        ALF=1./ALF
        K=MAX
        IF (K .GT. IDM) K=IDM
        DO 60 I=1,K
60      BJ(I)=BJ(I)*ALF
        BP(1)=-BJ(2)
        YP(1)=-BY(2)
        DO 80 I=2,K
        IM=I-1
        FAC=I/X
        BP(I)=BJ(IM)-FAC*BJ(I)
80      YP(I)=BY(IM)-FAC*BY(I)
        RETURN
        END
C
C=======================================================================
C
C       ASSOCIATED LEGENDRE POLYNOMIAL SUBROUTINE
C
C       FOR HARRINGTON'S DEFINITION OF THE ASSOCIATED
C       LEGENDRE PLOYNOMIAL  DEF=-1.
C
C       FOR THE OTHER DEFINITION OF THE ASSOCIATED
C       LEGENDRE POLYNOMIAL  DEF=1.
C
        SUBROUTINE POLY2(DEF,X,M,MAXN,P)
        DOUBLE PRECISION DEF,X,P(1),SQ,DSQRT,DBLE
        DOUBLE PRECISION FL1,FL2,FL3
        SQ=DSQRT(1.0D0-X**2)
        P(1)=1.D0
        IF (M .EQ. 0) GOTO 1
        DO 2 L=1,M
```

```
      P(1)=DEF*DBLE(FLOAT(2*L-1))*SQ*P(1)
2     CONTINUE
1     P(2)=DBLE(FLOAT(2*M+1))*X*P(1)
      DO 3 K=3,MAXN
      I=K-1
      J=K-2
      N=M+K-1
      FL1=DBLE(FLOAT(N+N-1))
      FL2=DLBE(FLOAT(M+N-1))
      FL3=DBLE(FLOAT(N-M))
      P(K)=(FL1*X*P(1)-FL2*P(J))/FL3
3     CONTINUE
      RETURN
      END
C
C-------------------------------------------------------------
C
      FUNCTION ACOS(X)
      DOUBLE PRECISION DSQRT
      DATA PI/3.141593/
      IF (X .GE. 1.) GOTO 1
      IF (X .LE. -1.) GOTO 2
      ACOS=(PI/2.)-ATAN(X/DSQRT(1.D0-X*X))
      RETURN
1     ACOS=0.
      RETURN
2     ACOS=PI
3     RETURN
      END
C
C=============================================================
```

The following routine is the difference between BISPH.FOR and MONOSPH.FOR.

```
C     ==================<<< MONOSPH.FOR>>>==================
C
C     BISTATIC SCATTERING FROM A SPHERE
C
      open(unit=10,status='NEW',file=output_file,err=100)
      write(10,*) 'sph.    Sep. Angle      freq        Mono.'
      write(10,*) 'size    (deg)           (GHz)       RCS'
      write(10,*) '(in)'
      DO 45 jj=1,nba
            asd=asdp+jj-1
            thb=180.
            freq=fmin*1/(cos(.5*asd/rtd))
            KA=CKA*FREQ
            CALL FIELD(1.,KA,THB,PHB,ETH,EPH,IER)
```

```
C
C       RCS FOR HORIZONTAL POLARIZATION
C
                IF(VHP) THEN
                        RCS=AREACM*CABS(ETH)**2
                        PH(I)=CATAN2(ETH)*RTD
C
C       RCS FOR VERTICAL POLARIZATION
C
                ELSE
                        RCS=AREACM*CABS(EPH)**2
                        PH(I)=CATAN2(EPH)*RTD
                ENDIF
                AM(I)=10.*ALOG10(RCS)-40
                write(10,50) sdi,asd,freq,AM(I)
45      continue
        close(unit=10)
        goto 101
100     write(6,*) 'Filename already exists!!!'
50      FORMAT (f5.2,2X,F10.4,2X,F10.4,2X,F10.4)
101     continue
        STOP
        END
C
C=============================================================
```

Appendix C

This appendix presents the derivation of the mathematical model for the RCS of a square flat plate using physical optics approximations. Following the derivation is the computer programs used to calculate the bistatic and equivalent monostatic cross sections for a flat plate.

The geometry utilized in this derivation is given in Figure 70.

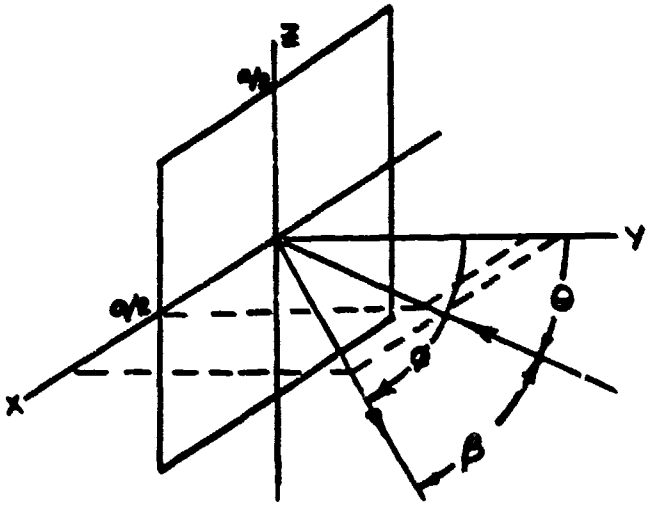

Figure 70. Scattering Geometry for a Square Flat Plate

The incident and scattered propagation vectors are constrained to lie in the x-y plane.

The incident electric field can be expressed as (Harrington, 1961:140)

$$E_z^i = E_o \, e^{jk(x\cos\theta + y\sin\theta)} \qquad (58)$$

The scattered electric field can be expressed as (Harrington, 1961:140)

$$E_z^s = \frac{kE_o a^2 e^{-jkr}}{j2\pi r} \cos\phi \frac{\sin[k(a/2)(\sin\theta + \sin\phi)]}{k(a/2)(\sin\theta + \sin\phi)} \qquad (59)$$

From eqs. (35) and (36), RCS is given by

$$\sigma = 4\pi \lim_{r\to\infty} \frac{|E_z^s|}{|E_z^i|} \qquad (60)$$

Substituting eqs. (58) and (59) into eq. (60) yields

$$\sigma = 4\pi \left[\frac{a^2}{\lambda} \cos\phi \frac{\sin[k(a/2)(\sin\theta + \sin\phi)]}{k(a/2)(\sin\theta + \sin\phi)}\right]^2 \qquad (61)$$

From Figure (70), it can be seen $\phi = \theta+\beta$. Substituting this relationship into eq. (61) gives the expression for bistatic RCS in terms of angle of incidence and bistatic angle:

$$\sigma = 4\pi \left[\frac{a^2}{\lambda} \cos(\theta+\beta) \frac{\sin[k(a/2)(\sin\theta + \sin(\theta+\beta))]}{k(a/2)(\sin\theta + \sin(\theta+\beta))}\right]^2 \qquad (62)$$

In accordance with Kell's hypothesis, the aspect angle for the equivalent monostatic case is equal to the angle of incidence plus half the bistatic angle. Applying this concept to eq. (61) gives the equivalent monostatic RCS as

$$\sigma = 4\pi \left[\frac{a^2}{\lambda} \cos(\theta+\beta/2) \frac{\sin[ka \sin(\theta+\beta/2)]}{ka \sin(\theta+\beta/2)}\right]^2 \qquad (63)$$

The computer programs calculating the bistatic and equivalent monostatic RCS follow. These programs are written in BASIC and run on a Zenith Z-100 computer using an 8-bit CP/M operating system.

```
1     '*********************BISTATIC RCS************************
2     'THIS PROGRAM CALCULATES THE BISTATIC RCS OF A SQUARE
3     'FLAT PLATE
4     '
5     'OUTPUT:  10*LOG(RCS); RCS IN SQUARE METERS
6     '
10    OPEN "O",1,"B:FPRCSB.DAT"
11    '
12    'DEFINE VARIABLES
13    'L = LENGTH OF ONE SIDE IN METERS
14    'WL = WAVELENGTH IN METERS
15    'THETA = ANGLE OF INCIDENCE
16    'BETA = BISTATIC ANGLE
17    '
20    L=0.3048
30    PI=3.141593
40    DIM RCS(181)
44    '
45    'I = ANGLES OF INCIDENCE
46    '
50    FOR I=0 TO 40 STEP 8
60      A$ = "ANGLE OF INCIDENCE="
70      PRINT#1,A$;I
74      '
75      'N = BISTATIC ANGLE
76      '
80      FOR N = 0 TO 60
90        THETA = PI*I/180
100       BETA = N*PI/180
110       WL=0.03
140       J = L*PI*(SIN(THETA)+SIN(THETA+BETA))/WL
150       IF J = 0 THEN 162 ELSE 160
160       RCS(N)=4*PI*(L^2*COS(THETA+BETA)*SIN(J)/(J*WL))^2
161       GO TO 170
162       RCS(N) =  4*PI*(L^2*COS(THETA+BETA)/WL)^2
170     NEXT N
190     FOR K=0 TO 60
210       RCS(K)=10*LOG(RCS(K))/2.3025851
220       PRINT#1,USING"####.###       ";K,RCS(K)
230     NEXT K
235   NEXT I
240   CLOSE#1
250   STOP
260   '************************************************************
```

```
1     '***************EQUIVALENT MONOSTATIC RCS*************
2     '
3     'THIS PROGRAM CALCULATES THE MONOSTATIC RCS OF A SQUARE
4     'FLAT PLATE AS A FUNCTION OF FREQUENCY IN ACCORDANCE
5     'WITH KELL'S HYPOTESIS
6     '
7     'OUTPUT:  10*LOG(RCS); RCS IN SQUARE METERS
8     '
10    OPEN "O",1,"B:FPRCSF.DAT"
11    '
12    'DEFINE VARIABLES
13    'L = LENGTH OF SIDE IN METERS
14    'WL = WAVELENGTH IN METERS
15    'THETA = MONOSTATIC ASPECT ANGLE
16    'BETA = BISTATIC ANGLE
17    '
20    L=0.3048
30    PI=3.141593
40    DIM RCS(181)
45    DIM FREQ(100)
47    '
48    'I = ANGLE OF INCIDENCE FOR BISTATIC CASE
49    '
50    FOR I=0 TO 40 STEP 8
60      A$ = "ANGLE OF INCIDENCE="
70      PRINT#1,A$;I
74      '
75      'N = BISTATIC ANGLE IN DEGREES
76      '
80      FOR N = 0 TO 60
90        THETA = PI*(I+N/2)/180
100       BETA = N*PI/180
110       WL=0.03*COS(BETA/2)
130       FREQ(N) = 3E8/(WL*1E9)
140       J = L*PI*2*SIN(THETA)/WL
150       IF J = 0 THEN 162 ELSE 160
160       RCS(N)=4*PI*(L^2*COS(THETA)*SIN(J)/(J*WL))^2
161       GO TO 170
162       RCS(N) =  4*PI*(L^2*COS(THETA)/WL)^2
170     NEXT N
190     FOR K=0 TO 60
210       RCS(K)=10*LOG(RCS(K))/2.3025851
220       PRINT#1,USING"####.###       ";FREQ(K),RCS(K)
230     NEXT K
235   NEXT I
240   CLOSE#1
250   STOP
260   '************************************************************
```

Appendix D

This appendix presents the derivation of the RCS model for a right circular cylinder and the computer programs used to calculate its bistatic and equivalent monostatic RCS. The derivation of the RCS is taken from "Project DISTRACT--Distributed Radar Concepts and Techniques," Appendix A, Cornell Aeronautical Laboratory, Inc.

The RCS of a finite cylinder is dominated by diffracted returns. For this reason, geometrical theory of diffraction (GTD) is used to compute the RCS. A general diffraction coefficient is written as

$$D = \frac{e^{i\pi/4}\,\mathrm{Sin}(\pi/n)}{n\,\mathrm{Sin}\phi'(2\pi k)^{1/2}}\left[(\mathrm{Cos}(\pi/n)-\mathrm{Cos}(\theta'-\alpha'))^{-1}\right.$$

$$\left. \mp\,(\mathrm{Cos}(\pi/n)-\mathrm{Cos}((\theta'+\alpha'+\pi)/n))^{-1}\right] \qquad (64)$$

where α' = angle of incidence

θ' = angle of diffraction

$n = \gamma/\pi$ (γ = exterior wedge angle)

ϕ' = angle between the incident ray and the positive tangent to the edge ($\phi' = \pi/2$ in this appendix)

$k = 2\pi/\lambda$ (wave number)

Polarization determines the choice of signs used in eq.(64). Vertical polarization ($\vec{E}$ parallel to the edge of the wedge)

uses the upper sign. Horizontal polarization uses the lower. Angles θ' and α' are defined graphically in Figure 71. Because a right circular cylinder has $\gamma = 270°$, $n = 3/2$. With $\phi' = \pi/2$, eq.(64) becomes

$$D = \frac{2}{3}\frac{e^{i\pi/4}\mathrm{Sin}(2\pi/3)}{(2\pi k)^{1/2}}\left[(\mathrm{Cos}(2\pi/3)-\mathrm{Cos}(\theta'-\alpha'))^{-1}\right.$$

$$\left. \mp (\mathrm{Cos}(2\pi/3)-\mathrm{Cos}(2(\theta'+\alpha'+\pi)/3))^{-1}\right] \quad (65)$$

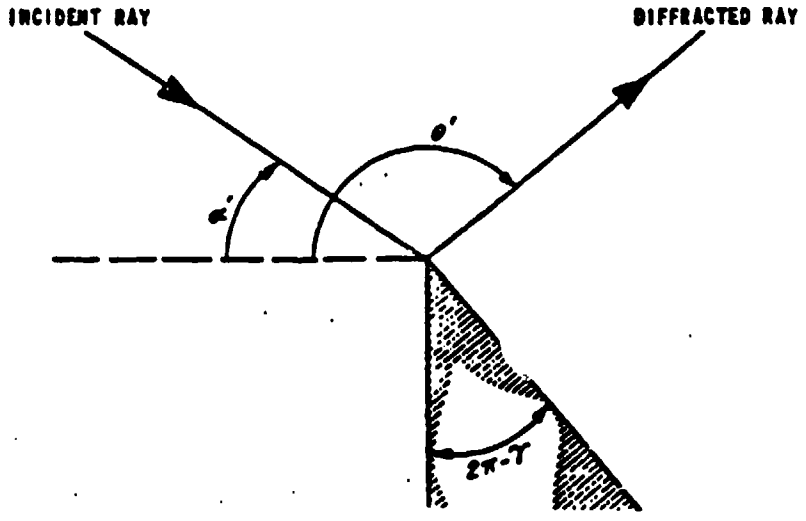

Figure 71. Diffraction at Edge of Conducting Wedge (Anderson, 1965:A-3)

The diffraction coefficients for the cylinder shown in Figure 72 can now be derived in terms of the incident and diffracted fields angles of incidence and diffraction, ψ_i and ψ_s, respectively. The edges contributing to the RCS are labelled S_1, S_2, and S_3. The fourth corner is not illuminated and does not effect RCS if the cylinder is large compared to a wavelength. Conventional references for ψ_i and ψ_s are shown at the center of the cylinder.

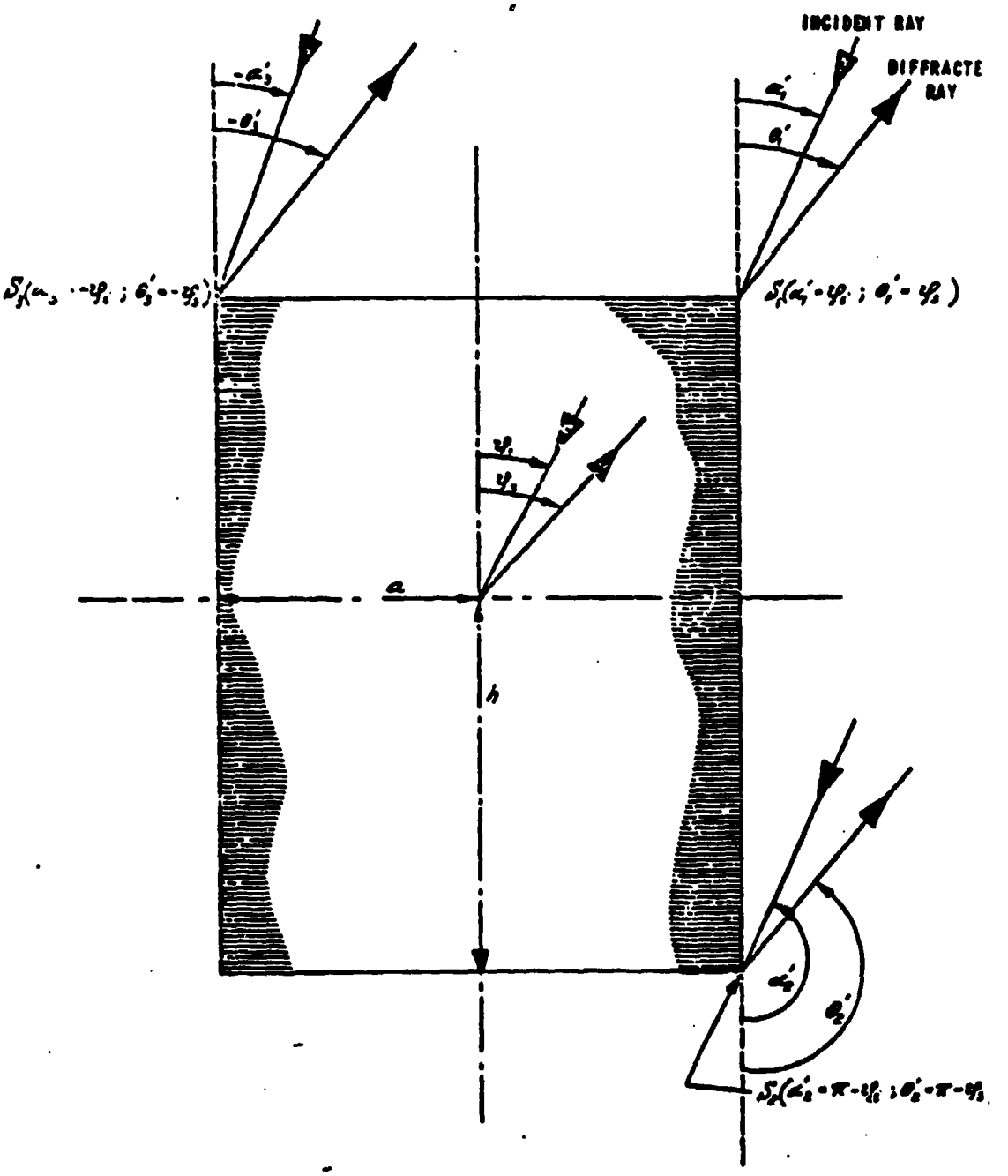

Figure 72. Diffraction by a Right Circular Cylinder (Anderson, 1965:A-4)

The diffraction coefficients resulting from each illuminated edge in Figure 72 are

$$D_{1_H}^{V} = \frac{2}{3}\frac{e^{i\pi/4}\mathrm{Sin}(2\pi/3)}{(2\pi k)^{1/2}}\left[(\mathrm{Cos}(2\pi/3)-\mathrm{Cos}(\psi_s-\psi_i))^{-1}\right.$$

$$\left. \mp\ (\mathrm{Cos}(2\pi/3)-\mathrm{Cos}(2(\pi+\psi_s+\psi_i)/3))^{-1}\right] \quad (66a)$$

$$D_{2_H}^{V} = \frac{2}{3}\frac{e^{i\pi/4}\mathrm{Sin}(2\pi/3)}{(2\pi k)^{1/2}}\left[(\mathrm{Cos}(2\pi/3)-\mathrm{Cos}(\psi_s-\psi_i))^{-1}\right.$$

$$\left. \mp\ (\mathrm{Cos}(2\pi/3)-\mathrm{Cos}(2(\psi_s+\psi_i)/3))^{-1}\right] \quad (66b)$$

$$D_{3_H}^{V} = \frac{2}{3}\frac{e^{i\pi/4}\mathrm{Sin}(2\pi/3)}{(2\pi k)^{1/2}}\left[(\mathrm{Cos}(2\pi/3)-\mathrm{Cos}(\psi_s-\psi_i))^{-1}\right.$$

$$\left. \mp\ (\mathrm{Cos}(2\pi/3)-\mathrm{Cos}(2(\pi-\psi_s-\psi_i)/3))^{-1}\right] \quad (66c)$$

The diffraction coefficients given in eq. (66) are for two-dimensional right-angle edges. Because a cylinder has curved edges it is three dimensional. The curvature is accounted for with a geometrical spreading factor used as a weighting function. Letting s be the distance from the edge to the receiver along the scattered ray and ρ_1 be the radius of curvature of the of the diffracted wave front, the weighting function can be written as

$$[s(1 + \rho_1^{-1}s)]^{-1/2} \quad (67)$$

Because $s \gg \rho_1$, eq.(67) can be written

$$(\rho_1)^{1/2}/s \quad \text{as} \quad \rho_1/s \rightarrow 0 \quad (68)$$

The curvature of the diffracted wavefront, ρ_1, is related to the angles of incidence and diffraction and the cylinders curvature by

$$\rho_1 = \frac{\rho}{\text{Cos}\Theta + \text{Cos}\delta} \qquad (69)$$

where ρ is the cylinder's radius and Θ and δ are defined in Figure 73.

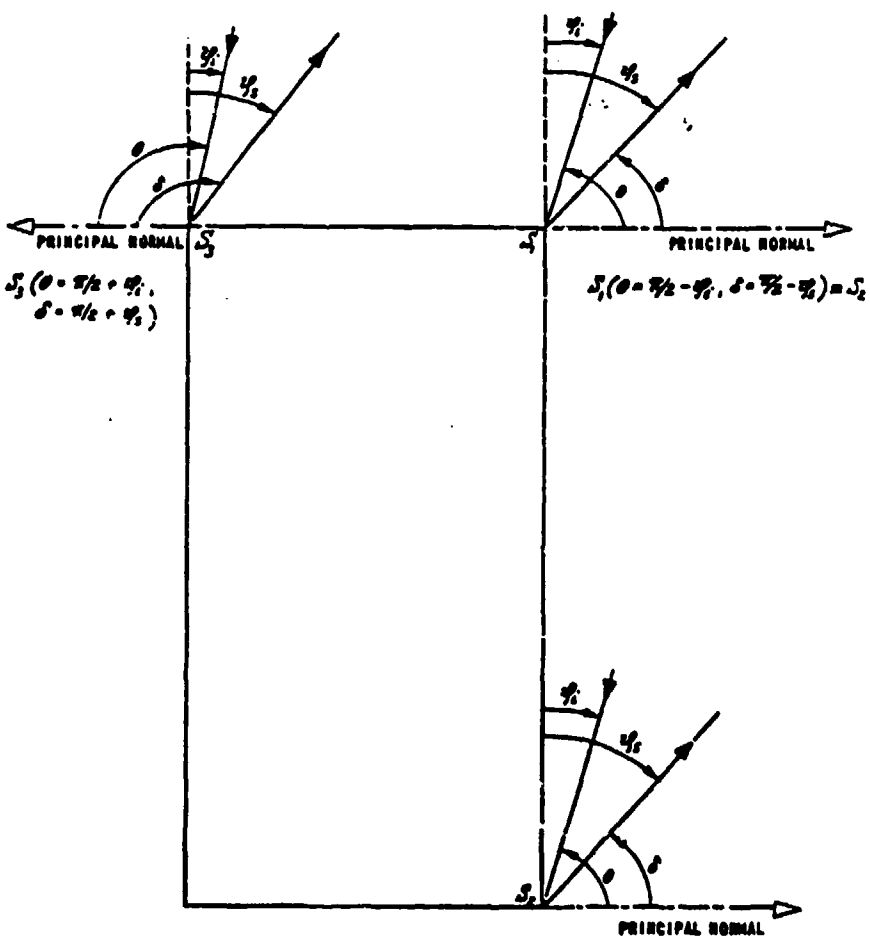

Figure 73. Angular Relationships for Geometric Factors (Anderson, 1965:A-7)

From this, the geometrical spreading factors for each edge are

$$[(\rho_{11})^{1/2}]/s = [(\rho_{12})^{1/2}]/s = \{[a/(\sin\psi_i+\sin\psi_s)]^{1/2}\}/s \quad (70a)$$

$$[(\rho_{13})^{1/2}]/s = \{[a/(-\sin\psi_i - \sin\psi_s)]^{1/2}\}/s \quad (70b)$$

The minus sign occurs in eq. (70b) because the edge at S_3 curves in the opposite direction when compared to S_1 and S_2.

The phase angle associated with a diffraction point is related to the distances the incident and scattered fields travel. With s defined as the distance from the point of diffraction with respect to a fixed reference plane and b the distance the incident field travels relative to a fixed reference plane, then from Figure 74, $s = r_s - d_s$, and $b = r_i - d_i$, for edge S_1.

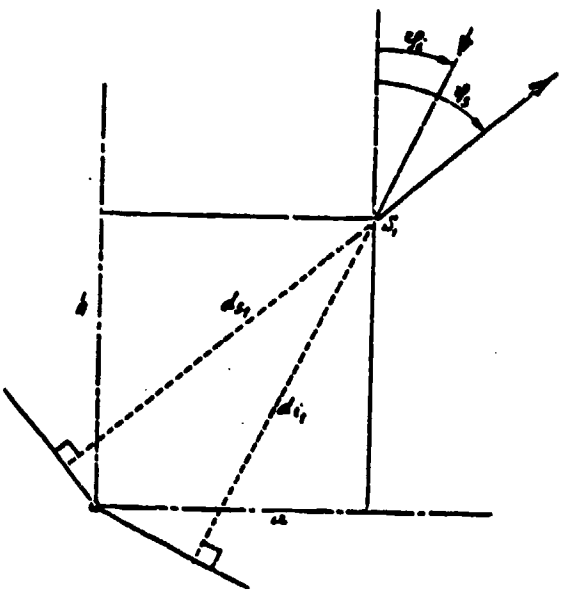

Figure 74. Phase of a Diffracted Ray (Anderson, 1965:A-8)

It can be derived from Figure 74 that

$$d_{i1} = a\mathrm{Sin}\psi_i + h\mathrm{Cos}\psi_i \tag{71a}$$

and

$$d_{s1} = a\mathrm{Sin}\psi_s + h\mathrm{Cos}\psi_s \tag{71b}$$

Using this logic, the phase terms can be written

$$e^{ik(s_1+b_1)} = e^{ik[2r-a(\mathrm{Sin}\psi_i+\mathrm{Sin}\psi_s)-h(\mathrm{Cos}\psi_i+\mathrm{Cos}\psi_s)]} \tag{72a}$$

$$e^{ik(s_2+b_2)} = e^{ik[2r-a(\mathrm{Sin}\psi_i+\mathrm{Sin}\psi_s)+h(\mathrm{Cos}\psi_i+\mathrm{Cos}\psi_s)]} \tag{72b}$$

$$e^{ik(s_3+b_3)} = e^{ik[2r+a(\mathrm{Sin}\psi_i+\mathrm{Sin}\psi_s)-h(\mathrm{Cos}\psi_i+\mathrm{Cos}\psi_s)]} \tag{72c}$$

By GTD, RCS as a function of the angles of incidence and diffraction is given by

$$\sigma(\psi_i, \psi_s) = 4\pi r^2 \left| \frac{\mu_{total}}{A} \right|^2 \tag{73}$$

where μ_{total} = sum of all rays diffracted toward the receiver

Combining eqs. (66), (70), and (72), diffraction at each illuminated edge is given by

$$\mu_{s1} = \mp\frac{2}{3}\,\frac{Ae^{i\pi/4}Sin(2\pi/3)}{(2\pi k)^{1/2}}\,\frac{[a/(Sin\psi_i+Sin\psi_s)]^{1/2}}{s}$$

$$x\ exp\{ik[2r-a(Sin\psi_i+Sin\psi_s)-h(Cos\psi_i+Cos\psi_s)]\}$$

$$x\ [(Cos(2\pi/3)-Cos(\psi_s-\psi_i))^{-1}$$

$$\mp\ (Cos(2\pi/3)-Cos(2(\pi+\psi_s+\psi_i)/3))^{-1}] \qquad (74a)$$

$$\mu_{s2} = \mp\frac{2}{3}\,\frac{Ae^{i\pi/4}Sin(2\pi/3)}{(2\pi k)^{1/2}}\,\frac{[a/(Sin\psi_i+Sin\psi_s)]^{1/2}}{s}$$

$$x\ exp\{ik[2r-a(Sin\psi_i+Sin\psi_s)+h(Cos\psi_i+Cos\psi_s)]\}$$

$$x\ [(Cos(2\pi/3)-Cos(\psi_s-\psi_i))^{-1}$$

$$\mp\ (Cos(2\pi/3)-Cos(2(\psi_s+\psi_i)/3))^{-1}] \qquad (74b)$$

$$\mu_{s3} = \mp\frac{2}{3}\,\frac{Ae^{i\pi/4}Sin(2\pi/3)}{(2\pi k)^{1/2}}\,\frac{[a/(-Sin\psi_i-Sin\psi_s)]^{1/2}}{s}$$

$$x\ exp\{ik[2r-a(Sin\psi_i+Sin\psi_s)-h(Cos\psi_i+Cos\psi_s)]\}$$

$$x\ [(Cos(2\pi/3)-Cos(\psi_s-\psi_i))^{-1}$$

$$\mp\ (Cos(2\pi/3)-Cos(2(\pi+\psi_s+\psi_i)/3))^{-1}] \qquad (74c)$$

where $s \approx r$ in the far field.

From Figure 72 it can be seen $\psi_s = \psi_i + \beta$. To remain consistent with other derivations in this study let $\psi_i = \theta$. Using the relationship $\psi_s = \theta + \beta$, bistatic RCS can be computed as a function of the angle of incidence and the bistatic angle. Eq. (74) is now

$$\mu_{s1} = \mp\frac{2}{3}\,\frac{Ae^{i\pi/4}\,Sin(2\pi/3)}{(2\pi k)^{1/2}}\,\frac{[a/(Sin\theta+Sin(\theta+\beta)]^{1/2}}{r}$$

$$x\ exp\{-ik[a(Sin\theta+Sin(\theta+\beta))+h(Cos\theta+Cos(\theta+\beta))]\}$$

$$x\ [(Cos(2\pi/3)-Cos(2\beta/3))^{-1}$$

$$\mp\ (Cos(2\pi/3)-Cos(2(\pi+2\theta+\beta)/3))^{-1}] \quad (75a)$$

$$\mu_{s2} = \mp\frac{2}{3}\,\frac{Ae^{i\pi/4}\,Sin(2\pi/3)}{(2\pi k)^{1/2}}\,\frac{[a/(Sin\theta+Sin(\theta+\beta)]^{1/2}}{r}$$

$$x\ exp\{-ik[a(Sin\theta+Sin(\theta+\beta))-h(Cos\theta+Cos(\theta+\beta))]\}$$

$$x\ [(Cos(2\pi/3)-Cos(2\beta/3))^{-1}$$

$$\mp\ (Cos(2\pi/3)-Cos(2(2\theta+\beta)/3))^{-1}] \quad (75b)$$

$$\mu_{s3} = \mp\frac{2}{3}\,\frac{Ae^{i\pi/4}\,Sin(2\pi/3)}{(2\pi k)^{1/2}}\,\frac{[a/(Sin\theta+Sin(\theta+\beta)]^{1/2}}{r}$$

$$x\ exp\{ik[a(Sin\theta+Sin(\theta+\beta))-h(Cos\theta+Cos(\theta+\beta))]-i\pi/2\}$$

$$x\ [(Cos(2\pi/3)-Cos(2\beta/3))^{-1}$$

$$\mp\ (Cos(2\pi/3)-Cos(2(\pi-2\theta-\beta)/3))^{-1}] \quad (75c)$$

Summing eqs.(75a), (75b), and (75c) and inserting this sum in eq.(73) gives the bistatic RCS. For the equivalent monostatic RCS, ψ_i and ψ_s are equal to $\theta + \beta/2$. Substituting this into eq.(74) gives

$$\mu_{s1} = \mp\frac{2}{3}\,\frac{Ae^{i\pi/4}Sin(2\pi/3)}{(2\pi k)^{1/2}}\,\frac{[a/(2Sin(\Theta+\beta/2)]^{1/2}}{r}$$

$$x\ exp\{-i2k[aSin(\Theta+\beta/2)+hCos(\Theta+\beta/2)]\}$$

$$x\ [(Cos(2\pi/3)-Cos(2\beta/3))^{-1}$$

$$\mp\ (Cos(2\pi/3)-Cos(2(\pi+2\Theta+\beta)/3))^{-1}] \quad (76a)$$

$$\mu_{s2} = \mp\frac{2}{3}\,\frac{Ae^{i\pi/4}Sin(2\pi/3)}{(2\pi k)^{1/2}}\,\frac{[a/(2Sin(\Theta+\beta/2)]^{1/2}}{r}$$

$$x\ exp\{-i2k[aSin(\Theta+\beta/2)-hCos(\Theta+\beta/2)]\}$$

$$x\ [(Cos(2\pi/3)-Cos(2\beta/3))^{-1}$$

$$\mp\ (Cos(2\pi/3)-Cos(2(2\Theta+\beta)/3))^{-1}] \quad (76b)$$

$$\mu_{s3} = \mp\frac{2}{3}\,\frac{Ae^{i\pi/4}Sin(2\pi/3)}{(2\pi k)^{1/2}}\,\frac{[a/(2Sin(\Theta+\beta/2)]^{1/2}}{r}$$

$$x\ exp\{i2k[aSin(\Theta+\beta/2)-hCos(\Theta+\beta/2)]-i\pi/2\}$$

$$x\ [(Cos(2\pi/3)-Cos(2\beta/3))^{-1}$$

$$\mp\ (Cos(2\pi/3)-Cos(2(\pi-2\Theta-\beta)/3))^{-1}] \quad (76c)$$

Monostatic RCS is then computed by summing eqs. (76a), (76b), and (76c) in eq. (73).

In eqs. (75c) and (76c) the phase contains the term $(-i\pi/2)$. This comes from $(-Sin\psi_i - Sin\psi_s)$ in the denominator of the geometrical spreading factor.

Computer programs written in FORTRAN 77 to calculate the biatatic and equivalent monostatic RCS are listed below.

```
C*********************<<< BICYL.FOR >>>*************************
C
C      THIS PROGRAM COMPUTES THE BISTATIC RCS OF A
C      RIGHT CIRCULAR CYLINDER, HORIZONTAL POLARIZATION.
C
C      OUTPUT:  10*LOG(RCS/1.E4); RCS IN SQUARE CM
C
C***********************************************************
C
       REAL A,H,F,G,K,U,V,X,ALPH(451),LAMBDA
       REAL BETA,PI,RC(451),S1,S2,S3,II,Q,Q1,Q2,Q3
       COMPLEX J,Y,P1,P2,P3
       J = (0.,1.)
       PI = 3.141593
C
C      DEFINE VARIABLES
C
C      A = RADIUS OF CYLINDER LIN CM
C      H = HALF CYLINDER'S LENGTH IN CM
C      LAMBDA = WAVELENGTH IN CM
C      THETA = ANGLE OF INCIDENCE (END-ON = 0°)
C      BETA = BISTATIC ANGLE
C
       A = 7.50
       H = 30.0
       OPEN (1,STATUS='NEW',FILE='B:SIGMA_BV.DAT')
C
C      I = ANGLE OF INCIDENCE
C
       DO 40 I = 0,90,15
         THETA = PI*FLOAT(I)/180.
         WRITE(1,*) 'THETA =',I
C
C      N = BISTATIC ANGLE
C
         DO 30 N = 0,60
           WRITE(*,*) I,N
           BETA = FLOAT(N)*PI/180.
           LAMBDA = 3.0
           K = 2.*PI/LAMBDA
           F = 2.*SIN(2.*PI/3.)/(3.*SQRT(2.*PI*K))
           X = 1./(COS(2.*PI/3.)-COS(2.*BETA/3.))
           L1 = 180-N-I
           Q = COS(2.*PI/3.)
           Q1 = COS(2.*(PI+2.*THETA+BETA)/3.)
           Q2 = COS(2.*(2.*THETA+BETA)/3.)
           Q3 = COS(2.*(PI-2.*THETA-BETA)/3.)
           IF (I.EQ.0) THEN
```

```
        RCS = PI*(A**2*K*COS(BETA/2.))**2
            ELSEIF (I.EQ.90) THEN
              RCS = 4*K*A*H**2*COS(BETA/2.)
C
C       DIVIDE BY 0 ERRORS OCCUR IN THE DIFFRACTION
C       COEFFICIENT.  THE FOLLOWING INSTRUCTIONS GIVE THE
C       RCS FOR THE PREVIOUS BISTATIC ANGLE WHEN THIS OCCURS.
C
            ELSEIF (Q1.EQ.Q) THEN
              GO TO 20
            ELSEIF (Q2.EQ.Q) THEN
              GO TO 20
            ELSEIF (Q3.EQ.Q) THEN
              GO TO 20
            ELSEIF (I.EQ.L1) THEN
              GO TO 20
C
            ELSE
       G = SQRT(A/(SIN(ALPHA)+SIN(ALPHA+BETA)))
       U = A*(SIN(ALPHA)+SIN(ALPHA+BETA))
      &     +H*(COS(ALPHA)+COS(ALPHA+BETA))
       V = A*(SIN(ALPHA)+SIN(ALPHA+BETA))
      &     -H*(COS(ALPHA)+COS(ALPHA+BETA))
       S1= X+1./(Q-Q1)
       S2= X+1./(Q-Q2)
       S3= X+1./(Q-Q3)
       P1= F*G*S1*CEXP(J*(PI/4.-K*U))
       P2= F*G*S2*CEXP(J*(PI/4.-K*V))
       P3= F*G*S3*CEXP(J*(-1.*PI/4.+K*V))
       Y = P1+P2+P3
       RCS = 4.*PI*CABS(Y)**2
            ENDIF
            RC(N) = 10.*ALOG10(RCS/1.E4)
            GO TO 30
20          M = N-1
            RC(N) = RC(M)
30        CONTINUE
C
C       OUTPUT THE BISTATIC ANGLE AND THE CORRESPONDING RCS
C
          DO 35 M = 0,60
            WRITE(1,32) M,RC(M)
32          FORMAT(I3,F12.4)
35        CONTINUE
40      CONTINUE
        CLOSE(UNIT=1)
        END
C
C*****************************************************************


C*******************<<< MONOCYL.FOR >>>*************************
C
```

```
C      THIS PROGRAM CALCULATES THE MONOSTATIC RCS,
C      HORIZONTAL POLAARIZATION, CORRESPONDING TO A GIVEN
C      BISTATIC GEOMETRY ACCORDING TO KELL'S MONOSTATIC      C
   BISTATIC RELATIONSHIP.
C
C      OUTPUT:  10*LOG(RCS/1.E4); RCS IN SQUARE CM
C
C*************************************************************
C
       REAL A,H,F,G,K,U,V,X,FREQ(451),LAMBDA
       REAL BETA,PI,RC(451),S1,S2,S3,II,Q,Q1,Q2,Q3
       COMPLEX J,Y,P1,P2,P3
       J = (0.,1.)
       PI = 3.141593
C
C      DEFINE VARIABLES
C
C      A = RADIUS OF CYLINDER IN CM
C      H = HALF CYLINDER'S LENGTH IN CM
C      LAMBDA = WAVELENGTH IN CM
C      THETA = ANGLE OF INCIDENCE (END-ON = 0°)
C      BETA = BISTATIC ANGLE
C
       A = 7.50
       H = 30.0
       OPEN (1,STATUS='NEW',FILE='B:SIGMA_FV.DAT')


C
C      I = ANGLE OF INCIDENCE
C
       DO 40 I = 0,90,15
         WRITE(1,*) 'ALPHA =',I
C
C      N = BISTATIC ANGLE
C
         DO 30 N = 0,60
           THETA = PI*(FLOAT(I)+FLOAT(N)/2.)/180.
           WRITE(*,*) I,N
           BETA = FLOAT(N)*PI/180.
C
C      FREQUENCY IS ADJUSTED ACCORDING TO KELL'S
C      RELATIONSHIP.
C
           LAMBDA = 3.0*COS(BETA/2.)
           K = 2.*PI/LAMBDA
           F = 2.*SIN(2.*PI/3.)/(3.*SQRT(2.*PI*K))
           X = 1./(COS(2.*PI/3.)-1.)
           THET = FLOAT(I)+FLOAT(N)/2.
           TERM = THET + FLOAT(I)
           Q = COS(2.*PI/3.)
           Q1 = COS(2.*(PI+2.*THETA)/3.)
           Q2 = COS(2.*(2.*THETA)/3.)
```

```
            Q3 = COS(2.*(PI-2.*THETA)/3.)
            IF (THET.EQ.0.) THEN
          RCS = PI*(A**2*K*COS(BETA/2.))**2
            ELSEIF (N.EQ.0) THEN
              GO TO 10
10          ELSEIF (THET.EQ.90) THEN
              RCS = 4*K*A*H**2*COS(BETA/2.)
            ELSEIF (TERM.EQ.210.) THEN
              GO TO 30
            ELSE
         G = SQRT(A/(SIN(THETA)+SIN(THETA)))
         U = A*(SIN(THETA)+SIN(THETA))
        &     +H*(COS(THETA)+COS(THETA))
         V = A*(SIN(THETA)+SIN(THETA))
        &     -H*(COS(THETA)+COS(THETA))
         S1= X+1./(Q-Q1)
         S2= X+1./(Q-Q2)
         S3= X+1./(Q-Q3)
         P1= F*G*S1*CEXP(J*(PI/4.-K*U))
         P2= F*G*S2*CEXP(J*(PI/4.-K*V))
         P3= F*G*S3*CEXP(J*(-1.*PI/4.+K*V))
         Y = P1+P2+P3
         RCS = 4.*PI*CABS(Y)**2
            ENDIF
            RC(N) = 10.*ALOG10(RCS/1.E4)
30        CONTINUE
C
C       OUTPUT THE BISTATIC ANGLE AND CORRESPONDING RCS
          DO 35 M = 0,60
            WRITE(1,32) M,RC(M)
32          FORMAT(I3,F12.4)
35        CONTINUE
40      CONTINUE
        CLOSE(UNIT=1)
        END
```

Bibliography

Adams, John A. "How to Design an Invisible Aircraft," IEEE Spectrum, 25: 26-31 (April 1988)

Anderson, L.J. Project DISTRACT--Distributed Radar Concepts and Techniques--Second Year Final Report, 18 November 1964-18 November 1965. Contract AF 30(6020-3289). Cornell Aeronautical Laboratory, Inc.

Biggs, A.W. and S.B. McMillen. Analytical Study of the Bistatic Radar Cross Section of a Prolate Spheroid. Contract AFOSR-79-0105. Lawrence, Kansas: University of Kansas, March 1979 (AD-A086846).

Bowman, J.J. Electromagnetic and Acoustic Scattering by Simple Shapes. Amsterdam: New Holland Publishing Company, 1969.

Coleman, J.R. Radar Cross Section Calculations, Vol. I. Contract DAAK40-77-0166. Hawthorne, CA: Northrup Corporation, December 1977 (AD-B066854L).

Crispin, J.W. and others. Methods of Radar Cross-Section Analysis. New York: Academic Press, 1968.

Dynalectron Corporation. The Air Force Radar Target Scatter Facility. Contract F08635-85-C-0141. Holloman AFB, NM.

Harrington, Roger F. Time-Harmonic Electromagnetic Fields. New York: McGraw-Hill Book Company, 1961.

Hunka, John F. and others. "A Technique for Rapid Measurements of Bistatic Radar Cross Sections," IEEE Transactions on Antennas and Propagation, AP-25 243-248 (March 1977).

Kell, Robert E. "On the Derivation of Bistatic RCS from Monostatic Measurements," Proceedings of the IEEE: 983-988 (August 1965).

Kerr, Donald E. Propagation of Short Radio Waves. New York: McGraw-Hill Book Company, 1951.

Knott, Eugene F. and others. Radar Cross Section. Norwood MA: Artech House, 1985.

Siegel, K.M. and others. "Bistatic Radar Cross Sections of Surfaces of Revolution," Journal of Applied Physics, 26: 297-305 (March 1955).

-----. Studies in Radar Cross Section VIII: Theoretical Cross Section as a Function of Separation Angle Between Transmitter and Receiver at Small Wavelengths. Contract W 33(08)-ac-14222. University of Michigan, Ann Arbor, Michigan. October 1953.

Skinner, Capt Paul and Capt Randy Jost. A Short Tutorial on the Methods of Physical Optics for Electromagnetic Scattering. AFWAL/AAWP, Wright-Patterson AFB OH, February 1988.

Stratton, John A. Electromagnetic Theory. New York: McGraw-Hill Book Company, 1941.

Tomko, Capt Frank, Chief, Radar Analysis Branch. Telephone interview. Air Force Target Scatter Facility, Holloman AFB NM, 6 May 1988.

VITA

Capt Jeffrey M. MacLennan was born on 27 February, 1951, in Seattle, Washington. He graduated from high school in Anchorage, Alaska, in 1969 and attended the University of Wyoming. He enlisted in the Marine Corps in 1972 and served in North Carolina, Thailand, Japan, and California as a combat engineer. Upon discharge from the Marine Corps in 1975, he attended Pacific Lutheran University from which he received a Bachelor of Arts Degree in Education in January 1979. He was then employed as a physical education teacher in Edmonds, Washington. He joined the Air Force in June 1982 and graduated from Officer Training School in August 1982. He then attended Louisiana Tech University earning a Bachelor of Science Degree in Electrical Engineering in May 1984. He then served as an avionics engineer on the F/FB-111 Avionics Modernization Program at McClellan AFB, California, until entering the School of Engineering, Air Force Institute of Technology, in June 1987.

Permanent address: 5004 Brentwood Dr.
Lacey, Washington 98503

SECURITY CLASSIFICATION OF THIS PAGE

REPORT DOCUMENTATION PAGE

Form Approved OMB No. 0704-0188

1a. REPORT SECURITY CLASSIFICATION UNCLASSIFIED	1b. RESTRICTIVE MARKINGS
2a. SECURITY CLASSIFICATION AUTHORITY	3. DISTRIBUTION/AVAILABILITY OF REPORT Approved for public release; distribution unlimited
2b. DECLASSIFICATION/DOWNGRADING SCHEDULE	
4. PERFORMING ORGANIZATION REPORT NUMBER(S) AFIT/GE/ENG/88D-24	5. MONITORING ORGANIZATION REPORT NUMBER(S)
6a. NAME OF PERFORMING ORGANIZATION School of Engineering 6b. OFFICE SYMBOL (If applicable) AFIT/ENG	7a. NAME OF MONITORING ORGANIZATION
6c. ADDRESS (City, State, and ZIP Code) Air Force Institute of Technology Wright-Patterson AFB, OH 45433	7b. ADDRESS (City, State, and ZIP Code)
8a. NAME OF FUNDING/SPONSORING ORGANIZATION 6585 Test Group 8b. OFFICE SYMBOL (If applicable) RXR	9. PROCUREMENT INSTRUMENT IDENTIFICATION NUMBER
8c. ADDRESS (City, State, and ZIP Code) HOLLOMAN AFB, NM 88330-5000	10. SOURCE OF FUNDING NUMBERS PROGRAM ELEMENT NO. / PROJECT NO. / TASK NO. / WORK UNIT ACCESSION NO.

11. TITLE (Include Security Classification)
(U) Verification and Limitations of the Monostatic-Bistatic Radar Cross Section Relationship Derived by Kell

12. PERSONAL AUTHOR(S)
Jeffrey M. MacLennan, B.S., Captain, USAF

13a. TYPE OF REPORT	13b. TIME COVERED	14. DATE OF REPORT (Year, Month, Day)	15. PAGE COUNT
Thesis	FROM _____ TO _____	1988, December	125

16. SUPPLEMENTARY NOTATION

17. COSATI CODES			18. SUBJECT TERMS (Continue on reverse if necessary and identify by block number)
FIELD	GROUP	SUB-GROUP	
17	09		Bistatic Scattering, Radar Cross Section, Monostatic-Bistatic RCS Equivalence
20	14		

19. ABSTRACT (Continue on reverse if necessary and identify by block number)

Thesis Advisor: Harry H. Barksdale, Major, USAF

Abstract: See back

12 Jan 1989

20. DISTRIBUTION/AVAILABILITY OF ABSTRACT	21. ABSTRACT SECURITY CLASSIFICATION
☒ UNCLASSIFIED/UNLIMITED ☐ SAME AS RPT. ☐ DTIC USERS	UNCLASSIFIED

22a. NAME OF RESPONSIBLE INDIVIDUAL	22b. TELEPHONE (Include Area Code)	22c. OFFICE SYMBOL
Harry H. Barksdale, Major USAF	513/255-6027	AFIT/ENG

DD Form 1473, JUN 86 Previous editions are obsolete. SECURITY CLASSIFICATION OF THIS PAGE

Abstract

Robert Kell developed a relationship between monostatic radar cross section (RCS) and bistatic RCS whereby bistatic RCS can be predicted from monostatic RCS measurements under certain conditions. This study found Kell's relationship to be mathematically sound given certain assumptions. Kell's relationship was then tested by comparing computer generated bistatic and monostatic cross sections for simple shapes. Four parameters were varied during testing in order to discern possible limitations of Kell's method: bistatic angle, angle of incidence, electrical size of the target, and continuity. Results of the testing show Kell's method has some merit. The difference between the bistatic RCS and its related monostatic RCS for electrically large spheres is less than 1-dB up to bistatic angles of 80°. For electrically large flat and singly curved surfaces the monostatic and bistatic cross sections were within 3-dB for angles of incidence up to 30° from broadside and bistatic angles up to 15°. Finally, the accuracy of Kell's relationship proved to be polarization dependent when surface discontinuities in the form of 90° wedges were present.